Molecules to Burn:
A Mechanistic Characterization of Cyanobacterial Aldehyde Deformylating Oxygenase

by

Matthew William Waugh

A dissertation submitted in partial fulfillment
of the requirements for the degree of
Doctor of Philosophy
(Chemical Biology)
in the University of Michigan
2015

Doctoral Committee:

Professor E. Neil G. Marsh, Chair
Associate Professor Nina Lin
Associate Professor Bruce A. Palfey
Professor Stephen W. Ragsdale

Dedication

I would like to dedicate this body of work to my grandfather Bruce Merrifield for teaching me the scientific method, to my grandmother Elizabeth Merrifield for encouraging a young scientist, to my parents William and Nancy Waugh for instilling in me a thirst for knowledge, and to my brothers Mark, James, and John for all of their support.

Acknowledgements

First and foremost, I would like to thank my advisor, Prof. E. Neil G. Marsh, for his support and direction. I have truly learned an incredible amount from him about scientific writing, the practical application of the scientific method, and about how to conduct myself as a scientist and an independent investigator. In particular, I would like to thank him for his patience and understanding during the most difficult time in my life. I would like to thank my committee members Prof. Bruce Palfey, Prof. Stephen Ragsdale, and Prof. Nina Lin for their suggestions and guidance. I would like to thank Prof. Stephen Maldonado and Tim Zhang for helping to teach me electrochemistry and their contributions the protein film voltammetry portion of this project. I would like to thank Dr. Debasis Das, Dr. Bekir Eser, Dr. Bishuajit Paul, Dr. Fengming Lin, Dr. Ben Buer, Dr. Jae Han, and Ben Ellington for their help and efforts on the project. I would also like to thank them, Dr. Tad Ogorzalek, Mckenna Schroeder, and my other lab mates for making coming to the lab fun. I would like to thank my friends Chris Tom, Dr. Hong Tran, Dr. Eli Eismann, JP Carolan, Matt Pauley, Laura Cessa, and Dr. Brian Devree for making grad school a singular experience. I would like to thank my family for all their love and support.

Table of Contents

List of Figures

List of Abbreviations

Φ	Fractionation Factor
Φ_{obs}	Observed Fractionation Factor
AcP	Acyl Carrier Protein
AD	Aldehyde Decarbonylase
ATP	Adinene Triphosphate
BAIB	[Bis(acetoxy)iodo]benzene
C_1	Carbonyl Carbon
C9	Nonanal
C10	Decanal
cAD	Cyanobacterial Aldehyde Decarbonylase
cADO	Cyanobacterial Aldehyde Deformylating oxygenase
C-C	Carbon-Carbon Bond
cer	*eceriferum*
cer1	Cer1 encoding gene
Cer1	Plant Aldehyde Decarbonylase
Cer3	Plant Acyl-CoA Reductase
CO	Carbon Monoxide
CO_2	Carbon Dioxide
CODH	Carbon Monoxide Dehydrogenase
CODH-ACS	Carbon Monoxide Dehydrogenase Acyl-Carrier Synthase
CV	Cyclic Voltammetry
CYP2B4	Cyclohexanecarboxaldehyde Decarbonylase
CYP6A1	Insect Aldehyde Decarbonylase
Cytb5	Cytochrome b_5
D_2O	Deuterium Oxide
$^{D_2O}SIE_{obs}$	Observed Deuterium Oxide Solvent Isotope Effect
DCM	Dichloromethane
D-HEPES	Deuterated (4-(2-hydroxyethyl)-1-piperazineethanesulfonic acid
DMSO	Dimethyl Sulfoxide
DNA	Deoxyribonucleic Acid
DPV	Differential Pulse Voltammetry
ε	Extinction Coefficient
EIE	Equilibrium Solvent Isotope Effect
EPT	Electron Proton Transfer
Fd	Ferredoxin
FDR	Ferredoxin Reductase
FID	Flame Ionization Detector
GC	Gas Chromatography

H_2O_2	Hydrogen Peroxide
HEPES	(4-(2-hydroxyethyl)-1-piperazineethanesulfonic acid
HCl	Hydrochloric Acid
HCO_2H	Formic Acid
HF	Hi-Fidelity
GC-MS	Gas Chromatography Mass Spectrometry
Hi-res MS	High-resolution Mass Spectrometry
HRP	Horseradish Peroxidase
i_{lim}	Limiting Current
IPTG	Isopropyl β-D-1-Thiogalactopyranoside
k_{app}	Apparent Rate Constant
k_{obs}	Observed Rate Constant
k_{cat}	Catalytic Rate Constant
KCL	Potassium Chloride
K_i	Inhibitor Dissociation Constant
K_M	Michaelis Constant
$LiAl_4$	Lithium Aluminum Hydride
MeOH	Methanol
MMO	Methane Monooxygenase
MMOB	Methane Monooxygenase B Component
MMOH	Methane Monooxygenase Hydroxylase Subunit
MMOR	Methane Monooxygenase Reductase Subunit
$M\text{-}OL_2$	Metal bound water ligand
$M\text{-}OL^-$	Metal bound hydroxyl ligand
MS	Mass Spectrometry
MS-EPT	Multiple Site Electron Proton Transfer
NADH	Nicotinamide Adinine Dinucleotide
NADPH	Nicotinamide Adinine Dinucleotide Phosphate
NaH	Sodium Hydride
NMR	Nuclear Magnetic Resonance
NTP	Nucleotide Triphosphate
^{OMe}PMS	O-Methoxy Phenazine Methosulfate
O_2	Oxygen Gas
PCR	Polymerase Chain Reaction
pD	Negative log of deuterium ion concentration
PDC	Pyridinium Dichromate
Pd on C	Palladium on Carbon
PFV	Protein Film Voltammetry
pH	Negative log of hydrogen ion concentration
pK_a	Acid Dissociation Constant
pL	Negative log of ligand ion concentration
PMS	Phenazine Methosulfate
$R\text{-}NL_2$	Amine functionality
RDS	Rate Determining Step
SAM	Self-Assembled Monolayer
SHE	Standard Hydrogen Electrode

SIE	Solvent Isotope Effect
SOCl2	Thionyl Chloride
TCEP	(tris(2-carboxyethyl)phosphine)
TEMPO	(2,2,6,6-Tetramethylpiperidin-1-yl)oxyl
THF	Tetrahydrofuran
V/K	k_{cat}/K_M
V_{max}	Maximum Velocity

Abstract

The development of next generation, “drop-in” biofuels that can replace conventional fossil fuels is essential to address the challenge of energy sustainability. These hydrocarbon based biofuels improve on the current generation of bioethanol based biofuels with greater energy densities, direct compatibility with modern fuel infrastructure, and significantly reduced resource requirements in production and refinement. However, there are very few known biosynthetic pathways to produce these molecules and, generally, they are not well understood. The focus of this dissertation is to explore one of the very few biosynthetic routes to produce entirely unfunctionalized hydrocarbons through investigation of the highly unusual reaction catalyzed by cyanobacterial aldehyde deformylating oxygenase (cADO).

Whereas the proton in the product alkane derives ultimately from the solvent, the identity of the proton donor in the active site remains unclear. To investigate the proton transfer step, solvent isotope effect (SIE) studies were undertaken. The rate of alkane formation was found to be maximal at pH 6.8 and to be the same in D_2O or H_2O within experimental error, implying that proton transfer is not a kinetically significant step. However, when the ratio of protium to deuterium in the product alkane was measured as a function of the mole fraction of D_2O, a $^{D_2O}SIE_{obs}$ of 2.19 ± 0.02 was observed. The SIE was invariant with the mole fraction of D_2O, indicating the involvement of a single protic

site in the reaction. We interpret this SIE as most likely arising from a reactant state equilibrium isotope effect on a proton donor with an inverse fractionation factor, for which $\Phi = 0.45$. These observations are consistent with an ironbound water molecule being the proton donor to the alkane in the reaction.

Substrate analogs and binding channel mutations were used to investigate substrate binding and/or product release acting as a non-chemical rate limiting step. The kinetics of the mutants were investigated using octadecanal and, although no increase apparent rate was observed, two mutants displayed significant shifts in apparent K_M. These results suggest the hydrophobic pocket is important in determining the binding specificity of long chain aldehyde substrates.

Protein film voltammetry experiments were undertaken to explore the electrochemistry of cADO and the possibility of electron transfer as a rate limiting step. The midpoint reduction potential was determined to be $E^o_{mid} = -73 \pm 10$ mV (vs SHE), 153 mV lower than the electron mediator used in solution experiments. Catalytic cyclic voltammetry with heptanal indicated an i_{lim} at E = -340 mV and a lower limit on alkane turnover of $k_{obs} > 0.43\ s^{-1}$, significantly faster than the rate of ~1 min^{-1} observed in solution. These data suggest that electron transfer was likely rate limiting in previous *in vitro* kinetic measurements. Interestingly, an alternative reaction was observed between enzyme and O_2, with a lower limit on turnover of $k_{obs} > 0.20\ s^{-1}$, consuming reducing equivalents to form H_2O_2 in a futile cycle previously attributed the reducing system and O_2. These observations suggest that inefficient interactions with the *in vitro* reducing system or a partitioning effect between alkane and H_2O_2 turnover may be responsible for the sluggish activity of cADO.

Chapter 1 Introduction

1.1 Biofuels and Sustainability

This chapter has been published in part as: Marsh, E. N. G., and Waugh, M. W. (2013) Aldehyde Decarbonylases: Enigmatic Enzymes of Hydrocarbon Biosynthesis, *ACS Catal*. 3, 2515-2521.

1.1.1 Sustainability

As the global population approaches the United Nations prediction of 9 billion by the middle of this century (Figure 1), perhaps the most significant and imminent challenge facing humanity is that of sustainability.[1] In the last century and a half the exponential growth of our society, and the globalization of communication and economic networks, has been dependent on fossil fuels derived from ancient, sequestered carbon reserves. Not only are these resources finite and being depleted, but their increasing scarcity results in international conflicts over limited resources. Combustion of these fuels, of which alkanes are a major component, is a substantial source of the greenhouse gas carbon dioxide (CO_2). The influx of this formerly sequestered carbon into the biosphere continues to unbalance the global carbon cycle leading to increasing acidification of the oceans, a rise in temperature of approximately 1^oC in the last century, and an estimated increase in temperature of between 0.5^oC and 4.8^oC in the 21^{st} century (Figure 1 inset).[2] The political, economic, and environmental concerns surrounding fuel

sustainability in particular have driven a need for green energy solutions to reduce fuel prices, replace rapidly depleting fossil fuels, and counteract global warming. Towards this end, a major focus of the renewable energy effort has been the research and development of liquid fuels produced by conversion of biomass, or biofuels, in a net carbon neutral biosynthetic pathway.

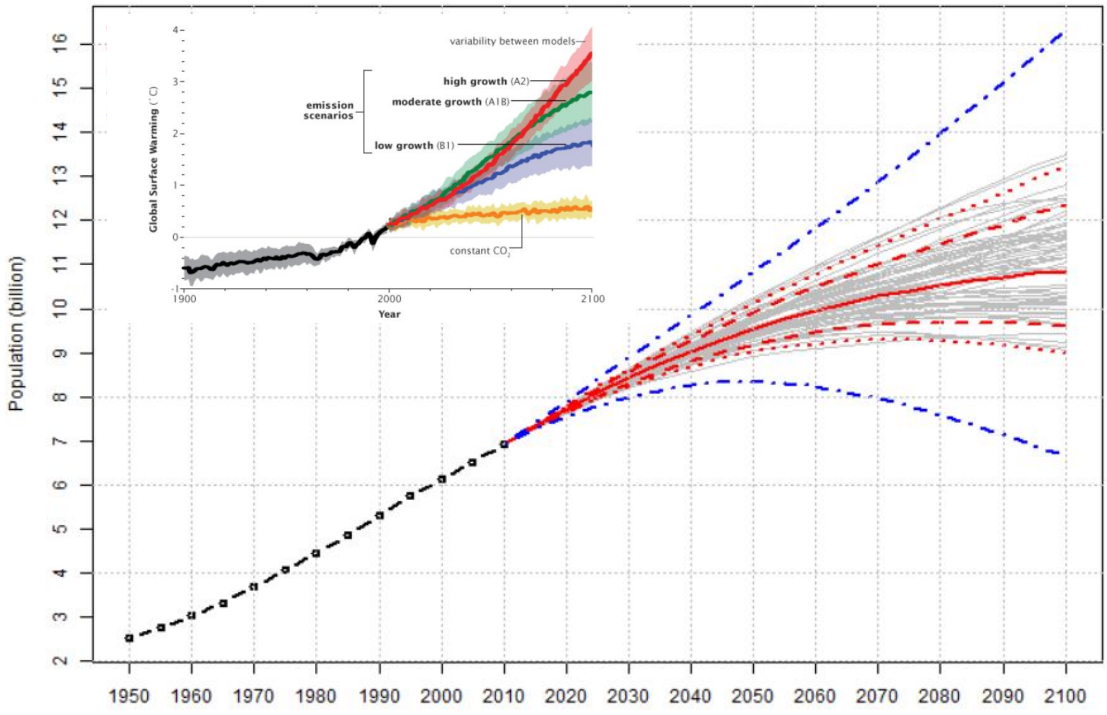

Figure 1.1 – United Nations projected world population growth model. The black line shows observed population, the solid red line shows the median, the blue lines show the high and low predictions. The inset graph displays estimated global surface temperature increase based on high, moderate, low, or constant CO_2 emission scenarios. Figures are based on references 1 and 2.

1.1.2 Biofuels

Currently, biomass provides approximately 10% of the global energy supply.[3] Refined biofuels only account for 2-3% of transportation fuel usage, with bioethanol providing roughly 75% of the market, but this is expected to continue to increase to

between 5 and 20% due to government mandated targets. First generation biofuels are derived directly through fermentation of sugars readily available from food crops such as wheat or corn, although this has raised concerns over the resource requirements involved including the subversion of food stocks and arable land. [4,5] Second generation biofuels focus on non-food crops such as wood, food crop waste, and specific biomass crops such as switchgrass.[6] A large portion of the field is still dedicated to the study and improvement of methods involved in the breakdown of lignocellulosic biomass to release previously inaccessible fermentable sugars.[7,8] Third generation biofuels utilize specially engineered energy crops such as algae to produce a highly renewable and energy dense feedstock, but are expensive to cultivate and extract.[9] However, each of these generations of biofuels still relies on the fermentation of sugars to bioethanol, which is inherently a flawed prospect. Although industrial production of ethanol is highly efficient after millennia of selecting for alcohol tolerant yeast in the pursuit of our fascination with imbibing alcohol, ethanol is highly miscible with water. Being both hydroscopic and corrosive make it incompatible with modern infrastructure, as in high concentrations it causes damage to all but specially designed engines and pipelines. Furthermore, being energetically intensive to separate and only 67% as energy dense as gasoline diminishes bioethanol as a viable alternative to fossil fuel both in its ability to reduce fuel price and carbon footprint. The challenge of producing the next generation of hydrocarbon based biofuels, those that can effectively function as “drop-in” replacements for gasoline, diesel, and jet fuel, has led to renewed interest, especially in the area of mechanistic enzymology, in how alkanes are biosynthesized.[10]

1.1.3 Hydrocarbon Biosynthesis in Nature

Drop-in biofuels, those that are direct substitutes for fossil fuels, such as hydrocarbons are ideal as the next generation of biofuels, however, the synthesis of completely unfunctionalized molecules presents a challenge for a cell.[11] Long-chain alkane waxes are synthesized by a wide variety of organisms, including plants, animals and microorganisms, and while chemically they are among the most boring of organic molecules, devoid of functionality and thus unreactive, they play essential roles in these organisms' survival.[12-15] Plants secrete what are termed "very long chain" alkane waxes (i.e. chain length ~ 30 carbons) onto their leaves and stems.[16] These, together with wax esters formed from aliphatic alcohols and carboxylic acids of similar chain length, serve as a waterproof barrier to prevent desiccation. A wide variety of hydrocarbons, including branched and unsaturated molecules, are biosynthesized by insects.[17] These are secreted onto the cuticle and play an important role as contact pheromones that mediate all manner of insect:insect recognition and social behaviors; they are also important in preventing desiccation, especially of larval forms.[18] Waterfowl secrete alkane-rich oils from their uropygial (preening) glands; these are essential for waterproofing the birds' feathers, which would otherwise become waterlogged and thus useless for insulation and flight.[12] Many algae synthesize large amounts of long-chain alkanes that can comprise up to 30 % of the algae's dry weight.[19] These accumulate in the area contained by the inner and outer cell walls known as the trilamellar structure and can be utilized to provide energy when photosynthesis is not possible.[20]

Historically, an important observation was that naturally-synthesized alkanes invariably comprise an odd number of carbons, suggesting that they are derived from fatty acid biosynthesis through loss of the carboxyl carbon.[21] It was subsequently established that long-chain alkanes are synthesized from fatty acids through the intermediacy of the corresponding fatty aldehydes. These are the substrates for the only known enzymes to actually perform alkane-forming chemistry, the aldehyde decarbonylases (ADs), which catalyze the carbon-carbon bond cleavage of aliphatic aldehydes to their respective n-1 alkanes. ADs come in three classes named for their respective organisms, plant, insect, and cyanobacteria. They are differentiated by both mechanism and structure.

1.2 Aldehyde Decarbonylases

The biosynthesis of aliphatic hydrocarbons appears to have evolved several times in Nature, resulting in three mechanistically distinct classes of decarbonylases, although each appears to synthesize unfunctionalized alkanes using fatty aldehydes as the precursor (Figure 2). In insects, the enzyme has been shown to be a cytochrome P450 protein,[22,23] whereas in cyanobacteria it is a non-heme diiron enzyme that is structurally related to enzymes such as ferritin and methane monooxygenase.[16,24] In plants, the enzyme is an integral membrane protein that has some sequence similarity to the fatty acid hydroxylase superfamily and stearoyl-CoA desaturase.[25] On this basis, it too is presumed to be a metalloenzyme, with iron the most likely metal. The different mechanisms of decarbonylation are reflected in the fate of the aldehyde carbon, which is

converted to CO_2 in insects,[23] formic acid (HCO_2H) in cyanobacteria,[26,27] and carbon monoxide (CO) in plants and algae.[19,28] The common mechanistic link between the decarbonylases appears to be iron-mediated oxygenation reactions, although this remains rather speculative in the case of the plant decarbonylases. In each case decarbonylation involves a novel biochemical reaction that represents a new variation on the oxidative chemistry catalyzed by other members of the respective enzyme families.

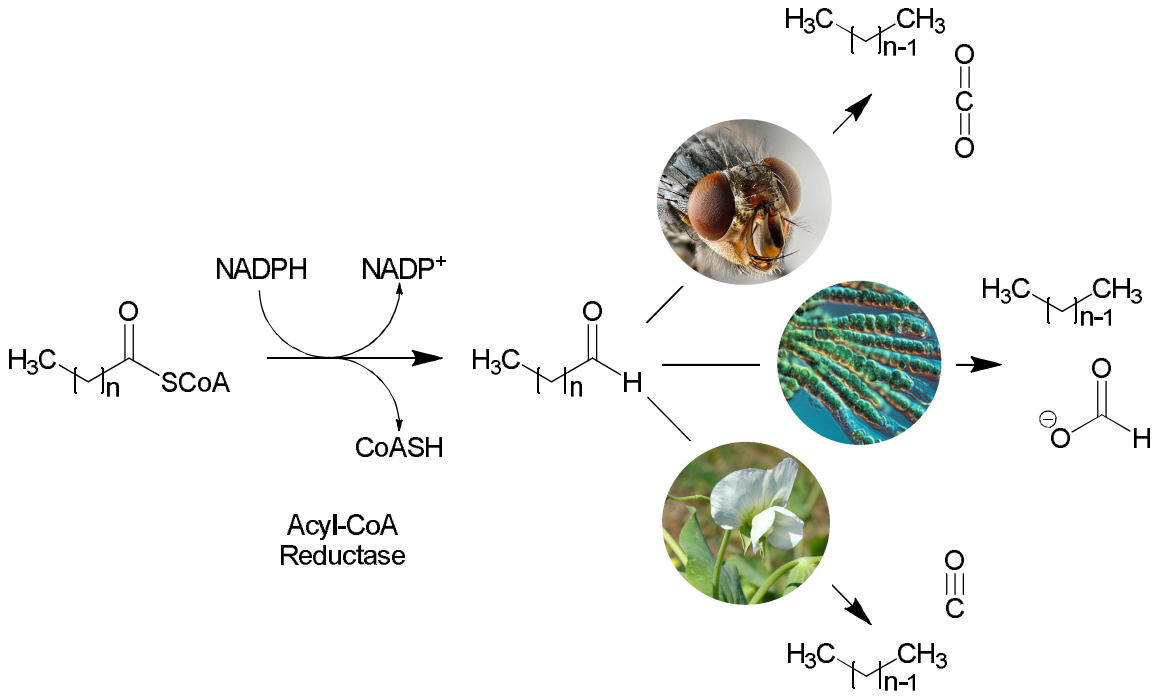

Figure 1.2 – The biosynthesis of alkanes proceeds in two steps from fatty acyl-CoA esters. The decarbonylation of the intermediate fatty aldehyde proceeds by one of three different mechanisms depending upon the organism. The insect AD is a membrane-bound P450 type enzyme. The cyanobacterial AD is a soluble non-heme diiron oxygenase. The plant AD is thought to be similar to the non-heme iron membrane proteins represented by stearoyl desaturase and fatty acid hydroxylase.

1.2.1 Insect Aldehyde Decarbonylase

The biosynthesis of hydrocarbons has been studied in a number of insect species

including the domestic house fly, *Musca domestica*, the fruit fly *Drosophila melanogaster*, cockroaches *Periplaneta americana* and *Blattella germanica*, and the termite *Zootermopsis angusticollis.*[29] Experiments on microsomal preparations of *M. domestica* demonstrated that molecular oxygen and NADPH were required for the conversion of (Z)-15-tetracosenal to (Z)-9-tricosene and, using 1-^{14}C-material, that the aldehyde carbon was oxidized to CO_2 in the process.[23] Furthermore, antibodies to either house fly cytochrome P450 reductase or to a cytochrome P450 (CYP6A1) purified from the house fly inhibited (Z)-9-tricosene.[30] These initial observations provided support for the involvement of a P450 enzyme in the reaction; this was more recently confirmed with the cloning and heterologous expression of the enzyme, CYP4G1, from *Drosophila*.[22]

Further clues to the mechanism of hydrocarbon formation came from analyses of n-tricosane formed by *M. domestica* microsomal preparations incubated with [2,2-$^{2}H_2$,2-^{13}C]-tetracosanoyl-CoA and [3,3-$^{2}H_2$,3-^{13}C]-tetracosanoyl-CoA which demonstrated that the deuterium atoms on the 2- and 3-positions were retained in the hydrocarbon product.[30] Analysis of [l-^{2}H]-tetracosenal incubated with microsomal preparations demonstrated that the aldehyde proton on C-l was transferred to the (Z)-9-tricosene product. Alternative oxidizing agents such as hydrogen peroxide, cumene hydroperoxide, and iodosobenzene were shown to substitute for O_2 and NADPH in the reaction. To accommodate these observations, a mechanism has been proposed, shown in Figure 1.3 A, in which the high valent iron-oxo species, resulting from heterolytic cleavage of the O-O bond of the iron-peroxy intermediate, abstracts an electron from the carbonyl group of the aldehyde.[30] The reduced iron-oxo species then attacks the carbonyl carbon of the aldehyde to form an iron-hemiacetal diradical. This intermediate is

proposed to fragment to form an alkyl radical and an iron-bound formyl radical. In the final step, the alkyl radical then abstracts the formyl hydrogen to produce the hydrocarbon and CO_2.

P450 enzymes catalyze a notably diverse range of oxidative transformations on a very wide range of substrates.[31] Even so, the decarbonylase reaction stands out as being unusual. In most cases P450 enzymes oxidize aldehydes to carboxylic acids through a well understood mechanism involving hydrogen atom abstraction by the high valent iron-oxo intermediate followed by "rebound" of the iron-bound hydroxyl group to give the hydroxylated substrate.[32] In some cases decarbonylation of the aldehyde does occur, notably in the aromatization reaction of androst-4-ene-3,17-dione to estrone catalyzed by human aromatase and the deformylation of cyclohexanal catalyzed by CYP2B4 (Figure 1.3 B).[31] However in these reactions, which are believed to involve the iron-peroxide form of P450, the aldehyde carbon is converted to formate, rather than CO_2, and a double bond is introduced into the oxidized product.[31] An intriguing question is how CYP4G1 controls the highly reactive iron-oxo intermediate to accomplish oxidative decarbonylation rather than simply oxidizing the aldehyde to a carboxylic acid, which, *a priori*, would appear to be a more likely fate for the substrate.

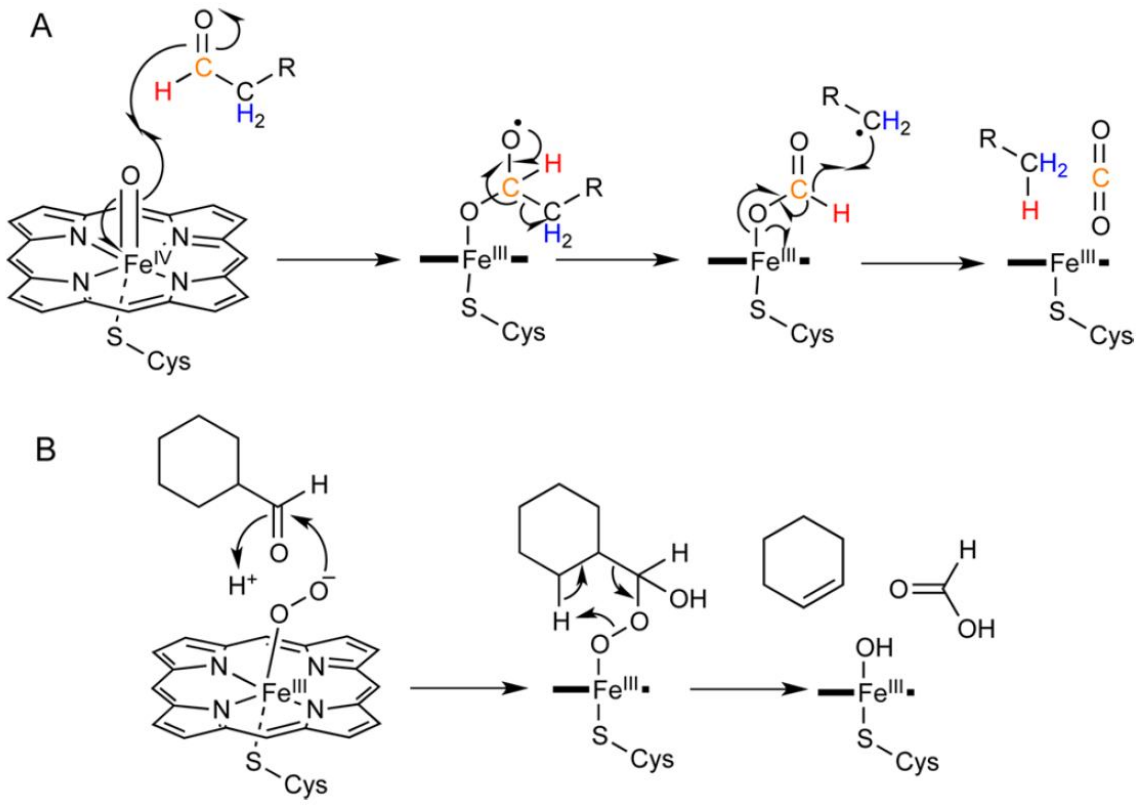

Figure 1.3 – Comparison of the deformylation reactions catalyzed by insect AD (CYP4G1) and CYP2B4. **A** – Deformylation of fatty aldehydes by the insect AD is proposed to start with the high-valent iron-oxo species and results in the formation of CO_2. The color-coding indicates positions in the substrate that have been isotopically-labeled to establish the mechanism. **B** - Decarbonylation of cyclohexanecarboxaldehyde by CYP2B4 is initiated by the iron peroxide species and results in the formation of cyclohexene and formic acid.

1.2.2 Plant Aldehyde Decarbonylase

Although alkane biosynthesis was first investigated in plants and green algae, these decarbonylases remain the least well-understood class, in large part because they are integral membrane proteins that are not highly expressed in native organisms and are hard to over-express and purify in expression organisms such as *E. coli* or yeast. Early experiments on crude microsomal preparations of pea leaves, *Pisum sativum*, and the green algae, *Botryococcus braunii*, demonstrated that these extracts were capable of

converting octadecanal to heptadecane.[19,28] A key finding was the demonstration, in experiments utilizing [1-^{3}H,1-^{14}C]octadecanal, that the carbonyl group was released as CO, which could be trapped by $RhClPh_3$.[28] The aldehyde hydrogen was, at least partly, transferred to the hydrocarbon as shown by the appearance of tritium in the heptadecane. The reaction required no additional cofactors and was inhibited by metal chelators, suggesting the enzymes were metallo-proteins.

Further purification of the decarbonylase from *B. braunii* (a technically challenging undertaking) yielded very small quantities of partially purified protein (a few tens of μg) but allowed some limited characterization of the algal enzyme.[33] The enzyme appeared to be membrane-associated with Mr ~ 66,000 Da, and a rather low specific activity: 3.5 nmol/min/mg. It was suggested on the basis of its UV-Visible spectrum, together with metal analysis, that it might contain a cobalt-porphyrin complex.[33] However, in the light of later genetic analyses discussed below, this appears most unlikely to be the case.

Genetic analysis has provided further insights into the plant decarbonylases. In land plants, very-long-chain alkanes are a major component of the waxy surface, known as the eceriferum, that cover the aerial organs and protect the plant against desiccation. Mutations or deletions in the *eceriferum* (or *cer*) genes result in a range of phenotypes including reduced hardiness to drought and reduced fertility, and have thus been studied quite extensively.[16,34] The aldehyde decarbonylase gene was identified as *cer1* through genetic studies in the model organism, *A. thaliana.*[25] The gene encodes a protein of 630 residues that is predicted to be an integral membrane protein and contains the "eight histidine" motif common to stearoyl desaturases and fatty acid hydroxylases.[35] These

latter enzymes are all integral-membrane, non-heme iron proteins, suggesting that Cer1 is likely also iron-dependent; however this has not been verified experimentally.

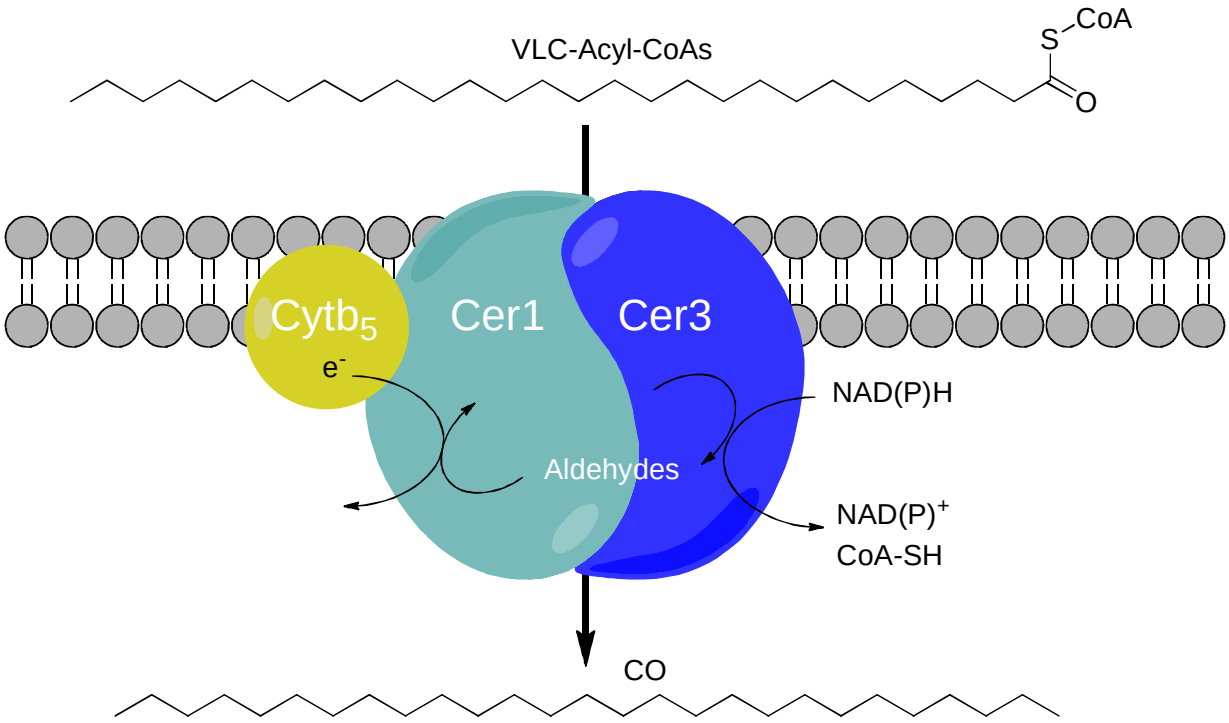

Figure 1.4 – The multi-enzyme complex comprising Cer1/Cer3/$Cytb_5$ that has been proposed to carry out the conversion of very long-chain acyl-CoA esters to alkanes and carbon monoxide in plants. Figure based on reference 38.

Confirmation that *cer1* actually encodes a decarbonylase has only recently been obtained, with the demonstration that heterologous expression of the gene in yeast results in the synthesis of small amounts of very long-chain alkanes, primarily 29 carbons in length.[36] However, to achieve this it was also necessary to introduce both the cognate acyl-CoA reductase, encoded by the *cer3* gene, and to introduce a mutated version of the yeast fatty acyl-CoA elongase component, Sur4, which allowed production of very long chain fatty acids (C28 and C30) that are not otherwise synthesized by yeast. *In vivo* protein:protein interaction screening indicated that Cer1 and Cer3 function as a complex in the membrane (Figure 1.4). The requirement for the mutant elongase component

further suggests that this complex is specific for very long chain acyl-CoA esters. Interestingly, the interaction screen also revealed an association between an endoplasmic reticulum-localized cytochrome b_5 isoform. The introduction of this cytochrome b_5 isoform into yeast enhanced Cer1/Cer3 alkane production, suggesting that cytochrome b_5 may be a cofactor for Cer1. Lastly, site-directed mutagenesis of the putative metal-binding histidine residues in Cer1 abolished alkane biosynthesis, demonstrating that they are essential for alkane synthesis.[36]

The reaction catalyzed by the plant AD enzymes remains the most enigmatic. With so little biochemical data on these enzymes, the mechanism of the reaction is hard to even guess at. Carbon monoxide-producing reactions are extremely rare in biology, and thus it is difficult to draw mechanistic comparisons with other enzymes. The observation that Cer1 is homolgous to stearoyl-CoA desaturase, together with its stimulation by cytochrome b_5, hints at the enzyme being iron and O_2-dependent, which would provide a common link to the insect and cyanobacterial enzymes. This raises the intriguing possibility that the plant decarbonylases may also employ a cryptic oxidation mechanism analogous to the cyanobacterial enzymes. It is, however, difficult to conceive of an oxygen-involving mechanism that would result in the formation of CO.

The non-enzymatic decarbonylation of aldehydes is catalyzed by a variety of transition metal complexes.[37] In particular, the decarbonylation of aldehydes by bi-dentate phosphine-ligated rhodium (I) complexes[38-40] has been studied in some detail. The reaction most likely occurs through the oxidative addition of the aldehyde to the metal to form a rhodium-formyl-hydride complex, followed by extrusion of CO, to yield a rhodium-alkyl-hydride complex, and lastly reductive elimination of the alkane.[39] The

only well-studied CO utilizing enzymes are carbon monoxide dehydrogenase (CODH) and carbon monoxide dehydrogenase–acetyl-CoA synthase (CODH-ACS). These enzymes are extremely oxygen sensitive (unlike aldehyde decarbonylases) and the coenzymes employed in these reactions are quite unlike the diiron center proposed for Cer1. The enzymes contain unique and complex metal clusters, in which CO is bound to either nickel ions that are part of modified iron-sulfur clusters, or a copper ion that is bound to molybdopterin though a bridging sulfide.[41] Whereas it seems highly unlikely that similar cofactors are contained within Cer1, it has been suggested that a di-nuclear nickel-iron center might function instead to catalyze decarbonylation chemistry in a manner analogous to that of the rhodium complex.[42]

The difficulties associated with expressing and purifying eukaryotic membrane proteins have hindered the mechanistic analysis of the insect and plant enzymes, although the recent reports of the cloning and recombinant expression of the *Drosophila* P450 enzyme in sf9 (insect gut) cell culture[43] and the *Arabidopis* enzyme (Cer 1) in yeast[36] hold out the prospect of being able to better characterize these enzymes in future. As such, the kinetics of the plant and insect enzymes have not been investigated, although the reported specific activity of the enzyme from algal preparations indicates that it is similarly slow.[33] The cyanobacterial enzyme being small, soluble, easily expressed and with the benefit of an x-ray structure, has so far been the subject of the most intense mechanistic interest and is the focus of this body of work.

1.2.3 Cyanobacterial Aldehyde Deformylating Oxygenase

The cyanobacterial pathway for alkane biosynthesis is the most recently discovered pathway,[24] and the only one for which, somewhat surprisingly, the acyl-CoA reductase and AD enzymes are soluble proteins. This fact has rendered the cyanobacterial enzyme more amenable to mechanistic analysis than the membrane-bound animal and plant decarbonylases. In the literature the cyanobacterial enzyme is referred to as either aldehyde decarbonylase (cAD) or, more recently, as aldehyde deformylating oxygenase (cADO),[44] which more accurately describes the reaction catalyzed by this enzyme. Although the biological functions of the hydrocarbon waxes produced by plants and animals are well understood, it is unclear why cyanobacteria biosynthesize these molecules, and indeed not all strains of cyanobacteria do. It was this latter observation that allowed the genes for alkane biosynthesis to be identified using a genomic subtraction approach to identify genes that were present in producing strains but absent in non-producers.[24]

cADO is the only decarbonylase for which x-ray structures are available.[45] The structure, shown in Figure 1.5 A, reveals it to be a member of the non-heme diiron family of oxygenases[42,46] exemplified by enzymes such as methane monooxygenase (MMO), class I ribonucleotide reductase, and fatty-acyl-ACP desaturase. The active site of the enzyme is housed within an antiparallel 4-helix bundle in which the two iron atoms are each coordinated by a histidine and two carboxylate ligands from the protein, shown in Figure 1.5 B. A further four α-helixes pack against the 4-helix bundle. One of the coordinating carboxylate ligands, Glu144, has been observed to perform a carboxylate shift, frequently observed in this family of enzymes, which allows for oxygen to bind the

diiron core.[30] The molecule of stearic acid frequently co-crystallized with cADO is thought to mimic the binding of the aldehyde substrate and suggests a substrate-binding pocket comprising a long hydrophobic channel that terminates at the diiron center.

Recently, our lab has produced novel crystal structures of wild-type (Wt) cADO, with and without iron bound, as well as the L194A mutant of cADO.[47] Co-crystallization of these enzymes with substrate analogs indicated multiple possible substrate binding conformations. Wt cADO was co-crystallized with two molecules of trans-2-nonylcyclopropane-1-carboxylic acid. In this structure, the first molecule lies adjacent to the active site and the diiron center, while the second molecule blocks the opening of the binding pocket with the polar head group exposed to solvent. The L194A mutant was co-crystallized with 11-(2-(2-ethoxyethoxy)ethoxy)undecanal partially occupying three different conformations in the hydrophobic channel. This structure confirms that the hydrophobic, substrate binding channel connects solvent to the buried active site and displays a distinct hydrogen bonding network indicative of a water channel. The metal free structure indicated that a conformational shift in a section of one of the primary α-helixes appears to act as a switch, becoming unstructured to allow for iron binding.[30,47]

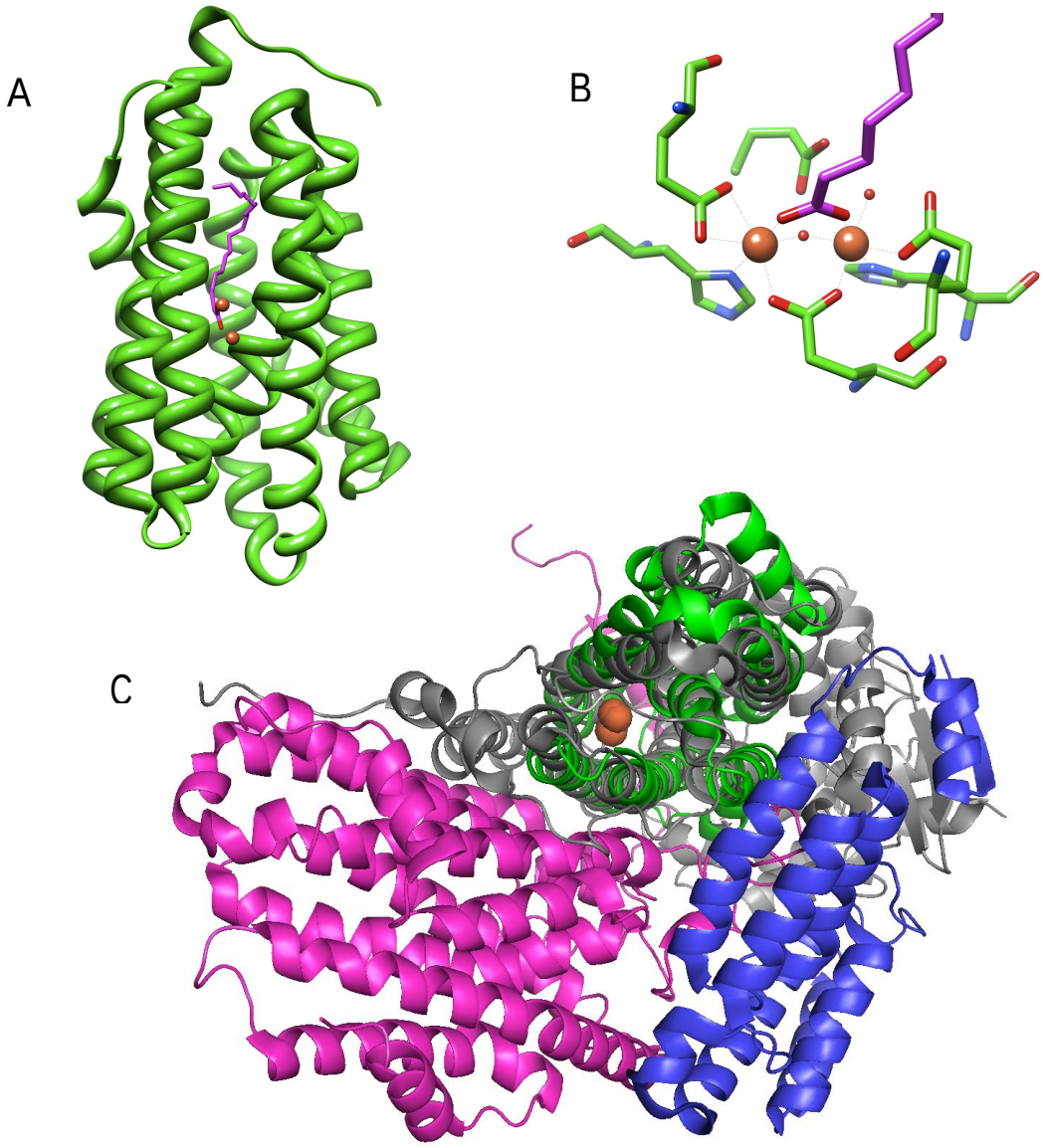

Figure 1.5 – A – Crystal structure of cADO (pdb 2OC5) from *P. marinus.* The iron atoms of the diiron center are shown in orange and the co-crystallized fatty acid is shown in purple. **B** – Detail of the active site of cADO showing the ligands to iron. **C** – Comparison of the structures of cADO and MMOH (pdb 1XVC). The structure of cADO, shown in green, is overlaid on the α subunit of MMOH, shown in gray. The additional β and γ subunits of MMOH are shown in pink and blue; the diiron centers of both enzymes closely overlay and are shown in orange. Figures 1.5 A and 1.5 B are based on reference 55.

Compared with other enzymes of this family, cADO presents a rather "minimalist" structure and the enzyme is much smaller (29 kDa monomer) than most other enzymes in this family. For example, the core structure of MMO, compared in Figure 1.5 C, is significantly larger (251 kDa $\alpha_2\beta_2\gamma_2$ homodimer) and the enzyme includes additional β and γ subunits that interact with the obligate reductase system (MMOR) as well as a regulatory component B (MMOB).[46,47] As discussed below, cADO similarly requires molecular oxygen and an external reducing system for activity, but proteins analogous to MMOR and MMOB, if they exist, have not yet been identified for this system.[48]

Our current understanding of the mechanism of cADO is drawn from a combination of isotopic labeling studies, reactions with radical clock substrate analogs, spectroscopic characterization by Mössbauer and EPR spectroscopy, and inferences based on its structural similarity to the MMO system. Initial studies established the conversion of aldehydes to alkanes required an external reducing system – either reduced ferredoxin or a chemical reducing system such as phenazine methosulfate (PMS)/NADH – to support activity.[27,48] In contrast to the insect or plant enzymes, the aldehyde carbon was shown to be converted to formate, rather than CO_2 or CO, in the reaction.[26,27] Deuterium labeling studies established that the aldehyde hydrogen was retained in formate, whereas the proton in the alkane derives from the solvent.[26,27] A key observation, based on $^{18}O_2$-labelling studies, was that one of the oxygen atoms in formate derives from molecular oxygen.[48] However, to accommodate the overall stoichiometry of the reaction it is necessary to invoke complete reduction of the oxygen consumed during turnover to give the equivalent of two molecules of water. In this respect cADO is

unique among iron oxygenases and the reaction has been referred to as a “cryptic” oxidation because the overall conversion of aldehyde to alkane + formate is redox neutral.

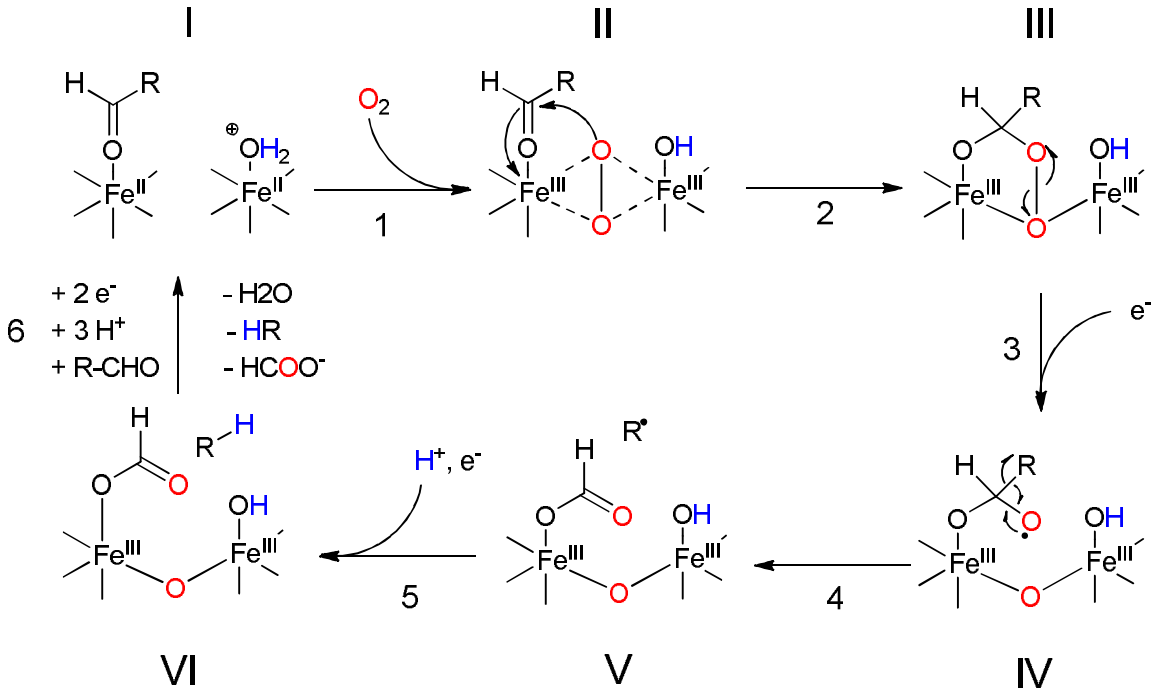

Figure 1.6 – Proposed mechanism for deformylation of aldehydes by cADO. The color-coding indicates the origins of oxygen atoms and protons in the products established by isotope-labeling.

Based on these observations, the mechanism shown in Figure 1.6 has been proposed that extrapolates from other, better-understood non-heme diiron oxygenases.[48] The reaction starts with the reduction of the diferric resting state of the enzyme to the active diferrous form that is able to bind molecular oxygen. It is hypothesized that oxygen forms an intermediate peroxo-bridged diiron core (P-type species), as has been observed in the MMO system. In the next step, the peroxo species undergoes nucleophilic addition to the aldehyde, forming a peroxy-hemiacetal intermediate. At this point it is necessary to invoke injection of a further electron into the active site that

results in breakdown of the peroxide and transiently generates a formyl radical. Fragmentation of this species results in homolytic cleavage of the carbon-carbon bond to produce a primary alkyl radical and formate as the co-product. Lastly, further reduction of the alkyl radical, possibly as a proton-coupled electron transfer reaction, results in formation of the alkane.

Support for a peroxy-hemiacetal species (intermediate III in Figure 1.6) comes from recent U.V.-Visible stopped-flow measurements and Mössbauer spectroscopy.[49] The formation of a $Fe_2^{III/III}$ bridged peroxide or peroxy-hemiacetal species was inferred from the appearance of a transient and characteristic band at 450 nm, whose appearance was dependent upon the presence of substrate. The freeze-quenched Mössbauer spectrum of this intermediate exhibited isomer shifts characteristic of a diferric core and consistent with the formation of a peroxy or peroxy-hemiacetal species. In the absence of external reductant the species was relatively stable, $t_{1/2}$ ~400 s; however upon addition of a stoichiometric amount of reduced O-methoxy-phenazine methyl sulfate (^{OMe}PMS) the intermediate rapidly decayed and resulted in ~0.50 equivalents of formate being produced. Reduction by ^{OMe}PMS resulted in the formation of an additional $Fe_2^{III/III}$ state distinct, as characterized by Mössbauer spectroscopy, from either the peroxy intermediate or the resting diferric enzyme, which likely reflects the presence of bound products.

Support for a radical mechanism for C-C bond scission (step 4 in Figure 1.6) comes from the reaction of cADO with aldehyde substrates containing either a strategically placed cyclopropyl or oxiranyl group that could act as a “radical clock”.[50,51] Cyclopropylcarbinyl and oxiranylcarbinyl radicals, formed when radicals are generated adjacent to a cyclopropyl or oxiranyl ring respectively, undergo very well characterized

ring-opening reactions and have been employed to investigate the reactions of many enzymes.[49,52-54] Cyclopropyl radical ring-opening rearrangements occur on a much faster timescale than their oxiranyl equivalents, allowing them to act as fast and slow radical clocks respectively.

When the cyclopropyl substrate was reacted with cADO only the rearranged alkene was observed as a product, indicating that an alkyl radical with a relatively long lifetime (> 10 ns) was formed as an intermediate.[50] Interestingly, the cyclopropyl aldehyde was found to partition approximately equally between turnover and acting as a mechanism-based inhibitor. Inactivation resulted from the covalent attachment of the alkyl chain to the enzyme through a phenylalanine residue that lines the substrate-binding channel. The modification was presumably a consequence of the cyclopropyl ring opening up, with the result that the repositioned alkyl radical could react with the protein.

Unlike the reaction with the cyclopropyl aldehyde, no covalent attachment and inhibition was observed in reactions with the oxiranyl aldehyde substrate and cADO. [51] Based on the partitioning between the rearranged (n-2 alkane) and un-rearanged (n-1 oxiranyl) products, the upper bound of the alkyl radical lifetime was estimated to be 100 μs. Therefore, the electron-proton transfer step occurs relatively fast, $k \sim 10^4 - 10^5\ s^{-1}$. This suggests the electron is transferred directly from a site on the protein rather than from the external reducing system, with the diiron center the most likely source of electrons. However the proton donor in the reaction remains unclear.

Most interestingly, it has recently been shown that cADO is capable of catalyzing other oxidative reactions.[53] The reactions of nonanal and decanal, which are very slow substrates, results in the formation of n-1 alcohols and aldehydes in addition to n-1

alkanes. These products may have been missed in previous studies because longer chain aldehydes typically used to assay the enzyme don't produce significant amounts of these side products. The oxygen in the alcohol was shown to derive from O_2, whereas the only C_1 product formed was formate. Intriguingly, simply incubating reduced cADO with alkanes or alcohols, in the absence of aldehydes, did not result in oxidation products. But when ^{13}C-labeled nonanol was incubated with the enzyme in the presence of unlabeled decanal ^{13}C-labeled nonanal was produced. These observations suggest the formation of a diffusible intermediate in the reaction, and to accommodate them a quite different mechanism for deformylation has been proposed (Figure 1.7).

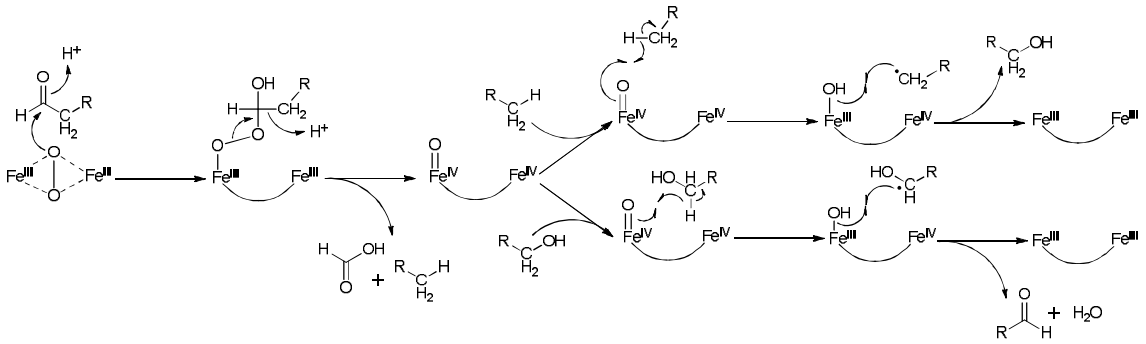

Figure 1.7 – Alternative carbanionic mechanism proposed for deformylation of aldehydes by cADO resulting in a reactive Fe^{IV} superoxo species capable of additional reactions producing n-1 alcohols and aldehydes.

The mechanism invokes heterolytic C-C bond cleavage to produce formate and a carbanion, which would be rapidly protonated, and a Fe^{IV} superoxo species. At this point the resulting alkane could undergo hydroxylation to give the n-1 alcohol, or alternatively diffuse from the enzyme. This would allow other alkanes or alcohols to enter the active site and be oxidized by the Fe^{IV} superoxo species. Although this mechanism accounts for the oxidation products observed with medium chain length aldehydes, it appears at odds

with the reductive homolytic bond cleavage previously proposed that is supported by the experiments discussed above, describing quite the mechanistic paradox.

The reaction catalyzed by cADO raises some intriguing mechanistic questions that are similar to those posed by the insect P450 AD, as the high-valent iron-oxo species formed by the non-heme diiron oxygenases are comparable in reactivity to those in P450 oxygenases. Thus, one likely fate of the aldehyde would be oxidation to a carboxylic acid through a mechanism analogous to alkane hydroxylation by MMOH. A further possibility would be oxidative deformylation to give formate and an alkene, as occurs in the aromatase reaction. Lastly, oxidative decarboxylation to give CO_2 and an alkane would also appear reasonable, given that this is the reaction catalyzed by the insect AD. Indeed, given the feasibility of this last reaction, it is all the more puzzling why the "cryptic" oxidation of aldehydes to alkanes would have evolved. How cADO discriminates against the many other potential oxidative pathways open to its substrates is one of the major challenges for understanding this enzyme.

cADO is the only decarbonylase for which the kinetics of the reaction have been investigated.[44,55,56] Kinetic analysis of the reaction is far from straightforward and is complicated by the very poor solubility of longer-chain aldehydes, and the requirement for an external reducing system. Nevertheless, it is clear that, in comparison with most enzymes, the reaction is extremely slow. Different laboratories have assayed the enzyme using different substrates, reducing agents and oxygen concentrations, making direct comparisons difficult, but the highest steady state turnover numbers reported are only about 1 min^{-1}. Given the interest in engineering this enzyme for use in biofuels

biosynthesis,[57,58] the reason why the reaction is so sluggish is of more than academic interest.

One should note that the extent to which the low activity measured *in vitro* represents the physiological activity of the enzyme *in vivo* is currently unclear. Cyanobacteria produce only low levels of hydrocarbons, the benefit of which to the organism, if any, is unknown, and the level at which cADO is expressed in cyanobacteria has not been reported. It is therefore quite possible that cADO may not be significantly more active *in vivo*. On the other hand, technical difficulties inherent to the assay, as discussed below, most likely contribute somewhat to the slow rates of turnover that have been reported.

In air-saturated buffer some amount of O_2 reacts non-enzymatically with the reducing system as both reduced ferredoxin and PMS are effective oxygen scavengers. This side reaction rapidly depletes both the reducing system and O_2 causing the enzyme-catalyzed reaction to cease after only a few turnovers. The total number of turnovers can be significantly increased by conducting the reaction at low oxygen concentrations, although under oxygen-limiting conditions the rate of reaction is several-fold slower.[55] An additional complication is that hydrogen peroxide generated by reaction of O_2 with the reducing system is an effective inhibitor of the enzyme ($K_i \sim 16\ \mu M$), further depressing turnover.[56] Addition of catalase was found to prolong the activity of cADO in the reaction, but it did not significantly increase the enzyme's specific activity.

Mechanistically, a more interesting reason for the enzyme's low activity is that additional protein cofactors may be necessary to activate it. One reason to suggest this is that in some mechanistically related enzymes, such as MMO, toluene monooxygenase,

and alkene monooxygenase, several additional subunits are required for activity.[47] The hydroxylase component of MMO (MMOH), for example, comprises an $\alpha_2\beta_2\gamma_2$-homodimer of Mr ~ 251 kDa. The β and γ subunits provide supporting protein architecture (Figure 1.5 C) that surrounds the catalytic α subunit and mediates interactions with the 39 kDa reductase component (MMOR) and an additional 16 kDa regulatory subunit, MMOB. This regulatory subunit, which is common to other enzymes in this group of oxygenases, dramatically alters the activity of the system by affecting a conformational change in the hydroxylase subunit.[59] MMOB binding results in up to a 1000-fold increase in activity.[46,47] The changes in structure are subtle and affect both the reduction potential of the iron center as well as the relative affinity of the enzyme for inhibitors and substrates.[59] It seems unlikely that cADO possesses additional tightly bound subunits analogous to the β and γ subunits of MMOH; if it did, the enzyme would probably not fold properly in their absence. However, a freely dissociable activating subunit, analogous to MMOB, seems at least a reasonable possibility.

Another possibility is that there is a specific, yet to be identified, reductase for the enzyme. Although ferredoxin supports activity, it interacts very weakly with cADO in comparison with most enzymes that use ferredoxin as a reductant. Moreover, cADO is unique in requiring additional electrons during the catalytic cycle, whereas in iron-oxygenase enzymes electrons are required only for initial reduction of the di-ferric resting state. The introduction of these additional electrons at the correct point in the catalytic cycle is crucial to the mechanism of deformylation as even pre-reduced enzyme will not turn over without the presence of the reducing system.[27] Thus a cADO-specific auxiliary

redox protein that could supply electrons at the right point in the catalytic cycle would be an appealing solution to this problem.

Lastly, several studies have sought to use cADO in metabolic engineering of hydrocarbon biosynthesis pathways.[24,45,57,58] So far the titres of alkanes produced have been modest, and it seems likely that this is at least in part due to the low actvity of cADO. However, there remains a distinct possibility that the deformylating activity of cADO may be an adventitious side reaction, and that the physiological role of the enzyme may involve a more conventional oxidation of an unknown substrate. In this context, the recent observation, albeit at very low activity, of n-1 alcohols and aldehydes derived from the reaction of C9 and C10 aldehydes is certainly intriguing.[53]

1.3 Goals

Over the last five years, previous studies by our lab, and others, have established a firm foundation from which we can investigate the mechanism of cADO. We know this non-heme diiron enzyme requires molecular oxygen and reducing equivalents to catalyze a radical-based aldehyde deformylation mechanism.[27,44,55,60,61] We know the rate constants for the formation of the key peroxy-hemiacetal intermediate,[62] as well as the lifetime of the radical species,[50,51] and that cADO is capable of a turnover rate with an upper limit of ~1 min^{-1}.[27,55] However, not only have these studies failed to answer a number of the basic questions surrounding this system including "What is the rate determining step?," they have in fact raised new ones such as "Why is the enzyme so slow when each of the chemical steps are relatively quick?" These questions have

implications both for the understanding of the unusual chemistry catalyzed by cADO as well as its future application towards sustainable drop-in biofuel production.

The research described in this thesis seeks to provide answers to these questions and others by continuing to explore the mechanistic underpinnings of cADO. First, in chapter 2, the final alkyl radical protonation, step 5 in Figure 1.6, was probed through the use of solvent isotope effects (SIEs). The proton donor was identified through the observation of an equilibrium isotope effect (EIE) on V/K. These experiments not only suggest proton transfer is not rate limiting, but that there may be a non-chemical RDS. Next, substrate analogs and binding pocket mutations were used in chapter 3 to investigate substrate binding and/or product release acting as a non-chemical rate limiting step. Although this could not be determined, insight was gained into the hydrophobic effects governing substrate specificity and the hydrophobic pocket was observed to be significant in substrate binding. Finally, the protein film voltammetry (PFV) experiments described in chapter 4 were used to explore the electrochemical nature of cADO and determine its reduction potential. Most interestingly, two separate catalytic signals were observed using cyclic voltammetry indicating an alternative pathway leading to a futile peroxide shunt. This work serves to expand our mechanistic understanding of cADO to include a branched pathway resulting in a partitioning effect that suggests a possible solution to the question of why the alkane forming activity is so slow.

1.4 References

(1) United Nations Department of Economic and Social Affairs/Population Division. *World Population Prospects The 2010 Revision Volume I: Comprehensive Tables*, United Nations, 2011.

(2) Meehl, G. A., T.F. Stocker, W.D. Collins, P. Friedlingstein, A.T. Gaye, J.M. Gregory, A. Kitoh, R. Knutti, J.M. Murphy, A. Noda, S.C.B. Raper,; I.G. Watterson, A. J. W. a. Z.-C. Z. (2007) *Global Climate Projections in Climate Change 2007: The Physical Science Basis. Contribution of Working Group I to the Fourth Assessment Report of the Intergovernmental Panel on Climate Change*.

(3) Esa Vakkilainen, K. K., Jussi Heinimö *Large Industrial Users of Energy Biomass*, Lappeenranta University of Technology, 2013.

(4) Farrell, A. E.; Plevin, R. J.; Turner, B. T.; Jones, A. D.; O'Hare, M.; Kammen, D. M. (2006) Ethanol can contribute to energy and environmental goals, *Science*, *311*, 506.

(5) Somerville, C.; Youngs, H.; Taylor, C.; Davis, S. C.; Long, S. P. (2010) Feedstocks for Lignocellulosic Biofuels, *Science*, *329*, 790.

(6) Kumar, R., Singh, S., and Singh, O. V. J. (2008) Bioconversion of lignocellulosic biomass: biochemical and molecular perspectives, *J. Ind. Microbiol. Biotechnol.*, *35*, 377.

(7) Wargacki, A. J.; Leonard, E.; Win, M. N.; Regitsky, D. D.; Santos, C. N.; Kim, P. B.; Cooper, S. R.; Raisner, R. M.; Herman, A.; Sivitz, A. B.; Lakshmanaswamy, A.; Kashiyama, Y.; Baker, D.; Yoshikuni, Y. (2012) An engineered microbial platform for direct biofuel production from brown macroalgae, *Science*, *335*, 308.

(8) Zhang, F.; Rodriguez, S.; Keasling, J. D. (2011) Metabolic engineering of microbial pathways for advanced biofuels production, *Curr Opin Biotechnol*, *22*, 775.

(9) Rosenberg, J. N., Oyler, G. A., Wilkinson, L., and Betenbaugh, M. J. (2008) A green light for engineered algae: redirecting metabolism to fuel a biotechnology revolution, *Curr. Opin. Biotechnol.*, *19*, 430.

(10) Ghim, C. M.; Kim, T.; Mitchell, R. J.; Lee, S. K. (2010) Synthetic Biology for Biofuels: Building Designer Microbes from the Scratch, *Biotechnol. Bioprocess Eng.*, *15*, 11.

(11) Buist, P. H. (2007) Exotic biomodification of fatty acids, *Natural Product Reports*, *24*, 1110.

(12) Cheesbrough, T. M.; Kolattukudy, P. E. (1988) Microsomal Preparation from an Animal Tissue Catalyzes Release of Carbon-Monoxide from a Fatty Aldehyde to Generate an Alkane, *J. Biol. Chem.*, *263*, 2738.

(13) Howard, R. W.; Blomquist, G. J. (2005) Ecological, behavioral, and biochemical aspects of insect hydrocarbons, *Annu. rev. entomology*, *50*, 371.

(14) Bernard, A.; Joubes, J. (2013) Arabidopsis cuticular waxes: advances in synthesis, export and regulation, *Prog Lipid Res*, *52*, 110.

(15) Ladygina, N.; Dedyukhina, E. G.; Vainshtein, M. B. (2006) A review on microbial synthesis of hydrocarbons, *Process Biochem.*, *41*, 1001.

(16) Bernard, A.; Joubes, J. (2013) Arabidopsis cuticular waxes: Advances in synthesis, export and regulation, *Prog Lipid Res*, *52*, 110.
(17) Howard, R. W.; Blomquist, G. J. In *Ann Rev Entomology* 2005; Vol. 50, p 371.
(18) Yoder, J. A.; Denlinger, D. L.; Dennis, M. W.; Kolattukudy, P. E. (1992) Enhancement of Diapausing Flesh Fly Puparia with Additional Hydrocarbons and Evidence for Alkane Biosynthesis by a Decarbonylation Mechanism, *Insect Biochemistry and Molecular Biology*, *22*, 237.
(19) Dennis, M. W.; Kolattukudy, P. E. (1991) Alkane Biosynthesis by Decarbonylation of Aldehyde Catalyzed by a Microsomal Preparation from Botryococcus-Braunii, *Arch Biochem Biophys*, *287*, 268.
(20) Wolf, F. R. (1983) BOTRYOCOCCUS-BRAUNII - AN UNUSUAL HYDROCARBON-PRODUCING ALGA, *Biotechnol. Appl. Biochem*, *8*, 249.
(21) Kolattukudy. P.E (1970) Plant Waxes, *Lipids*, *5*, 259.
(22) Qiu, Y.; Tittiger, C.; Wicker-Thomas, C.; Le Goff, G.; Young, S.; Wajnberg, E.; Fricaux, T.; Taquet, N.; Blomquist, G. J.; Feyereisen, R. (2012) An insect-specific P450 oxidative decarbonylase for cuticular hydrocarbon biosynthesis, *Proc. Natl. Acad. USA*, *109*, 14858.
(23) Reed, J. R.; Vanderwel, D.; Choi, S. W.; Pomonis, J. G.; Reitz, R. C.; Blomquist, G. J. (1994) Unusual mechanism of hydrocarbon formation in the housefly - cytochrome-P450 converts aldehyde to the sex-pheromone component (Z)-9-tricosene and CO_2, *Proc. Natl. Acad. USA*, *91*, 10000.
(24) Schirmer, A.; Rude, M. A.; Li, X. Z.; Popova, E.; del Cardayre, S. B. (2010) Microbial Biosynthesis of Alkanes, *Science*, *329*, 559.
(25) Aarts, M. G. M.; Keijzer, C. J.; Stiekema, W. J.; Pereira, A. (1995) Molecular characterization of the CER1 gene of arabidopsis involved in epicuticular wax biosynthesis and pollen fertility, *Plant Cell*, *7*, 2115.
(26) Warui, D. M.; Li, N.; Norgaard, H.; Krebs, C.; Bollinger, J. M.; Booker, S. J. (2011) Detection of Formate, Rather than Carbon Monoxide, As the Stoichiometric Coproduct in Conversion of Fatty Aldehydes to Alkanes by a Cyanobacterial Aldehyde Decarbonylase, *J. Am. Chem. Soc.*, *133*, 3316.
(27) Das, D.; Eser, B. E.; Han, J.; Sciore, A.; Marsh, E. N. G. (2011) Oxygen-independent decarbonylation of aldehydes by cyano-bacterial aldehyde decarbonylase: a new reaction of di-iron enzymes, *Angew. Chem.*, *50*, 7148.
(28) Cheesbrough, T. M.; Kolattukudy, P. E. (1984) Alkane Biosynthesis by Decarbonylation of Aldehydes Catalyzed by a Particulate Preparation from Pisum-Sativum, *Proc. Natl. Acad. USA -Biological Sciences*, *81*, 6613.
(29) Souda, P.; Ryan, C. M.; Cramer, W. A.; Whitelegge, J. (2011) Profiling of integral membrane proteins and their post translational modifications using high-resolution mass spectrometry, *Methods*, *55*, 330.
(30) Jia, C.; Li, M.; Li, J.; Zhang, J.; Zhang, H.; Cao, P.; Pan, X.; Lu, X.; Chang, W. (2015) Structural insights into the catalytic mechanism of aldehyde-deformylating oxygenases, *Protein & cell*, *6*, 55.
(31) Meunier, B.; de Visser, S. P.; Shaik, S. (2004) Mechanism of oxidation reactions catalyzed by cytochrome P450 enzymes, *Chem Rev*, *104*, 3947.

(32) Newcomb, M.; Hollenberg, P. F.; Coon, M. J. (2003) Multiple mechanisms and multiple oxidants in P450-catalyzed hydroxylations, *Archf Biochem Biophys*, *409*, 72.
(33) Dennis, M.; Kolattukudy, P. E. (1992) A Cobalt-Porphyrin Enzyme Converts a Fatty Aldehyde to a Hydrocarbon and Co, *Proc. Natl. Acad. USA*, *89*, 5306.
(34) Kunst, L.; Samuels, A. L. (2003) Biosynthesis and secretion of plant cuticular wax, *Progress in Lipid Research*, *42*, 51.
(35) Shanklin, J.; Whittle, E.; Fox, B. G. (1994) 8 Histidine-Residues Are Catalytically Essential in a Membrane-Associated Iron Enzyme, Stearoyl-Coa Desaturase, and Are Conserved in Alkane Hydroxylase and Xylene Monooxygenase, *Biochemistry*, *33*, 12787.
(36) Bernard, A.; Domergue, F.; Pascal, S.; Jetter, R.; Renne, C.; Faure, J.-D.; Haslam, R. P.; Napier, J. A.; Lessire, R.; Joubes, J. (2012) Reconstitution of Plant Alkane Biosynthesis in Yeast Demonstrates That Arabidopsis ECERIFERUM1 and ECERIFERUM3 Are Core Components of a Very-Long-Chain Alkane Synthesis Complex, *Plant Cell*, *24*, 3106.
(37) Modak, A.; Deb, A.; Patra, T.; Rana, S.; Maity, S.; Maiti, D. (2012) A general and efficient aldehyde decarbonylation reaction by using a palladium catalyst, *Chem Commun*, *48*, 4253.
(38) Doughty, D. H.; Pignolet, L. H. (1978) Catalytic decarbonylation of aldehydes, *J. Am. Chem. Soc.*, *100*.
(39) Fristrup, P.; Kreis, M.; Palmelund, A.; Norrby, P.-O.; Madsen, R. (2008) The mechanism for the rhodium-catalyzed decarbonylation of aldehydes: A combined experimental and theoretical study, *J. Am. Chem. Soc.*, *130*, 5206.
(40) Patra, T.; Manna, S.; Maiti, D. (2011) Metal-Mediated Deformylation Reactions: Synthetic and Biological Avenues, *Angew Chemie-Int Ed*, *50*, 12140.
(41) Ragsdale, S. W. (2006) Metals and their scaffolds to promote difficult enzymatic reactions, *Chem. Rev.*, *106*, 2217.
(42) Krebs, C.; Bollinger, J. M., Jr.; Booker, S. J. (2011) Cyanobacterial alkane biosynthesis further expands the catalytic repertoire of the ferritin-like 'di-iron-carboxylate' proteins, *Curr Opin Chem Biol*, *15*, 291.
(43) Qui, Y.; Tittiger, C.; Wicker-Thomas, C.; Le Goff, G.; Young, S.; Wajnberg, E.; Fricaux, T.; Taquet, N.; Blomquist, G. J.; Feyereisen, R. (2012) An insect-specific P450 oxidative decarbonylase for cuticular hydrocarbon biosynthesis, *Proc. Natl. Acad. Sci. (USA)*, *109*, 14858
(44) Li, N.; Chang, W.-C.; Warui, D. M.; Booker, S. J.; Krebs, C.; Bollinger, J. M. (2012) Evidence for Only Oxygenative Cleavage of Aldehydes to Alk(a/e)nes and Formate by Cyanobacterial "Aldehyde Decarbonylase", *Biochemistry*, *51,7908-7916*.
(45) Khara, B.; Menon, N.; Levy, C.; Mansell, D.; Das, D.; Marsh, E. N. G.; Leys, D.; Scrutton, N. S. (2013) Production of propane and other short-chain alkanes by structure-based engineering of ligand specificity in aldehyde-deformylating oxygenase, *Chembiochem*, *14*, 1204.
(46) Wallar, B. J.; Lipscomb, J. D. (1996) Dioxygen activation by enzymes containing binuclear non-heme iron clusters, *Chem Rev*, *96*, 2625.

(47) Buer, B. C.; Paul, B.; Das, D.; Stuckey, J. A.; Marsh, E. N. (2014) Insights into substrate and metal binding from the crystal structure of cyanobacterial aldehyde deformylating oxygenase with substrate bound, *ACS chem biol*, *9*, 2584.
(48) Li, N.; Norgaard, H.; Warui, D. M.; Booker, S. J.; Krebs, C.; Bollinger, J. M. (2011) Conversion of fatty aldehydes to alka(e)nes and foramte by a cyanobacterial aldehyde decarbonylase: crypric redox by an unusual dimetal oxygenase, *J. Am. Chem. Soc.*, *133*, 7148.
(49) Itzel, H., and Fischer, H. (1976) Electron spin resonance of oxiranyl radicals in solution: configurational stabilities and rearrangement reactions., *Helv. Chim. Acta*, *59*, 880−901.
(50) Paul, B.; Das, D.; Ellington, B.; Marsh, E. N. G. (2013) Probing the Mechanism of Cyanobacterial Aldehyde Decarbonylase Using a Cyclopropyl Aldehyde, *J. Am. Chem. Soc.*, *135*, 5234.
(51) Das, D.; Ellington, B.; Paul, B.; Marsh, E. N. (2014) Mechanistic insights from reaction of alpha-oxiranyl-aldehydes with cyanobacterial aldehyde deformylating oxygenase, *ACS chem biol*, *9*, 570.
(52) Newcomb, M.; Toy, P. H. (2000) Hypersensitive radical probes and the mechanisms of cytochrome P450-catalyzed hydroxylation reactions, *Accounts of Chem Res*, *33*, 449.
(53) Suda, K., Kikkawa, T., Nakajima, S., and Takanami, T. (2004) Highly regio- and stereoselective rearrangement of epoxides to aldehydes catalyzed by high-valent metalloporphyrin complex, Cr-(TPP)OTf, *J. Am. Chem. Soc.*, *126*, 9554−9555.
(54) Padwa, A., and Das, N. C. (1969) Oxirane radicals. The thermal decomposition of t-butyl cis- and trans-α,β-6-diphenylperglycidates., *J. Org. Chem.*, *34*, 816−821.
(55) Eser, B. E.; Das, D.; Han, J.; Jones, P. R.; Marsh, E. N. G. (2011) Oxygen-Independent Alkane Formation by Non-Heme Iron-Dependent Cyanobacterial Aldehyde Decarbonylase: Investigation of Kinetics and Requirement for an External Electron Donor, *Biochemistry*, *50*, 10743.
(56) Andre, C.; Kim, S. W.; Yu, X.-H.; Shanklin, J. (2013) Fusing catalase to an alkane-producing enzyme maintains enzymatic activity by converting the inhibitory byproduct H2O2 to the cosubstrate O-2, *Proc. Natl. Acad. Sci. USA*, *110*, 3191.
(57) Akhtar, M. K.; Turner, N. J.; Jones, P. R. (2013) Carboxylic acid reductase is a versatile enzyme for the conversion of fatty acids into fuels and chemical commodities, *Proc. Natl. Acad. Sci. USA*, *110*, 87.
(58) Howard, T. P.; Middelhaufe, S.; Moore, K.; Edner, C.; Kolak, D. M.; Taylor, G. N.; Parker, D. A.; Lee, R.; Smirnoff, N.; Aves, S. J.; Love, J. (2013) Synthesis of customized petroleum-replica fuel molecules by targeted modification of free fatty acid pools in Escherichia coli, *Proc. Natl. Acad. Sci. USA*, *110*, 7636.
(59) Lee, S. J.; McCormick, M. S.; Lippard, S. J.; Cho, U. S. (2013) Control of substrate access to the active site in methane monooxygenase, *Nature*, *494*, 380.
(60) Li, N.; Norgaard, H.; Warui, D. M.; Booker, S. J.; Krebs, C.; Bollinger, J. M. (2011) Conversion of fatty aldehydes to alka(e)nes and foramte by a

cyanobacterial aldehyde decarbonylase: crypric redox by an unusual dimetal oxygenase, *J. Am. Chem. Soc.*, *133*, 7148.

(61) Warui, D. M.; Li, N.; Norgaard, H.; Krebs, C.; Bollinger, J. M.; Booker, S. J. (2011) Detection of Formate, Rather than Carbon Monoxide, As the Stoichiometric Coproduct in Conversion of Fatty Aldehydes to Alkanes by a Cyanobacterial Aldehyde Decarbonylase, *J. Am. Chem. Soc.*, *133*, 3316.

(62) Pandelia, M. E.; Li, N.; Norgaard, H.; Warui, D. M.; Rajakovich, L. J.; Chang, W. C.; Booker, S. J.; Krebs, C.; Bollinger, J. M., Jr. (2013) Substrate-triggered addition of dioxygen to the diferrous cofactor of aldehyde-deformylating oxygenase to form a diferric-peroxide intermediate, *J Am Chem Soc*, *135*, 15801.

Chapter 2 Equilibrium Solvent Isotope Effects

2.1 Introduction

Aldehyde decarbonylases[1] (ADs) have attracted interest in the search for sustainable, drop-in biofuels because of their ability to produce long chain alkanes. Over the last five years, since Shirmer et al first identified the cyanobacterial alkane producing enzyme, cADO has become the most widely studied AD because, unlike the insect or plant ADs, it is a small, stable, soluble protein. Investigations of cADO have elucidated several key steps in the proposed mechanism, shown in Figure 2.1, however despite these efforts it remains unclear which step(s) in the mechanism are rate limiting.

In the proposed mechanism, an initial two-electron reduction of the resting diferric state to the active diferrous state (species I) initiates the reaction between cADO and molecular oxygen.[2,3] This forms an intermediate peroxo-bridged diiron core (species II). Next, nucleophilic addition to the aldehyde substrate results in the formation of a peroxy-hemiacetal intermediate (species III).[4] Addition of an electron results in breakdown of this intermediate, possibly through the formation of a transient formyl radical (species IV) that undergoes homolytic cleavage of the C_1-C_2 aldehyde bond, resulting in the formation of a primary alkyl radical and formate (species V).[5] Finally,

the alkyl radical is reduced to an alkane by electron-proton transfer (EPT) and the products are released from the enzyme (steps 5 and 6).

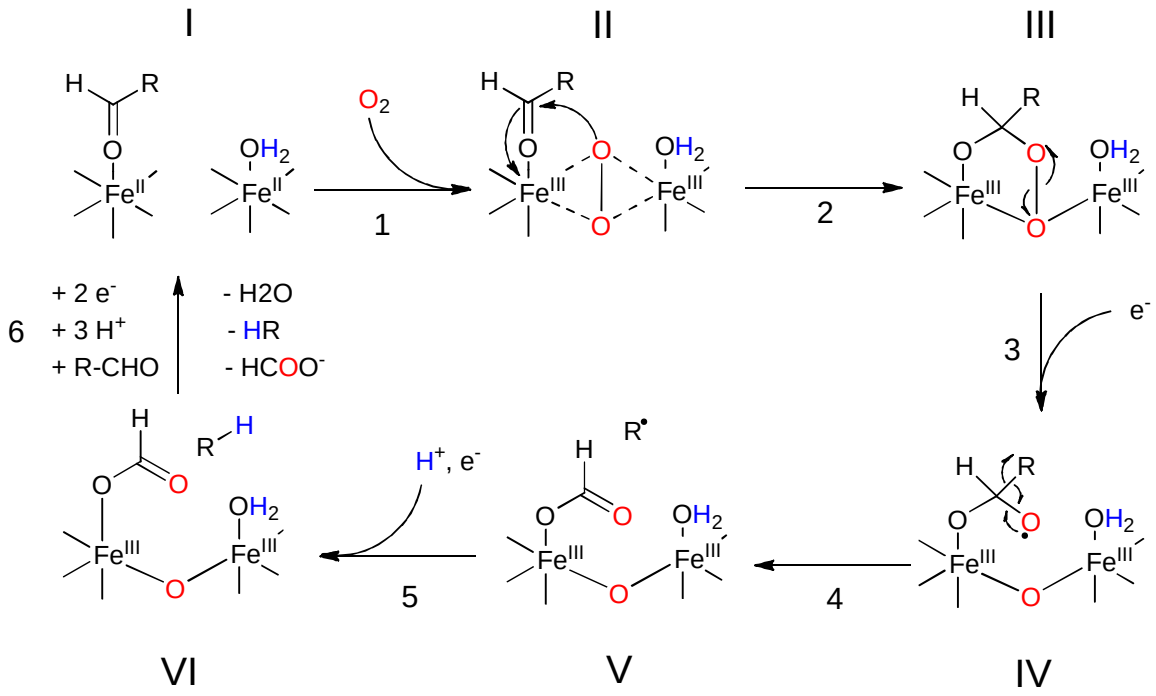

Figure 2.1 – Proposed mechanism for deformylation of aldehydes by cADO. The color-coding indicates the origin of the oxygen atoms and the protons in the product.

Experimental evidence supporting this mechanism comes from labeling studies indicating that the aldehyde proton is retained in formate whereas the alkane proton is derived from the solvent or an exchangeable site on the enzyme, [6,7] and that one atom of O_2 is retained in formate.[2,3] Recent spectroscopic evidence supports the formation of a peroxy-hemiacetal intermediate (species III) and its breakdown upon addition of exogenous reductant.[4] Recently, our laboratory has used both cyclopropyl- and oxiranyl-aldehydes designed to function as radical clocks to support a radical mechanism for C-C bond scission. From these experiments the lifetime of the alkyl radical was estimated to be in the region of 10 – 100 μs, implying that the EPT step occurs relatively

fast, k ~10^4 – 10^5 s^{-1}. [5,8] This suggests the electron is transferred directly from a site on the protein rather than from the external reducing system, with the diiron center the most likely source of electrons. However the proton donor in the reaction remains unclear.

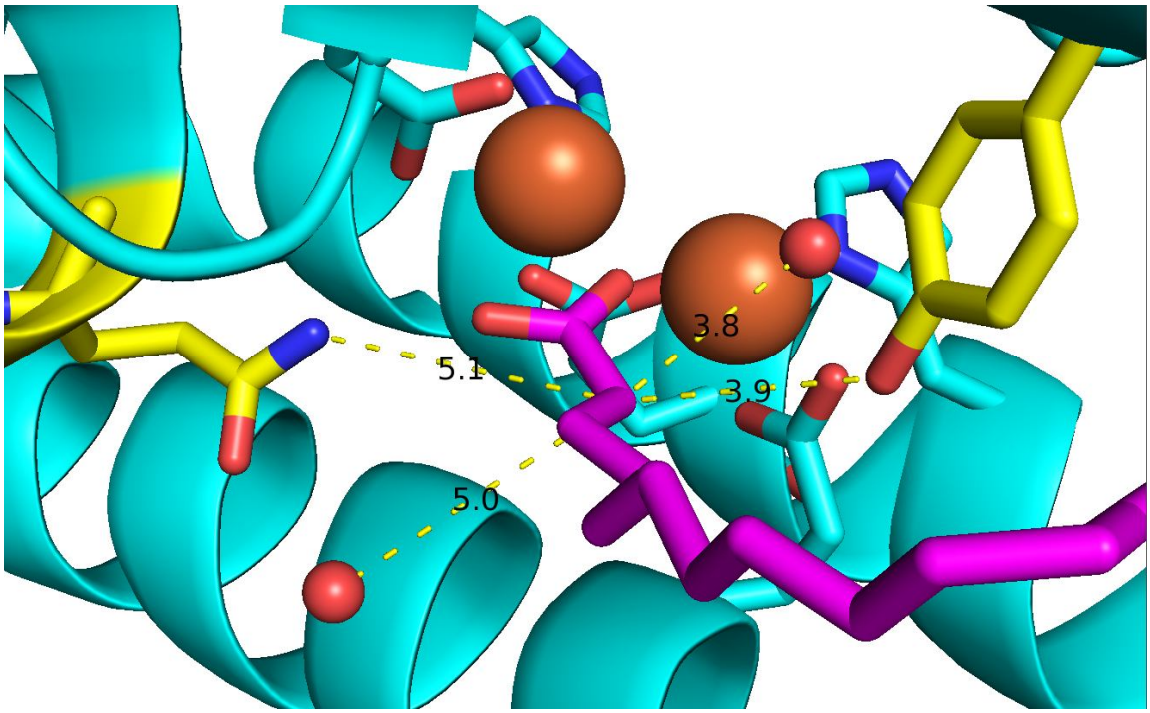

Figure 2.2 – Crystal structure of cADO with stearate (purple) bound (2OC5). Possible proton donors within ~5Å of the C_α in the active site are Gln123 and Tyr135 in yellow, or the two water molecules shown as red spheres. The diiron core is orange.

The crystal structures of wild-type cADO and two mutant forms have been determined with aliphatic carboxylic acids bound to the diiron center.[9] The carboxylic acid side chain occupies a hydrophobic channel leading from the metal center and likely closely mimics the binding of the aldehyde substrate. Close inspection of the structure of cADO with stearate bound reveals a network of hydrogen bonding residues and water molecules that leads from the exterior of the enzyme to the active site. This suggests a potential route by which the solvent derived proton transferred to the alkane gains access

to the active site. As shown in Figure 2.2, there are four potential proton-donating groups within 5Å of the α-carbon of stearate (corresponding to the carbon atom that would be the site of protonation in the reaction). These are the side chains of Gln123 and Tyr135, an iron-bound water, and a water molecule hydrogen-bonded to Gln123.

This chapter describes a series of solvent isotope effect (SIE) studies, which I undertook in order to further investigate the nature of the proton transfer step. SIEs are informative in identifying proton donors in enzymatic reactions if the donating group has an unusual fractionation factor and may also inform on the nature of the rate-determining step.

The work described in this chapter has been published as: Waugh, M. W., Marsh, E. N. G. M. (2014) Solvent Isotope Effects on Alkane Formation by Cyanobacterial Aldehyde Deformylating Oxygenase and Their Mechanistic Implications, *Biochemsitry*, 53, 5537-5543.

2.2 Materials and Methods

2.2.1 Materials

Recombinant cADO from *P. marinus* MIT9313 in a pET-28b(+) plasmid was expressed in BL21(DE3) *E. coli* for 12 h at 37^{o}C and purified by standard Ni-affinity chromatography using a 5 mL His-trap column in 100 mM HEPES, 100 mM KCl, and 10% glycerol at pH 7.2, as previously described.[6] After dialysis to remove immidazole to below 0.5 nM, enzyme was quantified by UV-vis spectroscopy using ε = 19.9 mM at A_{280}. Enzyme was loaded with Fe^{II} by anaerobic incubation with 10x ferrous ammonium

sulfate, and subsequently desalted using a 2 mL spin desalting column. The enzyme was quantified again and aliquoted for storage at -80^{o}C.

The His-Trap HP (5 ml) Ni-affinity column was obtained from GE Healthcare. Spin desalting columns were from Thermo Scientific. Octadecanal, heptanal, heptadecane, hexane, phenazine methosulfate (PMS), ferrous ammonium sulfate, NADH, and deuterium oxide were obtained from Acros Organics. 2xYT media, IPTG, kanamycin, potassium chloride and HEPES salts were from Fisher Chemicals.

2.2.2 Preparation of Deuterated Buffer

HEPES buffer was dissolved in 99.8% D_2O and lyophilized, twice, to produce deuterated HEPES (D-HEPES). Deuterated cADO assay buffer was prepared in 99.8% D_2O with 100 mM D-HEPES, pD 6.8, and 100 mM KCl. Proteated and deuterated buffers were purged with nitrogen for 2 hours before being transferred to an anaerobic chamber (Coy Laboratory Products Inc., Grass Lake, Mi), where they were allowed to equilibrate for at least a half hour before use. Mixed D_2O/H_2O buffers were prepared at various mole fractions by combining deuterated and proteated buffers to the desired ratios, differences in molar volumes between H_2O and D_2O were accounted for using the values of 18.126 mL/mol and 18.058 mL/mol respectively.[10] The mole fraction of D_2O in each assay was re-calculated to account for the isotopic purity of the D_2O and the addition of enzyme from stock solution in proteated buffer. The buffers were brought to pL 6.8 using the equation $pL = pH_{obs} + 0.311x + 0.0766x^2$ where x is the mole fraction of deuterium.[11]

2.2.3 Enzyme Assays

All assays were performed under microaerobic conditions in an anaerobic chamber under an atmosphere of 3% hydrogen: 97% nitrogen, O_2 < 20 ppm. Standard assay conditions include 10 µM Fe^{II} loaded cADO, 100 µM PMS, 1 mM NADH, and 300 µM substrate with a total assay volume of 500 µL in either 100 mM HEPES or D-HEPES buffer containing 100 mM KCl. All assays were initiated by addition of substrate and shaken at 37 ^{o}C.

We note the removing the tubes from the chamber allows the slow diffusion of O_2 into the sealed tubes so that the concentraton of oxygen is certainly significantly higher than 20 ppm (equivalent to ~26 nM dissolved O_2). However, as the enzyme turns over very slowly, the low O_2 concentration` does not appear to limit the overall rate of the reaction and minimizes side reactions that deplete the auxiliary reducing system, the products of which appear to inhibit the enzyme.

Assays containing octadecanal were performed in triplicate in 2 mL Eppendorf tubes for varying lengths of time. Octadecanal stocks solution were made up in DMSO and dissolved at 70 ^{o}C; the final concentration of DMSO in the assay was 2%. Assays were quenched with 500 µL of ethyl acetate, vortexed, and centrifuged to extract the heptadecane product to the organic layer, which was then combined with a tridecane internal standard for GC-MS analysis.

Assays containing heptanal were performed similarly to those described above except that 1.5 mL gas tight vials were substituted for Eppendorf tubes. At the end of the reaction period, the vials were shaken vigorously for 3 min to volatilize the hexane product. A gas tight syringe was used to extract 250 µL of headspace, which was

analyzed by GC-MS to quantify the total ion counts of labeled and unlabelled hexane produced.

2.2.4 Quantification of Hydrocarbon Products by GC-MS

Quantification of hydrocarbon products was performed using a Shimadzu QP-2010 GC-MS equipped with a DB-5 column (30 m x 0.25 mm x 0.25 µm). During heptadecane quantification the flow rate of helium carrier gas was 1.0 mL/min with an injection temperature of 200 ^{o}C. 8 µL of sample was injected in splitless mode. Initial temperature was held at 70^{o}C for 2 min, increased to 320 ^{o}C at a rate of 20 ^{o}C/min, and then maintained at 320^{o}C for 2 min. The interface temperature for the MS was 250 ^{o}C and the solvent cut time was 4.5 min. Heptadecane eluted between 8.9 and 9.1 min and concentration was determined using a calibration curve of heptadecane standards prepared in ethyl acetate.

For hexane quantification the flow rate of helium carrier gas was 24.0 mL/min with an injection temperature of 200.0 ^{o}C. 250 µL aliquots of gas were manually injected in splitless mode. Initial temperature was held at 70.0 ^{o}C for 2 min, increased to 275 ^{o}C at a rate of 20.0 ^{o}C/min, and then maintained at 275 ^{o}C for 1.75 min. The interface temperature for the MS was 250 ^{o}C and the solvent cut time was 4 min. Hexane eluted between 1.73 min and 1.98 min. Total ion counts for 86 and 87 amu, corresponding to the molecular ion peaks for proteated and deuterated hexane respectively, were generated for each sample and corrected for instrument background as well as natural ^{13}C isotope abundance. Chromatographic data were analyzed by Shimadzu GC-MS solution software.

2.3 Results and Discussion

Various assay conditions have been reported in mechanistic investigations of cADO.[6,7,12-14] Although the enzyme requires oxygen, in air-saturated buffer we have found that only 1-2 equivalents of product are formed, relatively rapidly, before the reaction nearly ceases. This is thought to be due to the auxiliary reducing system, which is necessary to supply the electrons needed in the reaction, but which also efficiently reacting with oxygen. This side reaction depletes the reducing system and produces H_2O_2 as a byproduct that has been shown to inhibit cADO.[13] However, at low oxygen concentrations, that have been termed microaerobic conditions, we have consistently found that the enzyme achieves multiple turnovers with the reaction rate remaining linear for several hours. For steady state kinetic measurements, it is, of course, necessary to take measurements over multiple turnovers, and therefore, we employed microaerobic conditions, as described in Materials and Methods, for these experiments.

2.3.1 Dependence of Rate on pL

SIEs can be a function of pL (L = H or D) because of kinetically significant ionizations of protic positions in the enzyme or substrate.[10] Therefore, we initially investigated the rate of reaction as a function of pL in H_2O and D_2O, both to determine the optimal pL for SIE measurements and to examine whether any isotope-dependent shift in activity was observed. cADO was assayed in proteated and deuterated buffers at various pL values between 6.0 and 8.4 using octadecanal as the substrate. Plots of reaction rate as a function of pL are shown in Figure 2.3. At pL < 6.0, cADO activity was too low to reliably measure. Activity increased to a maximum near pL 7.0 in either

proteated or deuterated buffers, before diminishing slightly at higher pL. The activity of the enzyme appears to be slightly lower in deuterated buffer, but given the experimental errors associated with these measurements, we do not consider the differences significant. The plots provide no evidence of a kinetically significant ionization occurring during the reaction.

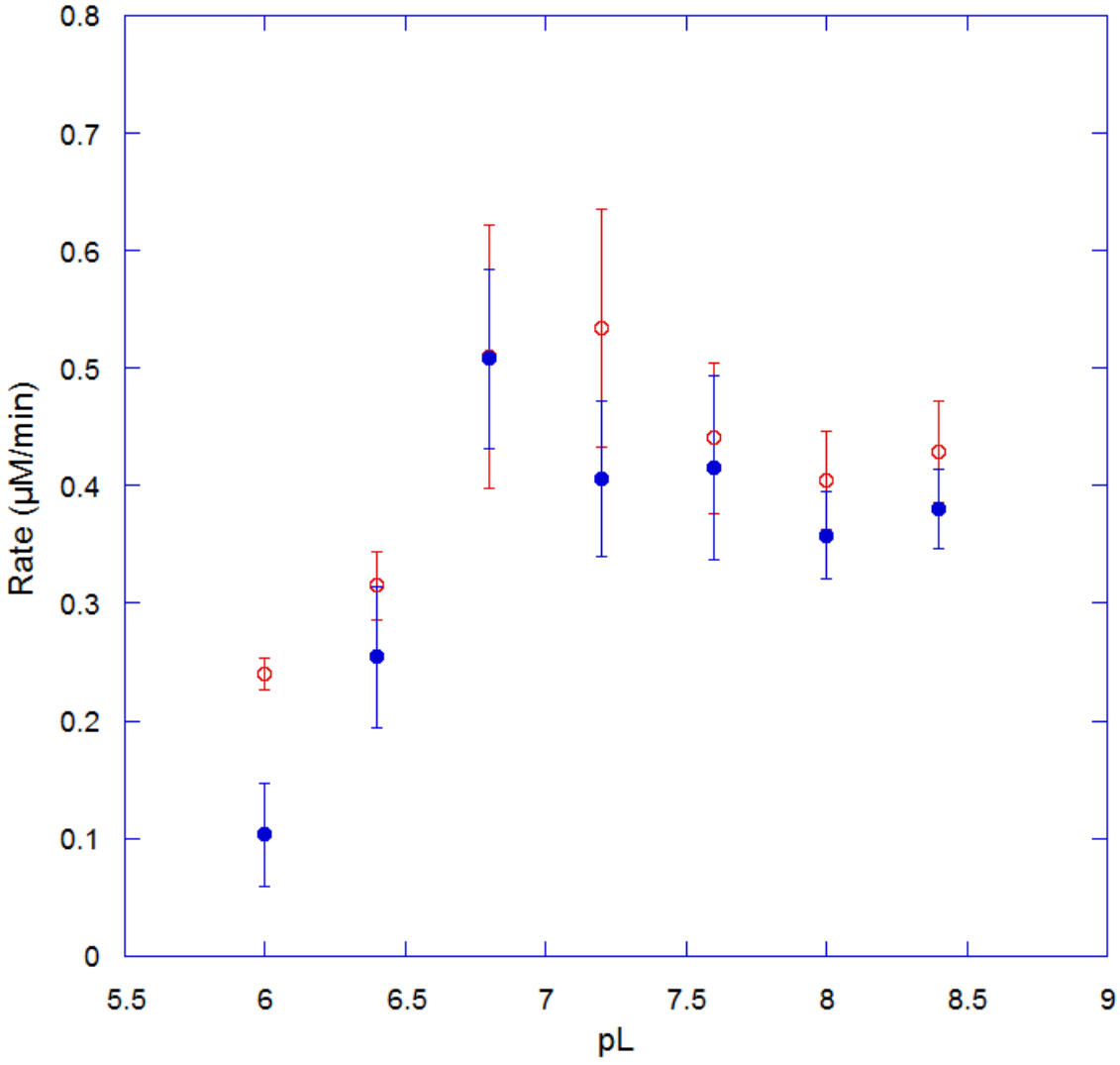

Figure 2.3 – pL rate profiles for cADO with octadecanal in H_2O (○) and D_2O (●).

2.3.2 Solvent Isotope Effect on the Transfer of Deuterium to Product

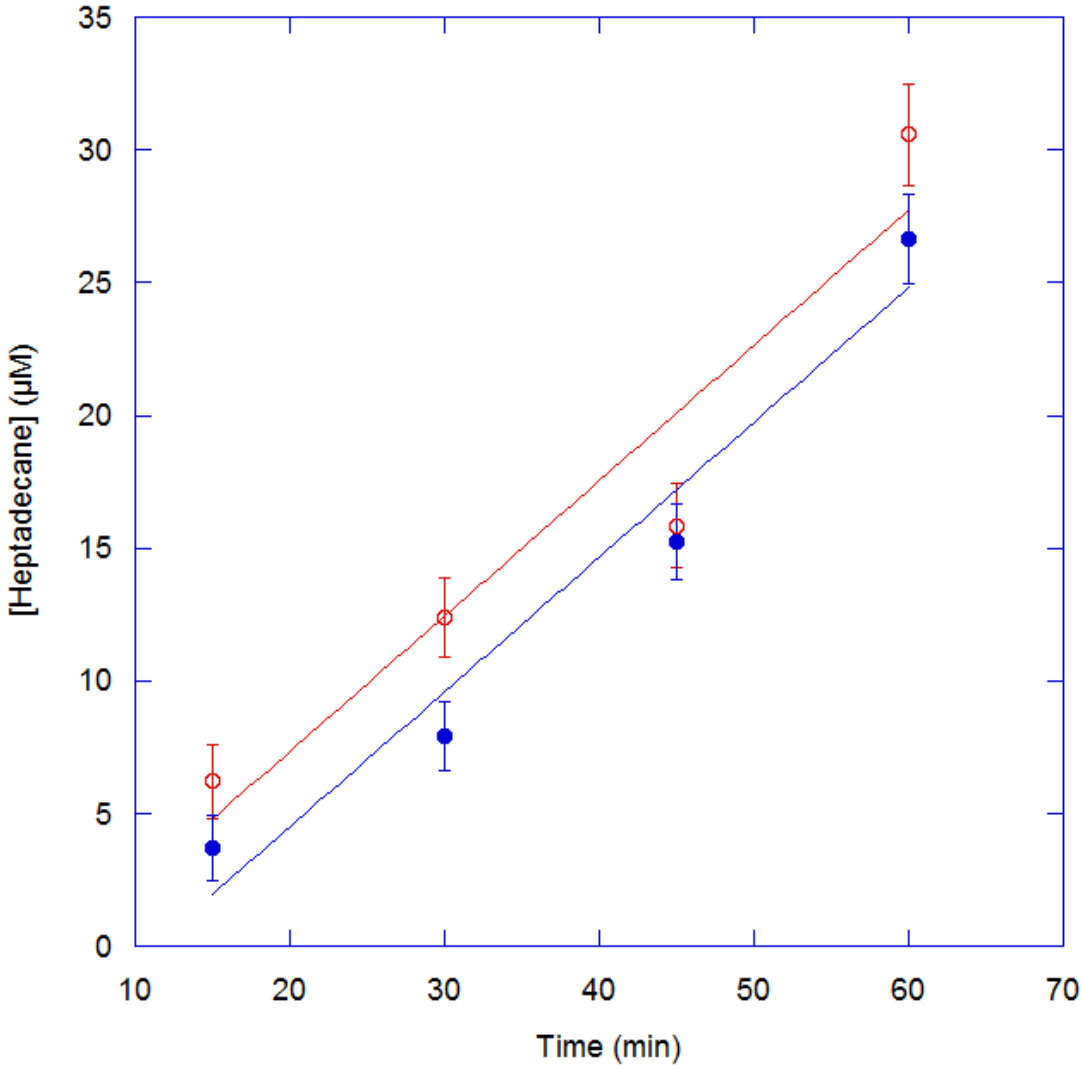

Figure 2.4 – Time course measurement of cADO with octadecanal at pL 6.8 in H_2O (○) and D_2O (●).

On the basis of the pL – rate profile, solvent isotope effect measurements were made at pL 6.8, shown in Figure 2.4, where enzyme activity was found to be near maximal in both H_2O and D_2O. At this pL, the nonenzymatic exchange of deuterium from the solvent with the α-carbon of the aldehyde was sufficiently slow that it did not interfere with the experiment. At pL 6.8, measurements of the rates of heptadecane

formation in H_2O and D_2O allowed the SIE on V_{max} for cADO reacting with octadecanal as a substrate to be calculated as 1.0 ± 0.2. This result is consistent with the pL-dependent activity of the enzyme discussed above.

This observation indicates that proton transfer is not a kinetically significant step in the reaction. Taken together with other experimental data, the absence of a solvent isotope effect on V_{max} suggests that all of the chemical steps are relatively fast compared to the steady state rate of turnover. Although spectroscopic studies of the formation of the differic-peroxide intermediate(s) appear to be complicated by multiple reactant states arising from the order of binding of aldehyde and O_2, the rate constants for the formation of the activated oxygen species (II or III in Figure 2.1) have been measured as 0.75 and 0.2 s^{-1} depending on which substrate binds first.[4] Subsequent reaction of species III with reduced ^{OMe}PMS, with concomitant formation of formate (species V), was reported to occur in < 1 s. Previous studies performed using an α-oxiranyl aldehyde as a radical clock indicated the rate at which species V was converted to VI was fast (~10^4 to ~10^5 s^{-1}).[8] These observations are in accord with chemical logic, in that species IV and V involve the formation of highly reactive radical species that would be expected to have very short lifetimes.

The preceding discussion points to a nonchemical step being rate-determining during turnover. We have discussed possible reasons for very slow turnover of substrates by cADO previously,[15] which we briefly summarize here. These include the insoluble nature of both the substrates and products, which may limit both diffusion of the substrate into the active site and release of the product alkane from the highly hydrophobic substrate-binding channel of cADO. As noted above, the inhibition of cADO by

hydrogen peroxide, which arises from the uncoupled reaction of the reducing systems employed to assay the enzyme with O_2, may also slow the reaction.[13] The transfer of reducing equivalents from the auxiliary reducing system, e.g., PMS or ferredoxin, to cADO during the catalytic cycle could also be rate-limiting during the reaction. In this respect, it should be noted that the physiological electron donor to cADO has yet to be identified, nor is the reason that some cyanobacteria produce alkanes understood. It is possible that the cADO may require other proteins to activate it,[16] similar to the plant decarbonylase, or that the deformylating activity could be a side reaction and that the enzyme catalyzes an oxidative reaction on an as yet undiscovered substrate.

2.3.3 Fractionation Factor for the Transfer of Deuterium to Product

Solvent fractionation factors (Φ) have the potential to discriminate between different proton donors in enzymatic reactions.[10] Therefore, we sought to generate a proton inventory for the cADO reaction that would allow Φ to be determined. If the proton donor was a free water molecule, Φ would be predicted to be near unity.[17] If Tyr135 or Gln123 were the proton donor, Φ would be predicted to be greater than one based on Φ for phenol and R-NL2 (Φ = 1.13 for each).[17] However, a water molecule bound to a Lewis acidic group, such as a metal ion, will behave more like a free hydroxyl group (Φ = 0.43) and will have a characteristically inverse Φ.[18-21]

Typically, proton inventories are calculated using the rate ratio of reactions in mixed isotopic versus pure protic solvents plotted against the mole fraction of deuterium (χ) in the mixed solvent.[10] In this case, the velocity of the reaction is independent of the isotopic composition of the solvent; therefore, we determined Φ by performing an

internal competition experiment in mixed isotopic solvents. We note that in this experimental design the observed fractionation factor (Φ_{obs}) is related to the observed solvent isotope effect ($^{D_2O}SIE_{obs}$) on V/K by the relationship $\Phi_{obs} = 1/ {}^{D_2O}SIE_{obs}$.

The ratio of protium to deuterium in the alkane product was determined as a function of χ using GC-MS. To obtain the requisite degree of precision in measuring the mass ratios of the product molecular ion peak, heptanal was used as a substrate for these experiments. Measurements with octadecanal proved to be unreliable because of the low abundance of the molecular ion peak. The ratios of unlabeled to deuterated hexane were determined at every tenth χ D_2O (average of five determinations per point) and were used to plot the data shown in Figure 2.5. The observed solvent isotope effect ($^{D_2O}SIE_{obs}$) on the reaction was calculated by

$$\chi_{product} = {}^{D_2O}SIE_{obs}(1/\chi_{solvent} - 1) \qquad (1)$$

From the data, a $^{D_2O}SIE_{obs}$ value of 2.19 ± 0.02 was calculated. Equation 1 assumes that $^{D_2O}SIE_{obs}$ does not vary as a function of χ, i.e., that only a single proton is involved in the transition state. The excellent fit of the data to eq 1 ($R^2 = 0.998$) indicates that this is indeed the case, and fits of the data to the linearized form of eq 1 give a straight line (Figure 2.5, inset).

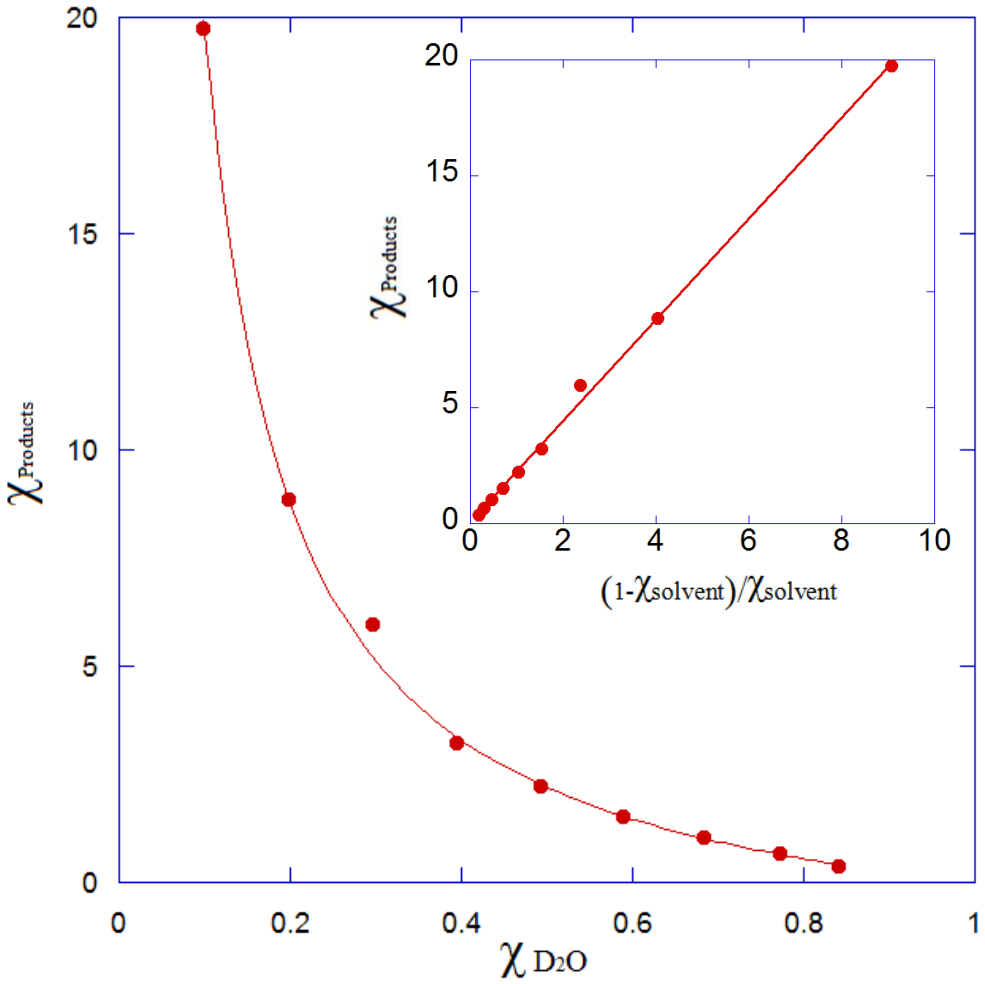

Figure 2.5 – Proton inventory for cADO. The mole fraction of D_2O in the solvent is plotted against the ratio of proteated to deuterated product alkane. The solid line represents the best fit to equation 1 where $R^2 = 0.998$. Error bars are contained within the points. The inset graph represents a fit to the linearized form of equation 1 ($R^2 = 0.999$).

2.3.4 Interpretation of Φ_{obs}

Isotope effect measurements seldom allow unambiguous mechanistic interpretations to be made; here we consider two interpretations that are consistent with our data. More likely, $^{D_2O}SIE_{obs}$ represents a reactant state equilibrium SIE arising from a protic site that is characterized by an inverse fractionation factor, Φ_{obs}. In this interpretation, the distribution of isotope is established at the proton-donating group prior

to the start of the catalytic cycle. Because the chemical steps in the reaction are irreversible, the enzyme is forced to take whichever isotope is present at the active site, and thus, the distribution of isotopes in the product alkane reflects the equilibrium distribution of isotopes at the proton donating group prior to the reaction, i.e., Φ_{obs}. In this case, $\Phi_{obs} = 1/{}^{D_2O}SIE_{obs} = 0.457 \pm 0.004$.

We are not aware of any experimentally determined fractionation factors for Fe-dependent enzymes. However, fractionation factors have been measured for two isoforms of carbonic anhydrase with Co^{II} bound, for which the M-OL_2 species has a Φ in the range of 0.81- 0.9 and the M-OL^- species has a Φ in the range of 0.72 - 0.77.[10,22,23] These agree quite well with the fractionation factor for $Co(H_2O)_6^{2+}$ in solution ($\Phi = 0.70$), and it is generally assumed that other divalent metals such as Zn and Fe^{II} have a Φ of ~0.7.[22,24] We note that Φ is calculated on a per-bond basis and is multiplicative. It is therefore diagnostic for the number of a metal-bound water molecules; for one water molecule, $\Phi_{obs} = \Phi^2 = \sim 0.49$.

The low value of Φ_{obs} for cADO is consistent with an iron bound water molecule being the proton donor in the reaction, as the experimentally determined Φ_{obs} of 0.457 is in good agreement with the predicted value of Φ^2 (0.49).[10] This value is similar to that determined for another non-heme iron enzyme, factor inhibiting hypoxia inducible factor-1α.[24] For this enzyme, fractionation factors were measured on k_{cat} ($\Phi_{obs} = 0.51$) and k_{cat}/K_M ($\Phi_{obs} = 0.40$) that were associated with a kinetically significant dissociation of an Fe^{II}-bound water molecule prior to O_2 binding. Thus, we conclude that the observed SIE may reasonably be interpreted as arising from a reactant state EIE due to the equilibration of H_2O and D_2O at the diiron core that leads to enrichment of H_2O at the metal site.

An alternative explanation is that $^{D_2O}SIE_{obs}$ arises from a kinetic competition between two equivalent proton donors at the active site. This can give rise to isotopic discrimination even if the preceding steps in the reaction are irreversible and in favorable cases can allow intrinsic kinetic isotope effects to be determined even when proton transfer is not rate-determining.[25,26] This would also be consistent with an iron-bound water molecule as the proton donor, as opposed to the active site tyrosine residue. However, in this case, the interpretation of the isotope effect would be complicated because of the expected additional discrimination against deuterium arising from the inverse fractionation factor. It is, however, unclear whether the two protons on a water molecule in the active site would behave as chemically equivalent given the strong propensity of the protons to form hydrogen bonds with polar groups at the active site. Therefore, although these findings are consistent with our experimental data, we consider this the less likely explanation, and we are not aware of a precedent in which SIEs have been demonstrated to arise by such a mechanism.

2.3.5 Mechanistic Implications

Interpreting the low Φ_{obs} value as arising from the donation of a proton by an iron-bound water molecule raises a question of whether the metal is in the ferric or ferrous oxidation state. Mechanistic considerations make it more likely that the proton donor is an Fe^{II}-OH_2 species rather than an Fe^{III}-OH_2 species. The pK_a values of Fe^{III}-OH_2 species are much lower than those of Fe^{II}-OH_2 species [cf. Fe^{3+}-$(OH_2)_6$ (pK_a = 2.2) and Fe^{2+}-$(OH_2)_6$ (pK_a = 9.5)] so that at neutral pH Fe^{III}-OH^- would predominate at the active site of cADO.[27] Also, donation of a proton from $Fe^{III}OH^-$ would result in the

formation of a terminal iron oxide species or would require the concerted transfer of a second proton from another site, which is not supported by the proton inventory.

In contrast, proton transfer coupled with electron transfer from Fe^{II}-OH_2 through a multiple-site electron-proton transfer (MS-EPT) reaction appears to be quite plausible (Figure 2.6 A).[28] In this case, an electron would be transferred to the alkyl radical from the metal and the proton transferred from the metal-bound water in a concerted manner. Here, oxidation of Fe^{II} to Fe^{III} facilitates proton transfer due to the increased Lewis acidity of the metal. Previous studies using an α-oxiranyl aldehyde as a radical clock provide evidence that the intermediate alkyl radical is reduced extremely rapidly, consistent with direct electron transfer from Fe^{II}, as opposed to long-range electron transfer from an external reductant.[8]

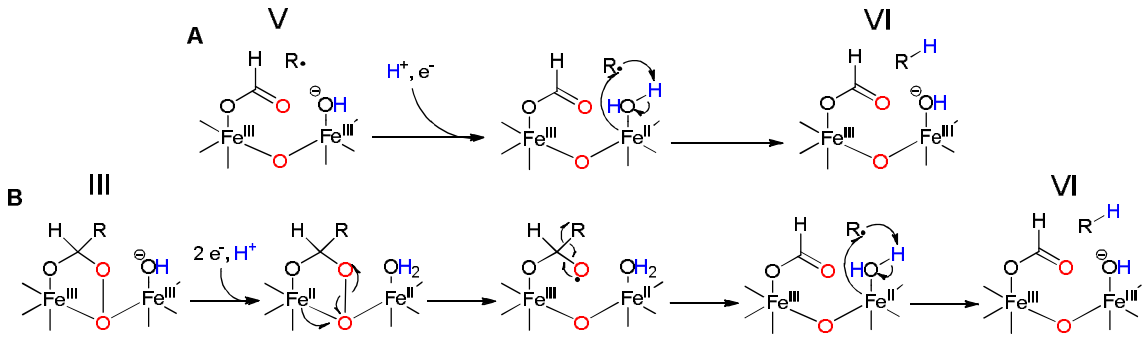

Figure 2.6 – Two potential mechanisms for multiple site electron-proton transfer (MS-EPT) from an Fe^{2+}-OH_2 species. **A –** single electron reduction of the diferric core after deformylation resulting a mixed valent $Fe^{III/II}$ species. **B –** two electron reduction of the diferric core *prior* to deformylation resulting in a divalent $Fe^{II/II}$ species that undergoes subsequent chemical steps.

The mechanism discussed above implies the formation of a mixed valent Fe^{II}/Fe^{III} metal center during the reaction, prior to reduction of the alkyl radical. We note that the previous step in the mechanism requires an electron to facilitate C-C bond cleavage and that this electron could also be transferred from iron. It is therefore an interesting

question of whether these steps occur sequentially through mixed valent metal species or whether, prior to C-C bond cleavage, complete reduction of cADO to the diferrous enzyme occurs, as shown in Figure 2.6 B. These mechanisms may be hard to distinguish experimentally given the short lifetimes of the reactive intermediates involved, but the attractive feature of forming a diferrous intermediate is that the enzyme is primed to complete the deformylation reaction without the need to shuttle further electrons into the active site.

Lastly, we note that a rather different mechanism for cADO has been proposed, shown in Figure 1.7, on the basis of the observation of low levels of hydroxylated products when cADO is reacted with medium chain-length aldehydes such as decanal and nonanal.[12] The mechanism involves the formation of a transient Fe^{IV} superoxo species that subsequently acts to hydroxylate the product alkane and does not require additional electrons to be introduced during the reaction. The experiments described here do not necessarily rule out such a mechanism as the proton transferred to form the n-1 alkane could still originate from an iron-bound aquo ligand that could give rise to the EIE observed in this study. However, we regard this mechanism as less likely to be operating, at least with octadecanal and heptanal, the substrates we commonly use to assay cADO, as no n-1 alcohol or n-2 alkane products were observed.

2.4 Conclusions

In conclusion, the solvent isotope effect measurements we have described provide information about the likely donor of the proton to the product alkane. The absence of any kinetic solvent isotope effect on the reaction, taken together with other experimental observations, points to a non-chemical step as likely being rate-determining in the reaction. With the caveat that intramolecular competition between two active site proton donors cannot be rigorously excluded, the $^{D_2O}SIE_{obs}$ measured in these studies most likely arises from a highly inverse reactant state fractionation factor associated with the active site group that donates the proton to the product alkane. The low Φ_{obs} value is characteristic of the pre-equilibrium binding of H_2O to an iron center, pointing to an iron-bound water molecule as the likely proton donor.

2.5 References

(1) Ghim, C. M.; Kim, T.; Mitchell, R. J.; Lee, S. K. (2010) Synthetic Biology for Biofuels: Building Designer Microbes from the Scratch, *Biotechnol. Bioprocess Eng.*, *15*, 11.

(2) Li, N.; Chang, W. C.; Warui, D. M.; Booker, S. J.; Krebs, C.; Bollinger, J. M., Jr. (2012) Evidence for only oxygenative cleavage of aldehydes to alk(a/e)nes and formate by cyanobacterial aldehyde decarbonylases, *Biochemistry*, *51*, 7908.

(3) Li, N.; Norgaard, H.; Warui, D. M.; Booker, S. J.; Krebs, C.; Bollinger, J. M., Jr. (2011) Conversion of fatty aldehydes to alka(e)nes and formate by a cyanobacterial aldehyde decarbonylase: cryptic redox by an unusual dimetal oxygenase, *J. Am. Chem. Soc.*, *133*, 6158.

(4) Pandelia, M. E.; Li, N.; Norgaard, H.; Warui, D. M.; Rajakovich, L. J.; Chang, W. C.; Booker, S. J.; Krebs, C.; Bollinger, J. M. (2013) Substrate-Triggered Addition of Dioxygen to the Diferrous Cofactor of Aldehyde-Deformylating Oxygenase to Form a Diferric-Peroxide Intermediate, *J. Am. Chem. Soc.*, *135*, 15801.

(5) Paul, B.; Das, D.; Ellington, B.; Marsh, E. N. (2013) Probing the mechanism of cyanobacterial aldehyde decarbonylase using a cyclopropyl aldehyde, *J. Am. Chem. Soc. 135*, 5234.

(6) Das, D.; Eser, B. E.; Han, J.; Sciore, A.; Marsh, E. N. (2011) Oxygen-independent decarbonylation of aldehydes by cyanobacterial aldehyde decarbonylase: a new reaction of diiron enzymes, *Angew Chem Int Ed Engl*, *50*, 7148.

(7) Warui, D. M.; Li, N.; Norgaard, H.; Krebs, C.; Bollinger, J. M., Jr.; Booker, S. J. (2011) Detection of formate, rather than carbon monoxide, as the stoichiometric coproduct in conversion of fatty aldehydes to alkanes by a cyanobacterial aldehyde decarbonylase, *J. Am. Chem. Soc.*, *133*, 3316.

(8) Das, D.; Ellington, B.; Paul, B.; Marsh, E. N. G. (2014) Mechanistic Insights from Reaction of alpha-Oxiranyl-Aldehydes with Cyanobacterial Aldehyde Deformylating Oxygenase, *ACS Chem. Biol.*, *9*, 570.

(9) Khara, B.; Menon, N.; Levy, C.; Mansell, D.; Das, D.; Marsh, E. N.; Leys, D.; Scrutton, N. S. (2013) Production of propane and other short-chain alkanes by structure-based engineering of ligand specificity in aldehyde-deformylating oxygenase, *Chembiochem : a European journal of chemical biology*, *14*, 1204.

(10) Quinn, D. M., Sutton, L. D. In *Enzyme Mechanism from Isotope Effects*; CRC Press: 1991.

(11) Vidakovic, M.; Sligar, S. G.; Li, H. Y.; Poulos, T. L. (1998) Understanding the role of the essential Asp251 in cytochrome P450cam using site-directed mutagenesis, crystallography, and kinetic solvent isotope effect, *Biochemistry*, *37*, 9211.

(12) Aukema, K. G.; Makris, T. M.; Stoian, S. A.; Richman, J. E.; Munck, E.; Lipscomb, J. D.; Wackett, L. P. (2013) Cyanobacterial aldehyde deformylase oxygenation of aldehydes yields n-1 aldehydes and alcohols in addition to alkanes, *ACS Catal*, *3*, 2228.

(13) Andre, C.; Kim, S. W.; Yu, X. H.; Shanklin, J. (2013) Fusing catalase to an alkane-producing enzyme maintains enzymatic activity by converting the

inhibitory byproduct H2O2 to the cosubstrate O2, *Proc. Natl. Acad. Sci. USA*, *110*, 3191.
(14) Schirmer, A.; Rude, M. A.; Li, X.; Popova, E.; del Cardayre, S. B. (2010) Microbial biosynthesis of alkanes, *Science*, *329*, 559.
(15) Marsh, E. N. G.; Waugh, M. W. (2013) Aldehyde Decarbonylases: Enigmatic Enzymes of Hydrocarbon Biosynthesis, *ACS Catal.*, *3*, 2515.
(16) Bourdenx, B.; Bernard, A.; Domergue, F.; Pascal, S.; Leger, A.; Roby, D.; Pervent, M.; Vile, D.; Haslam, R. P.; Napier, J. A.; Lessire, R.; Joubes, J. (2011) Overexpression of Arabidopsis ECERIFERUM1 promotes wax very-long-chain alkane biosynthesis and influences plant response to biotic and abiotic stresses, *Plant physiology*, *156*, 29.
(17) Jarret, R. M.; Saunders, M. (1985) A NEW METHOD FOR OBTAINING ISOTOPIC FRACTIONATION DATA AT MULTIPLE SITES IN RAPIDLY EXCHANGING SYSTEMS, *J. Am. Chem. Soc.*, *107*, 2648.
(18) Kresge, A. J., More O'Ferrall, R. A., and Powell, M. F. In *In Isotopes in Organic Chemistry*; Buncel, E., and Lee,, C., C., Eds.; Elsevier: Amsterdam, 1987.
(19) Schowen, K. B., and Schowen, R. L. (1982) Solvent Isotope Effects on Enzyme Systems, *Methods Enzymol*, *87*, 551−606.
(20) Galtress, C. L., Morrow, P. R., Nag, S., Smalley, T. L., Tschantz,; M. F., V., J. S., Wichems, D. N., Ziglar, S. K., and Fishbein, J. C. (1992) Mechanism for the Solvolytic Decomposition of the Carcinogen N-Methyl-N′-nitro-N-nitrosoguanidine in Aqueous Solutions., *J. Am. Chem. Soc.*, *114*, 1406−1411.
(21) Gold, V., and Grist, S. (1972) Deuterium Solvent Isotope-Effects on Reactions Involving Aqueous Hydroxide Ion., *J. Chem. Soc. Perkin Trans.*, *2*, 89−95.
(22) Kassebaum, J. W.; Silverman, D. N. (1989) HYDROGEN-DEUTERIUM FRACTIONATION FACTORS OF THE AQUEOUS LIGAND OF COBALT IN CO(H2O)62+ AND CO(II)-SUBSTITUTED CARBONIC-ANHYDRASE, *J. Am. Chem. Soc.*, *111*, 2691.
(23) Makinen, M. W.; Kuo, L. C.; Dymowski, J. J.; Jaffer, S. (1979) CATALYTIC ROLE OF THE METAL-ION OF CARBOXYPEPTIDASE-A IN ESTER HYDROLYSIS, *J. Biol. Chem.*, *254*, 356.
(24) Hangasky, J. A.; Saban, E.; Knapp, M. J. (2013) Inverse Solvent Isotope Effects Arising from Substrate Triggering in the Factor Inhibiting Hypoxia Inducible Factor, *Biochemistry*, *52*, 1594.
(25) Yoon, M., Song, H. T., Hakansson, K., and Marsh, E. N. G. (2010) Hydrogen Tunneling in Adenosylcobalamin-Dependent Glutamate Mutase: Evidence from Intrinsic Kinetic Isotope Effects Measured by Intramolecular Competition., *Biochemistry*, *49*, 3168−3173.
(26) Yoon, M., Kalli, A., Lee, H. Y., Hakansson, K., and Marsh, E. N.; G. (2007) Intrinsic deuterium kinetic isotope effects in glutamate mutase measured by an intramolecular competition experiment., *Angew. Chem., Int. Ed.*, *46*, 8455−8459.
(27) Gilson, R., and Durrant, M. C. (2009) Estimation of the pKa values of water ligands in transition metal complexes using density

functional theory with polarized continuum model solvent corrections., *J. Chem. Soc., Dalton Trans.*, 10223−10230.

(28) Weinberg, D. R., Gagliardi, C. J., Hull, J. F., Murphy, C. F., Kent,; C. A., W., B. C., Paul, A., Ess, D. H., McCafferty, D. G., and; Meyer, T. J. (2012) Proton-coupled electron transfer., *Chem. Rev.* , *112*, 4016−4093.

Chapter 3 Mutagenesis and Substrate Analogs

3.1 Introduction

cADO could potentially form the foundation of a commercially viable biosynthetic pathway for the production of net carbon neutral drop-in biofuels.[1,2] However, in reality cADO is too sluggish by several orders of magnitude. It may be possible to improve the activity of cADO through extensive protein engineering and fortunately cADO is extremely stable, which aids mutagenesis. For this approach to be feasible, reengineering this enzyme for practical biofuels applications requires that we must first identify the slow step of the mechanism. It is odd that while much of the mechanism has been explored, no RDS has yet been determined. The results of the SIE study in chapter 2, combined with evidence provided by previous mechanistic analysis, suggest the RDS may not be chemical in nature. This leaves few possible reasons for the slow nature of the enzyme.

First, it is possible that transfer of the reducing equivalents required for turnover of the catalytic cycle is rate limiting. This could be due to a slow binding interaction with a corresponding reductant or electron mediator, in this case PMS or ferredoxin, because the native reducing system has not been identified. It is possible that electron transfer itself is rate limiting. There is some evidence that the key electron injection in step 3 of the mechanism shown in Figure 3.1 occurs on the order of less than 1 s.[3] However, the

experiment did not report on the decay of the peroxy-hemiacetal intermediate III, and therefore the binding interaction between O-methoxy-PMS (^{OMe}-PMS) and cADO itself, but instead followed the corresponding decrease in NADH absorption by UV-vis spectroscopy. Our lab has previously shown NADH consumption to be decoupled from the aldehyde turnover and that it is not a good reporter for measuring activity, therefore, this crucial electron input step has not been entirely explored.[4]

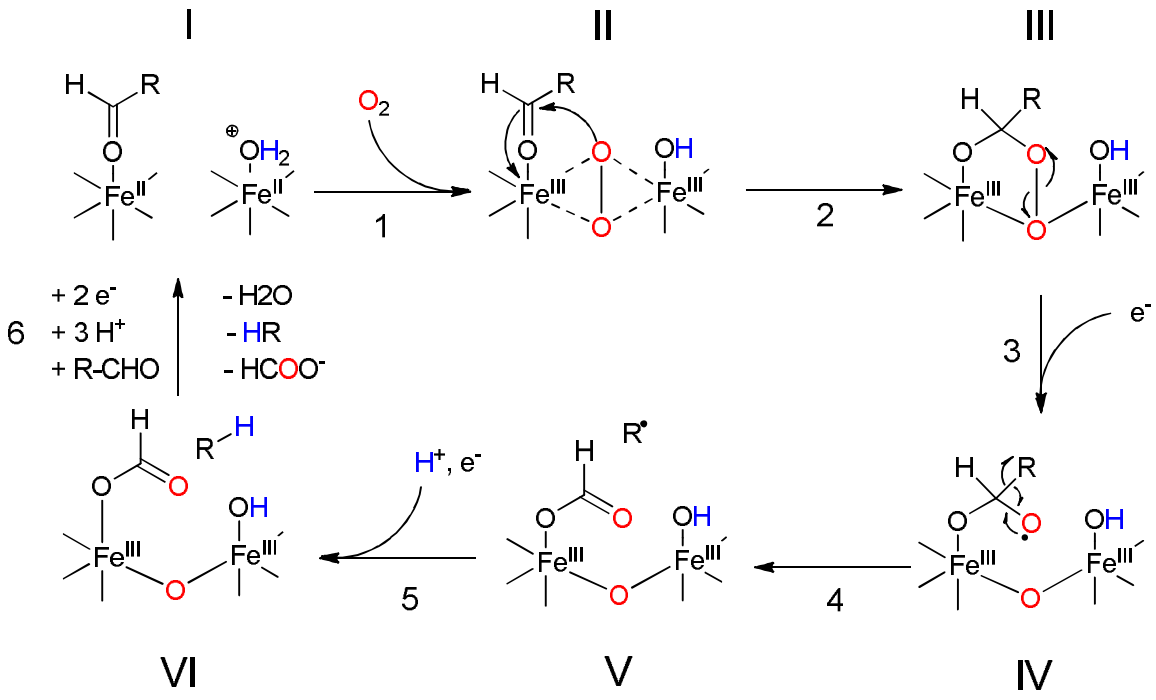

Figure 3.1 – Proposed mechanism for deformylation of aldehydes by cADO. The color-coding indicates the origins of oxygen atoms and protons in the products established by isotope-labeling.

Second, the mechanism may be insufficient to describe the reaction of cADO and an additional step that we are unaware of may be required that is slow. Based on the wealth of work done on cADO, this case may seem unlikely; however, recent studies by Wackett et al have indicated the possibility of an alternative reaction that is more like a P450 enzyme in which an Fe^{IV} superoxo species performs oxidative chemistry.[5] This

proposed pathway is capable of producing n-1 aldehydes and alcohols, as shown in Figure 3.2, through a proton abstraction followed by a hydroxyl radical rebound mechanism. Although it uses a different reactive oxygen species, this is somewhat similar to the activity of MMO.[6] This raises the question of whether the hydrocarbon-producing carbon-carbon bond cleavage is the primary activity of cADO and if instead we have simply not yet identified either the correct substrate or the physiological reaction.

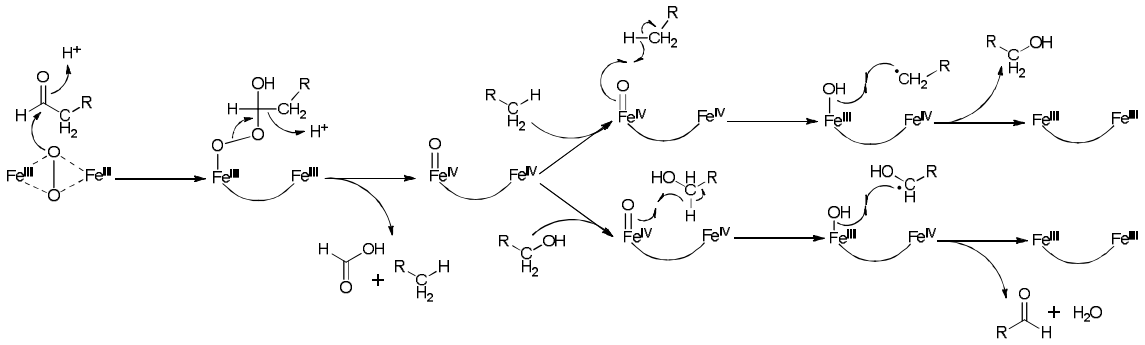

Figure 3.2 – Alternative carbanionic mechanism proposed for deformylation of aldehydes by cADO resulting in a reactive Fe^{IV} superoxo species capable of additional reactions producing n-1 alcohols and aldehydes.

Finally, as the substrates, products, and the binding channel are all highly hydrophobic, the RDS may be due to slow substrate binding and/or product release. Although, in theory, substrate binding cannot be rate determining, because as long as substrate concentration is sufficiently large the Michaelis-Menten equation predicts the reaction will approach V_{max}, the kinetics of cADO are complicated by the fact that the native substrate in not very soluble. Octadecanal forms micelles when in high enough concentrations, effectively capping the available substrate concentration.[7] In this way the apparent V_{max} may be artificially low and not accurately represent saturating substrate conditions. Alternatively, there may be a conformation change associated with aldehyde binding that triggers a carboxylate shift, common in the non-heme diiron oxygenases.[8,9]

This may be necessary to allow and has been suggested to trigger the oxygen binding event.[10] Neither the substrates, nor the products are particularly soluble and the hydrophobicity of the binding channel may prevent association of the substrate in the correct orientation or dissociation of the products once formed.

Our lab has determined several crystal structures indicating there are multiple binding modes for both long and short chain substrate analogs, as show in Figure 3.3 A and B respectively.[11] For long chain substrates there are two binding modes where the aldehyde functionality would have access to the active site. In one the hydrophobic tail of the aldehyde is buried in a hydrophobic pocket, shown on the left side of Figure 3.3 A, while in the second it occupies the putative substrate binding channel exposed to solvent, shown on the right side of the figure. Conversion to alkane product may be sterically favorable in only one, or neither, conformation as there are no specific side chain residues to anchor the substrate in the active site beyond the electrostatic interaction with the diiron core itself. Additionally, the alkane may be sterically hindered from leaving the active site in the buried conformation. In the third conformation, the polar head group is exposed to solvent while the nonpolar alkyl chain is buried in the hydrophobic pocket. This effectively blocks the binding channel entirely while keeping the substrate in what is presumably the most hydrophobically favorable and stable position. In the structure where short chain substrate analogs were co-crystallized, two molecules of acid were found to bind in the binding channel. The first with the polar head group presented to the active site and the second with its polar head group exposed to solvent. The same problems arise in that there is little to anchor the first substrate in the correct steric

configuration relative to the active site and, should it turn over, the second molecule blocking the binding pocket opening may prevent the dissociation of the product.

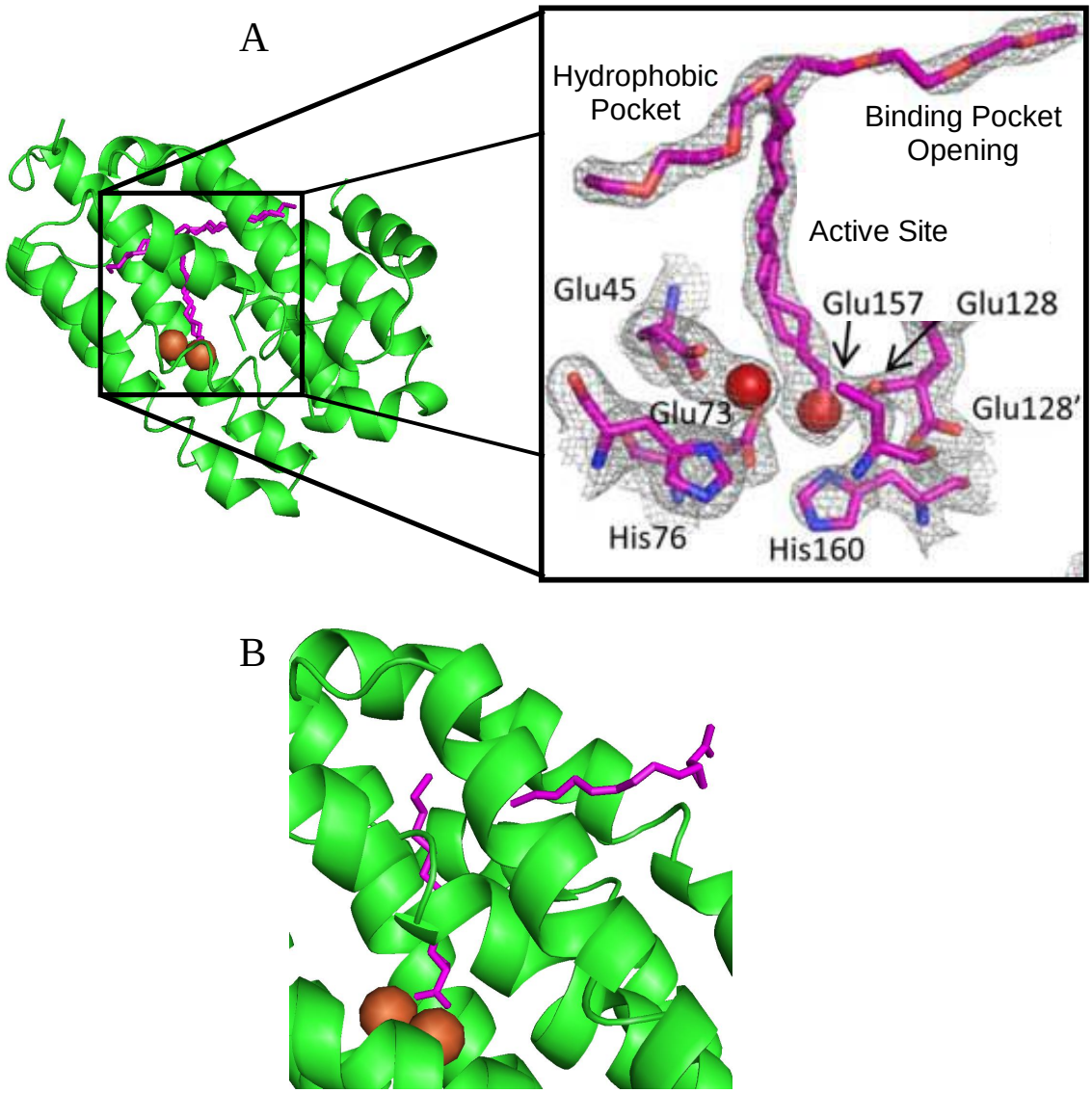

Figure 3.3 – **A** – Crystal structure of cADO mutant L194A (pdb 4PGI), shown in green, with multiple conformations of the substrate 11-(2-(2-ethoxyethoxy)ethoxy)undecanal bound, shown in purple. The window on the right shows an expanded view of the different binding modes in the active site and labels the three components of the binding channel. Parts of this figure were adapted from reference 11. **B** – Crystal structure of cADO with two molecules of trans-2-nonylcyclopropane-1-carboxylic acid, shown in purple, bound (pdb 4PG1). In both structures the diiron core atoms are shown in orange, the hydrophobic pocket is on the reader's left, and the opening to solvent is on the right.

It is unclear which, if any, of these scenarios may be occurring, but it seems plausible that one or more of these effects may contribute to the sluggishness of cADO as the only reporter we have for activity is product formation. The work described in this chapter focuses on exploring the third scenario, where substrate binding and/or product release acts as a non-chemical rate limiting step. I performed mutagenesis to perturb the substrate and product binding interactions in the active site, hydrophobic pocket, and opening of the binding pocket. If eliminating non-productive binding modes were to improve the activity of cADO, it would implicate substrate binding and/or product release as a non-chemical RDS. Also included in this chapter is the synthesis and characterization of substrate analogs designed to stabilize the proposed radical used to probe the mechanism and substrate binding affinity.

3.2 Materials and Methods

3.2.1 Materials

Wt and mutant recombinant cADO from *P. marinus* MIT9313 were purified as previously described in chapter 2 section 2.1. His-Trap HP (5 mL) Ni-affinity column was obtained from GE Healthcare. 2xYT media, IPTG, kanamycin, mono and dibasic potassium phosphate, potassium chloride, HEPES, glycerol, 9^oN DNA ligase buffer, 9^oN DNA ligase, ferrous ammonium sulfate, toluene, HCl, CH_2Cl_2, MeOH, acetone, potassium carbonate, 1-(bromomethyl)-4-methylbenzene, and *p*-cresol were from Fisher Scientific. ATP was from Roche Molecular Biochemicals. Phusion HF DNA polymerase, Phusion HF buffer, polynucleotide kinase buffer, T4 polynucleotide kinase, DpnI, and cutsmart buffer were obtained from New England Biolabs. dNTP mix was from

Invitrogen. Spin desalting columns were from Thermo Scientific. Octadecanal, phenylacetaldehyde, 3-bromoproan-1-ol, triphenylphosphine, phenyl lithium, THF, $SOCl_2$, Pd on C, $LiAl_4$ TEMPO, BAIB, 2-(4-(bromomethyl) phenyl)acetic acid, 2-(4-hydroxyphenyl)acetic acid, 1-bromopropane, heptadecane, 1-heptadecene, tridecane, hexane, phenazine methosulfate, and NADH were obtained from Acros Organics. Pentadecanal, dodecanal, butyraldehyde, PDC, 1-bromododecane, and NaH were from Sigma Aldritch.

3.2.2 Synthesis of Substrate Analogs

The chemical structures of the substrate analogs used in this chapter are shown in Figure 3.4. The detailed procedures of the syntheses and characterization of these compounds and the product standards **7**, **8**, and **11**, are described in Appendix A. The product standard **12** was obtained commercially. Product standards **9** and **10** were not synthesized and observation of the product was inferred by GC-MS analysis.

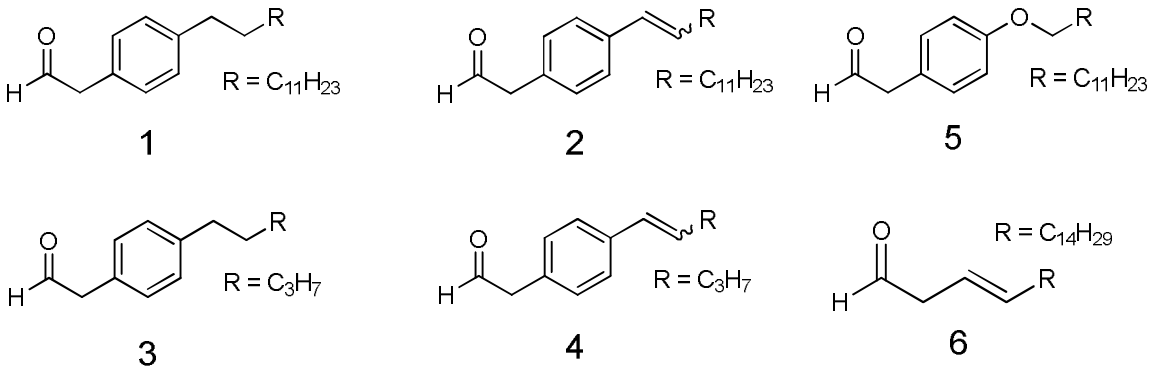

Figure 3.4 — The six substrate analogs synthesized to probe cADO were **1** — 2-(4-tridecylphenyl)acetaldehyde **2** — unsaturated 2-(4-(tridec-1-en-1-yl)phenyl) acetaldehyde **3** — 2-(4-pentylphenyl) acetaldehyde **4** — 2-(4-(penten-1-en-1-yl) phenyl)acetaldehyde **5** — 2-(4-(dodecyloxy)phenyl)acetaldehyde and **6** — (E)-octadec-3-enal.

3.2.3 Site Directed Mutagenesis

Primers were designed using the PrimerX design tool and ordered from IDT technologies. Primers were phosphorylated using a T4 polynucleotide kinase for 30 min at 37^{o}C, which was then heat-inactivated for 20 min at 65^{o}C. The reaction mixture contained 5 µM primer, 1 mM ATP, 1x polynucleotide kinase buffer, and 1 µL of T4 polynucleotide kinase in a 50 µL total reaction volume. 25 ng of parent plasmid template were then used in a PCR containing 500 nM of forward and reverse phsosphorylated primer, 250 µM dNTP mix, 0.5x Phusion HF buffer, 0.5x 9^{o}N DNA ligase buffer, 1 U of Phusion DNA polymerase, 20 U of 9^{o}N DNA ligase, and enough water to bring the reaction volume to 25 µL. A two-step PCR was run with an initial denaturing step at 98^{o}C for 30 s. The two steps comprised a 30 s denaturing step at 98^{o}C followed by a 210 s (30 s/kb of plasmid) combined annealing and elongation step at 68^{o}C. These two steps were repeated 30 times followed by a 5 min hold at 68^{o}C for final elongation. The parent plasmid template in the PCR mixture was then digested with 1 µL of DpnI, 1x New England Biolabs cutsmart buffer, and enough water to bring the volume to 50 µL at 37^{o}C for 4 h. The mutant plasmid was then purified from the mixture using a PCR purification kit and 2 µL was transformed into 40 µL of electrocompetent XL1-Blue cells. Cells were allowed to recover for 45 min and then plated on kanamycin resistant agar. Colonies were picked for overnight growth and their DNA was purified and verified by sequencing. Alignments to identify successful mutants were performed with Mega 4. Mutant plasmids were then transformed into BL21(DE3) cell lines for protein expression.

3.2.4 Enzyme Assays

Assays under microaerobic conditions were performed in an anaerobic chamber under an atmosphere of 3% hydrogen: 97% nitrogen, O_2 < 20 ppm (equivalent to ~26 nM dissolved O_2). Assays under aerobic conditions were first prepared in an anaerobic chamber, then removed and exposed to oxygen immediately prior to their initiation. Standard assay conditions include 10 µM Fe^{II} loaded cADO, 100 µM PMS, 1 mM NADH, and 300 µM substrate with a total assay volume of 500 µL in 100 mM HEPES buffer containing 100 mM KCl and 10% glycerol at pH 7.2. All assays were initiated by addition of substrate and shaken at 37 ^{o}C. Octadecanal assays for Michaelis-Menten analysis were performed with substrate concentrations varying from 10 µM to 500 µM. These data were analyzed and fit using Kaleidagraph 4.0.

Assays containing octadecanal, **1**, **2**, **3**, **4**, **5**, and **6** were performed in triplicate in 2 mL Eppendorf tubes for varying lengths of time. Stock solutions were made up in DMSO and dissolved at 70 ^{o}C; the final concentration of DMSO in the assays was 2%. Assays were quenched with 500 µL of ethyl acetate, vortexed, and centrifuged to extract the product to the organic layer, which was then combined with a tridecane internal standard for GC-MS analysis.

Assays containing phenylacetaldehyde were performed similarly to those described above except that 1.5 mL gas tight vials were substituted for Eppendorf tubes. At the end of the reaction period, the vials were shaken vigorously for 3 minutes to volatilize the product. A 1 mL Hamilton gas tight syringe was used to extract 1 mL of headspace for GC analysis.

3.2.5 Quantification of Liquid-Extracted Hydrocarbon Products by GC-MS.

Quantification of liquid extracted hydrocarbon products was performed using a Shimadzu QP-2010 GC-MS equipped with a DB-5 column (30 m x 0.25 mm x 0.25 µm). During hydrocarbon quantification the flow rate of helium carrier gas was 1.0 mL/min with an injection temperature of 200 ^{o}C. 8 µL of sample was injected in splitless mode. Initial temperature was held at 70^{o}C for 2 min, increased to 320 ^{o}C at a rate of 20 ^{o}C/min, and then maintained at 320^{o}C for 2 min. The interface temperature for the MS was 250 ^{o}C and the solvent cut time was 4.5 min. Heptadecane, **7**, **8, 11**, and **12** were identified by authentic standards and concentrations were determined using calibration curves of standards prepared in ethyl acetate. The expected product **9** was not observed. The expected product **10** was identified by observation of a new GC-MS peak and its associated mass. Heptadecane eluted between 8.9 and 9.1 min, **7** and **8** eluted between 11.3 and 11.35 min, **10** eluted between 6.4 and 6.45 min, **11** eluted between 11.35 and 11.4 min, and **12** eluted between 10.8 and 10.9 min. Chromatographic data were analyzed by Shimadzu GC-MS solution software.

3.2.6 Quantification of Headspace-Extracted Hydrocarbon Products by GC.

Quantification of headspace extracted hydrocarbon products was performed using an Agilent 6850 GC equipped with a flame ionization detector and a Restek Rtx-5 capillary column (30 m × 0.25 mm × 0.25 µm). The flow rate of the helium carrier gas was 1.1 mL/min, and the inlet temperature was maintained at 320 °C. Injections were made in split mode with a split ratio 2:1 and a total flow 2.2 mL/min. The oven

temperature was held at 40 °C for 2 min and then increased to 150 at 20 °C/min and finally maintained at that temperature for 2 min. The FID detector was at 260 °C with a continuous flow of H_2 at 40 mL/min and air at 400 mL/min. Toluene and ethylbenze eluted between 4.4 and 4.7 min. Concentrations were determined using calibration curves of standards prepared in buffer. Chromatographic data were analyzed using HP Chem station software.

3.3 Results and Discussion

The bulk of the experiments described here were performed microaerobically, unless otherwise specified, and it should be noted that removing the assay tubes from the anaerobic chamber allows the slow diffusion of O_2 into the sealed tubes so that the concentration of oxygen is certainly significantly higher than 20 ppm (equivalent to ~26 nM dissolved O_2). However, as the enzyme turns over very slowly, even with the relatively high concentration of enzyme (10 μM) the low O_2 concentration does not appear to limit the overall rate of the reaction and minimizes side reactions that deplete the auxiliary reducing system, the products of which appear to inhibit the enzyme. It should therefore be recognized that when measuring alkane formation, although we are not truly under steady state conditions with respect to oxygen (where $[O_2]$ is large relative to enzyme), the microaerobic assay conditions allow for continuous measurement of multiple turnovers and apparent steady state conditions as O_2 is still not the limiting factor in the reaction. This has been confirmed by testing the addition of increasing volumes of aerated buffer to microaerobic assays prepared in gas tight GC vials. The rate

of alkane production remained constant regardless of O_2 concentration as shown in Figure 3.5.

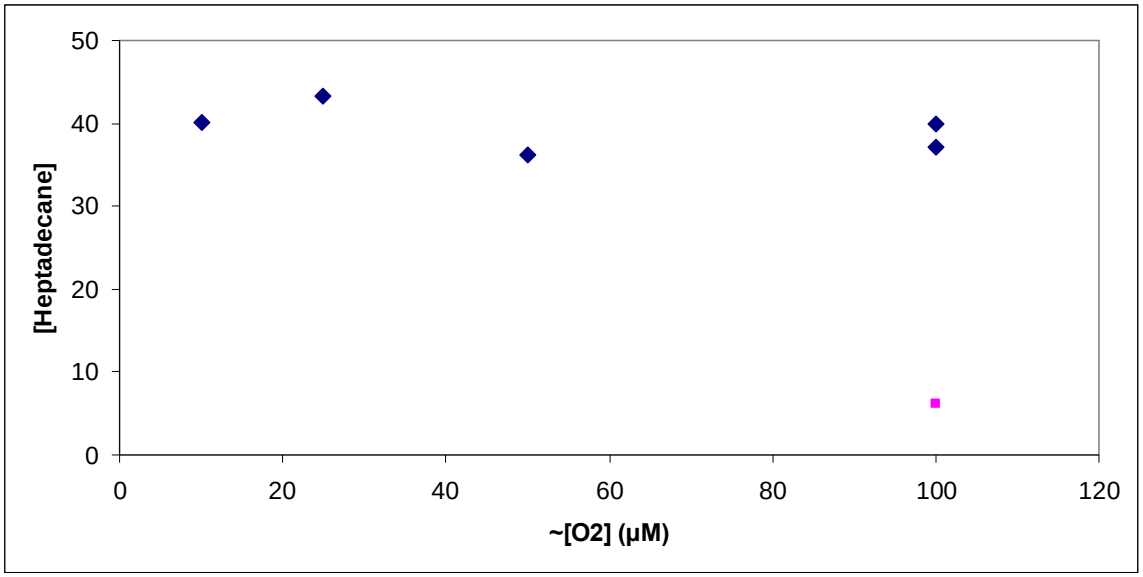

Figure 3.5 – Heptadecane formation in 1 h under standard assay concentrations (10 μM Wt cADO, 100 μM PMS, 1 mM NADH) with increasing O_2 concentration added by addition of aerated buffer, shown in blue. Shown in pink is the background heptadecane formation under conditions with the highest oxygen concentration tested.

3.3.1 Substrate Analogs

A major question posed in the early mechanistic investigations of cADO was whether the observed carbon-carbon bond cleavage proceeded through a radical-based mechanism as hypothesized.[12-14] Attempting to provide evidence for this mechanism, a number of potential substrate analogs were tested for activity with cADO. First, the relatively simple substrate **6** was synthesized with the expectation that the β-γ double bond would rearrange in a radical-based mechanism from the less stable primary to the more stable secondary radical resulting in the product **12**, as shown in Figure 3.8 A. However, under standard microaerobic assay conditions the β-γ double bond in substrate **6** proved to be unstable. The C_α proton was labile enough to allow rearrangement to the

α-β conjugated aldehyde on the timescale of the assay (1 h), which has been shown to inhibit cADO, and in some cases non-enzymatic decarbonylation was observed. As a result, no activity was discernable above the background signal.

The next potential substrate tested was phenylacetaldehyde. It was hypothesized that deformylation would produce a benzyl radical as shown in Figure 3.6 B, which, being more stabilized than the normal alkyl radical created in the deformylation of octadecanal, would allow observation, and possibly trapping, of the radical intermediate.[15-18] In initial aerobic and microaerobic activity assays the formation of the expected product, toluene, was monitored by GC using headspace assays as it was quite volatile, yet phenylacetaldehyde did not appear to interact with the enzyme as no product formation was observed above background. Competition assays with octadecanal initially suggested there was some interaction with the enzyme as octadecanal production was decreased in the presence of phenylacetaldehyde, however, later experiments indicated this was an artifact of the reactive aldehyde damaging the enzyme and no substrate was being turned over.

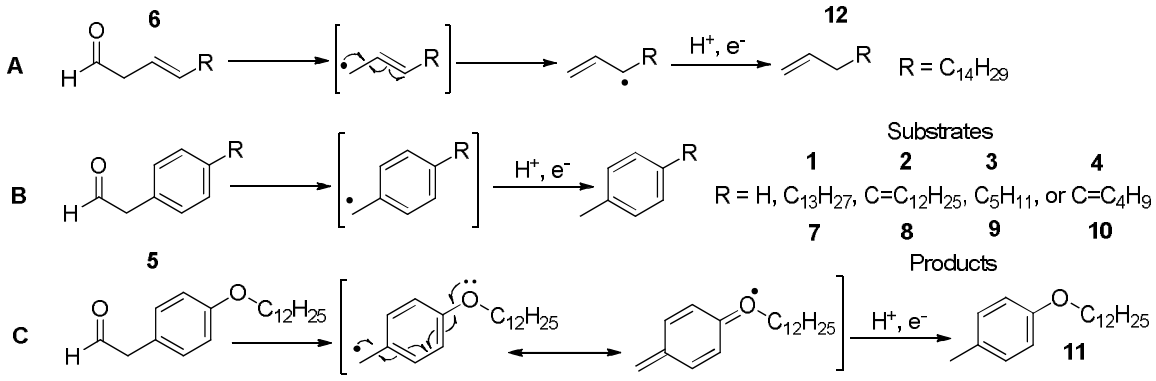

Figure 3.6 – Predicted reactions with substrate analogs. **A** – The mechanism of radical rearrangement by substrate **6** to form product **12**. **B** – The formation of a more stable, benzyl radical by phenylacetaldehyde and substrates **1, 2, 3,** and **4** to produce toluene or products **7**, **8**, **9**, and **10** respectively. **C** – The stabilization of the benzyl radical by formation of a resonance structure using substrate **5** to produce product **11**.

3.3.1.1 Phenylacetaldehyde-Derived Substrate Analogs

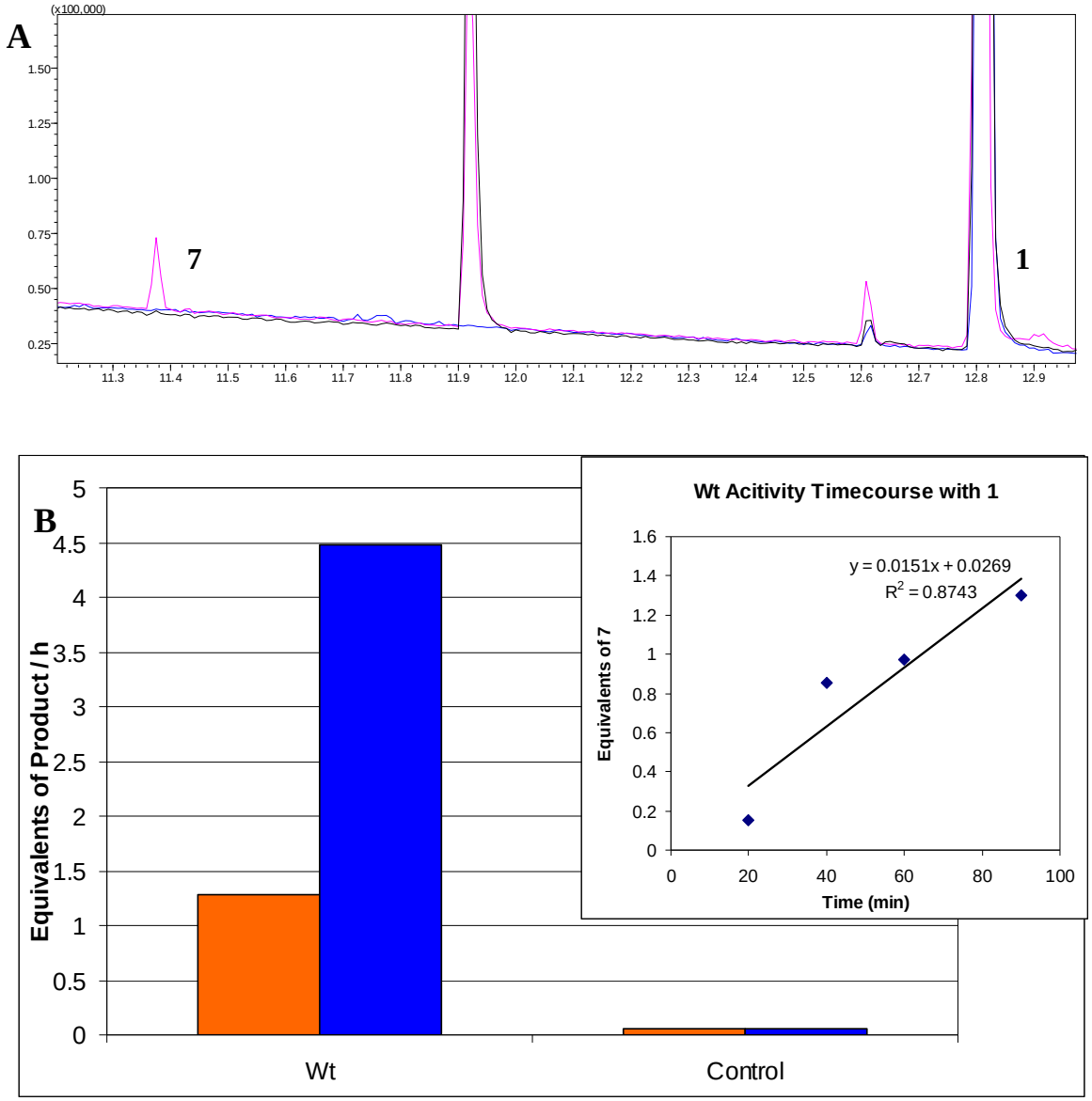

Figure 3.7 – A – GCMS trace of substrate **1** and product **7**. The pink trace indicates the product of a microaerobic assay and contains product **7**. The blue trace shows the no product formed with substrate and enzyme in the absence of reducing system. The black trace shows no product is formed with substrate and reducing system in the absence of enzyme. The y-axis displays peak area and the x-axis displays elution time (min).
B – Comparison of Wt activity with octadecanal, in blue, and substrate **1,** in orange, under microaerobic conditions. The inset shows the time dependent turnover of substrate **1**. The control indicates the background concentration observed in the GCMS traces.

Under the assumption that phenylacetaldehyde was unable to interact with the enzyme in a productive manner due to its steric bulk relative to the narrow and buried active site, we hypothesized that appending a long aliphatic tail to the benzene ring would allow hydrophobicity to dominate substrate binding effects and force the bulky phenylacetaldehyde moiety into the active site. Therefore, the phenylacetaldehyde derivative substrate **1** was synthesized with a $C_{13}H_{27}$ aliphatic tail to mimic the length of octadecanal. As shown in Figure 3.9, under microaerobic conditions substrate **1** did react with cADO, albeit to a much lesser extent than octadecanal. This result was interesting as it indicated that hydrophobicity was able to dominate over steric effects as the major force driving substrate binding.

To further probe this functionality the phenylacetaldehyde derivatives **2**, **3**, **4**, and **5** were synthesized. Substrate **2** was synthesized to explore the effect of further extending the conjugation and therefore the stabilizing effect of the phenyl group on the radical. Substrate **5** was synthesized with the intention of providing additional delocalization to further stabilize the radical on the more electronegative oxygen atom, as shown in Figure 3.8 C. Substrates **3** and **4** were prepared, with C_5H_{11} and C_5H_{10} aliphatic tails respectively, to mimic the length of heptanal and to test the effect of the length of the aliphatic chain, and therefore hydrophobicity, on the activity of the substrate. The activity comparison of these substrate analogs is shown in Figure 3.8 and clearly indicates a trend in the structure activity relationship of the substrates. For comparison, the microaerobic activity of substrate **1** represents the turnover of 1.3 equivalents per hour as shown in Figure 3.7.

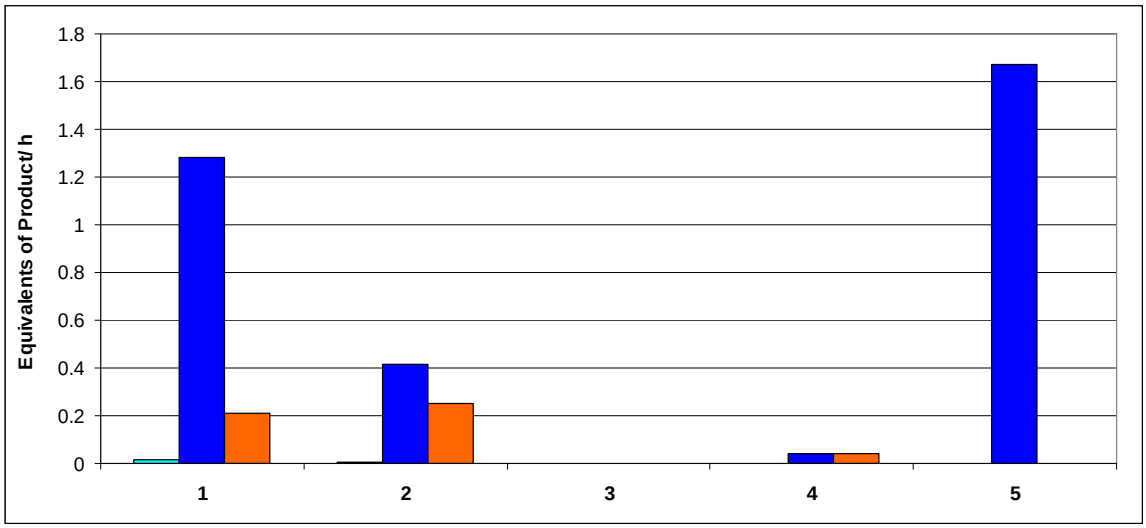

Figure 3.8 – Comparison of the relative activity of the phenylacetaldehyde derived substrate analogs under microaerobic assay conditions, shown in blue, and aerobic assay conditions, shown in orange. The no-enzyme control is shown in cyan.

Although compound **3** showed no product formation, the activity of the unsaturated form, substrate **4**, was observed at just above background levels. This represents only the smallest fraction of a turnover, but indicates that a shorter chain phenylacetaldehyde derived substrate analog could react with cADO. Comparing the saturated long and short chain substrates **1** and **3** or the unsaturated substrates **2** and **4** supports the hypothesis that increasing the hydrophobicity of a substrate improves the activity and, therefore, the binding of that substrate. Alternatively, it can be said that favorable hydrophobic binding effects are in a fine balance with unfavorable steric effects between substrate and enzyme. The significant loss in activity observed when decreasing the effective substrate length in the substrate analogs is not observed with the standard aldehydes, octadecanal and heptanal. This suggests that to overcome the steric effects, the hydrophobicity of a substrate needs to be increased as much as possible.

Comparison of long chain substrates **1** and **2** indicates that introducing the additional double bond in substrate **2** significantly lowers the activity under microaerobic conditions. This is likely due to increased steric hindrance of the substrate in the active site because the double bond would be planar with the benzene ring. This would act to increase the rigidity of the substrate, and therefore the inflexible steric volume occupied by the phenylacetaldehyde head group. Two product peaks were observed in the GC-MS trace for substrate **2**, indicating the cis and trans forms of the product **8**, in an approximately 60:40 split. This suggests that neither stereoisomer was significantly more active than the other and that sterics do not appear to be important. The trend appears to hold with the short chain substrates **3** and **4,** although, due to the very low activity with the short chain substrates it is difficult to make a strong claim.

Substrate **5** had comparable activity to substrate **1** and under microaerobic conditions and they both turned over more than one equivalent per hour, although no product was observed under aerobic conditions. It was predicted that the turnover of substrates **1** and **5** might be observable by UV-vis spectroscopy because the stabilized benzyl radicals have characteristic absorption maxima at 320 and 290 nm respectively.[18] However, the timescale of the reaction proved to be too slow to observe a significant absorption change at the expected wavelengths. Additionally, both the enzyme and the reducing system were in much higher concentrations than the product and absorbed in the same region, obscuring any possible observation of the intermediates.

Under aerobic conditions the phenylacetaldehyde substrate analogs were generally less active. This appeared to be due to the slow turnover rate that allowed the reducing system to be consumed through futile cycling before a significant concentration

of substrate could react, as has been observed previously with octadecanal. Turnover of small amounts of substrates **1, 3,** and **4** was observed, however, we attribute this to pre-equilibration of substrate and enzyme before the addition of oxygen allowing for a small burst phase production of products **7**, **8**, and **10** and not steady state conditions.

Ultimately, a different study using the cyclopropyl and oxiranyl substrate analogs, rather than these phenylacetaldehyde derivatives, confirmed the existence of a radical as central to the mechanism of cADO.[19,20] In that study, an irreversible side reaction with the enzyme was attributed to the stabilizing effect of the cyclropropyl radical clock substrate. Interestingly, the stabilized benzyl radical expected to form with the phenylacetaldehyde derived substrates did not appear to covalently modify the protein, as shown by LC-MS data in Figure 3.9.

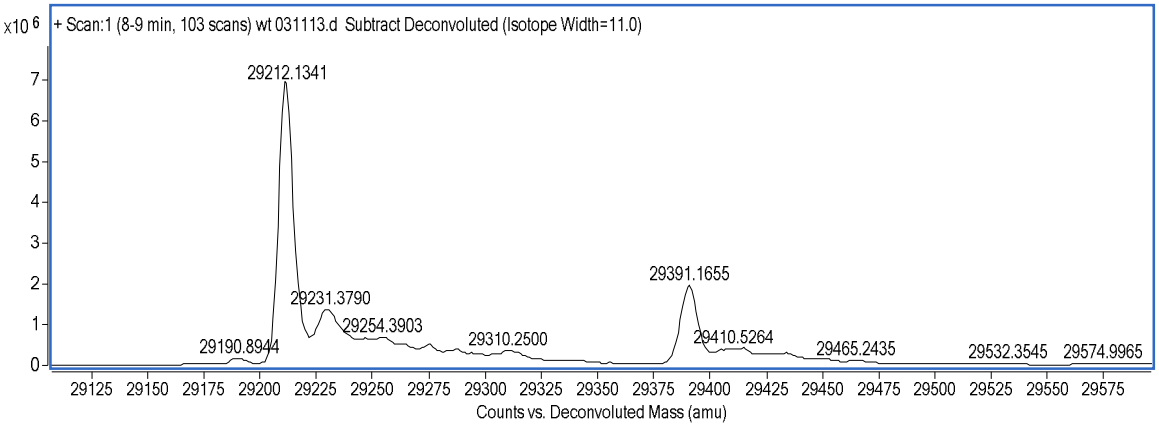

Figure 3.9 – LC-MS data indicating the expected mass of Wt enzyme (29212 amu) after reaction with **1** and that no covalently modified protein was observed (29484 amu).

3.3.2 Mutagenesis

Mutagenesis is a common tool used in enzyme investigations to explore the mechanism,[9,21,22] but based on analysis of the crystal structure and the SIE study there are

no residues that are directly involved in the mechanism of cADO. However, the SIE study in chapter 2 also suggested that substrate binding may be important as a non-chemical RDS and the structure activity relationships of the phenylacetaldehyde derived substrate analogs indicated that the high hydrophobicity of the binding pocket was important in mediating substrate binding. Analysis of the recent crystal structures of cADO, shown in Figure 3.3, shows three hydrophobic regions in the binding channel that may have an important effect on substrate specificity and binding affinity. Mutagenesis was performed to better understand the way substrates and products interact with the active site and these regions of the binding channel.

The first region was the area surrounding the active site. Analysis of the crystal structure in Figure 3.10 A shows the side chain of residue I127 in multiple conformations. This suggests it is flexible and potentially in a gating position where it may control substrate access or lock it in place. This residue was mutated to Leu, Val, and Ala to modulate the hydrophobic volume. The goal was to study the possibility of the I127 being a gating residue and whether changing the steric influence of this position would change the way the substrate would react with the enzyme. F100 was also chosen to be mutated to Ala to facilitate the binding of phenylacetaldehyde and other substrate analogs. Figure 3.10 B shows the overlay of phenylacetic acid in the active site, in place of the stearic acid, as a model for the substrate analogs and shows the clashing of the benzene ring with I127 and F100.

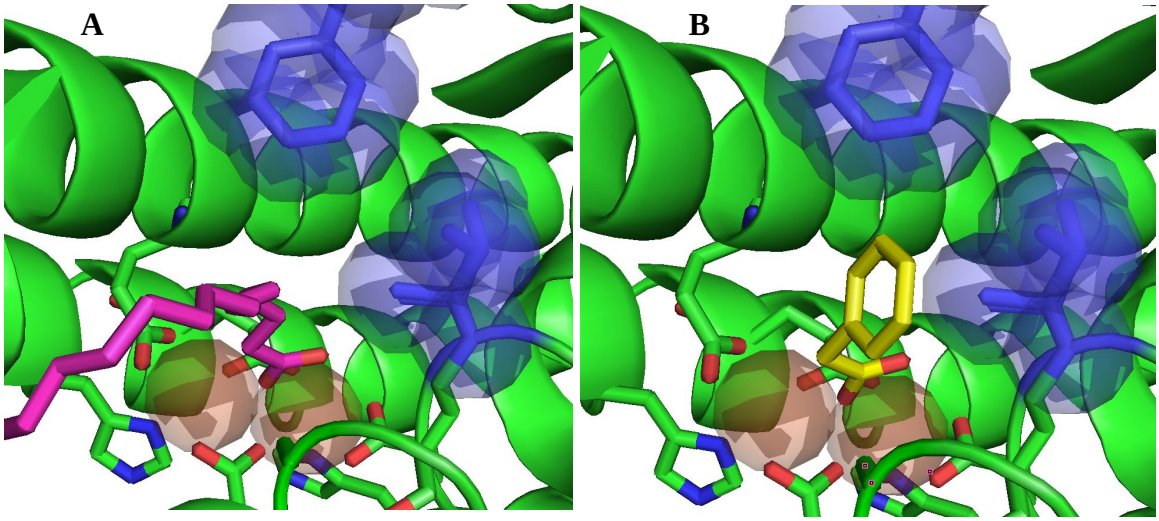

Figure 3.10 – A – Wt crystal structure of cADO (pdb 2OC5) showing the active site with stearic acid bound in purple. **B** – Wt crystal structure showing phenylacetic acid overlaid where the stearic acid is normally bound. The residues in blue were chosen for mutations. The iron atoms are shown as spheres in brown.

The second area to be mutated was the hydrophobic pocket. According to the recent structure shown in Figure 3.3 A, two of the long-chain substrate binding modes terminate with the alkyl chain in this buried region.[11] One is the first productive binding mode with the aldehyde presented to the diiron core. The other is an entirely non-productive binding mode where the remainder of the alkyl chain occupies the opening of the binding pocket and the polar head group is exposed to solvent. As there are no obvious residues involved involved in substrate binding interactions, this hydrophobic pocket may play a role in locking the substrate in position with the aldehyde functionality presented to the diiron core or it may be involved preventing product release. The residues I37 and V41 were chosen to be mutated to I37F and V41I to fill the hydrophobic void, restricting access to the hydrophobic pocket as shown in the overlaid Figures 3.11 A and B, and in doing so inform on the first productive binding mode.

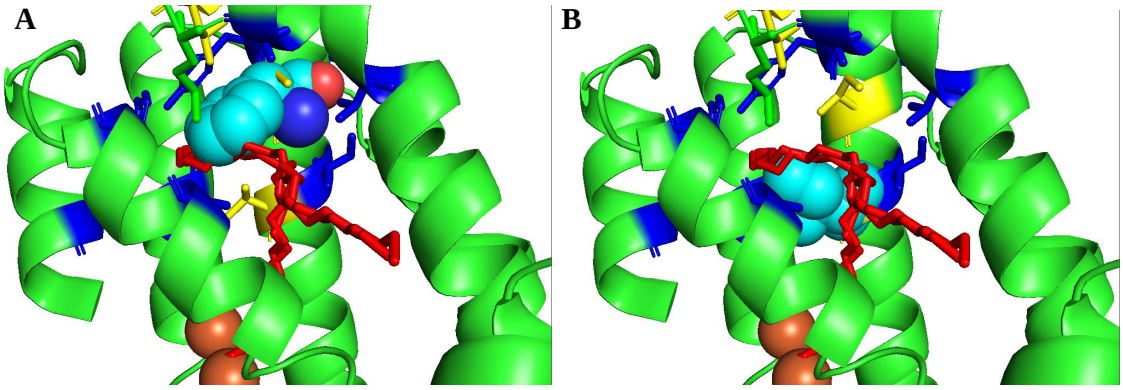

Figure 3.11 – Crystal structures cADO mutant L194A (pdb 4PGI) with an obscuring helix removed to show the hydrophobic binding pocket. Blue and yellow residues are those that make up the surface of the pocket. The substrate 11-(2-(2-ethoxyethoxy) ethoxy)undecanal is shown in red and partially occupies three different conformations. **A** – Shows the space filling overlay of Phe, in cyan, onto I37. **B** – Shows the space filling overlay of Ile, in cyan onto V41.

The third region to be mutated was the opening of the binding pocket. In the crystal structure with long chain substrate bound, this channel contained the tail of the substrate in the second productive configuration.[11] Most of the substrate in the entirely non-productive binding mode, where the polar head group would be exposed to solvent, occupies this space as well. In the second crystal structure with short-chain carboxylic acids bound, shown in Figure 3.12 A, a second carboxylic acid molecule is also apparently bound in this region. The intention here was to introduce polar and charged residues that would inform on the second productive binding conformation, potentially destabilize the non-productive binding configuration, and promote product release by making the binding pocket overall more hydrophilic. The residue I212 was mutated to Asn and L194 was mutated to Thr or Glu as shown in Figure 3.12 B.

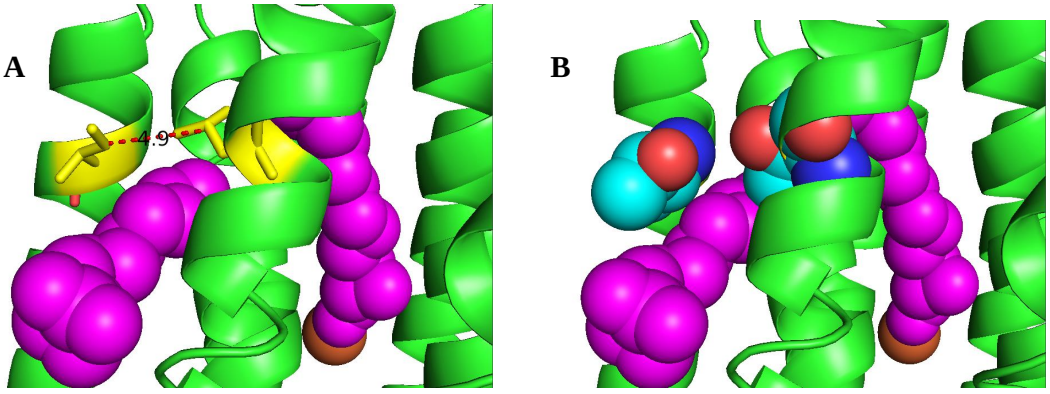

Figure 3.12 – Wt crystal structure of cADO with two molecules of trans-2-nonyl cyclopropane-1-carboxylic acid, shown in purple, bound (pdb 4PG1). **A –** Shows the mutation sites in yellow and **B –** Shows the space filling overlay of the Asn and Thr residues, in cyan, blue, and red, on I212 and L194 respectively.

3.3.2.1 Mutant Activity

Active site mutants I127L, I127V, and I127A decreased in activity as the hydrophobic void size increased, but were not significantly reduced relative to Wt, as shown in Figure 3.13. Although F100A was observed to be significantly less active than Wt, all of the active site mutants exhibited linear activity with respect to time as shown in Figure 3.14.

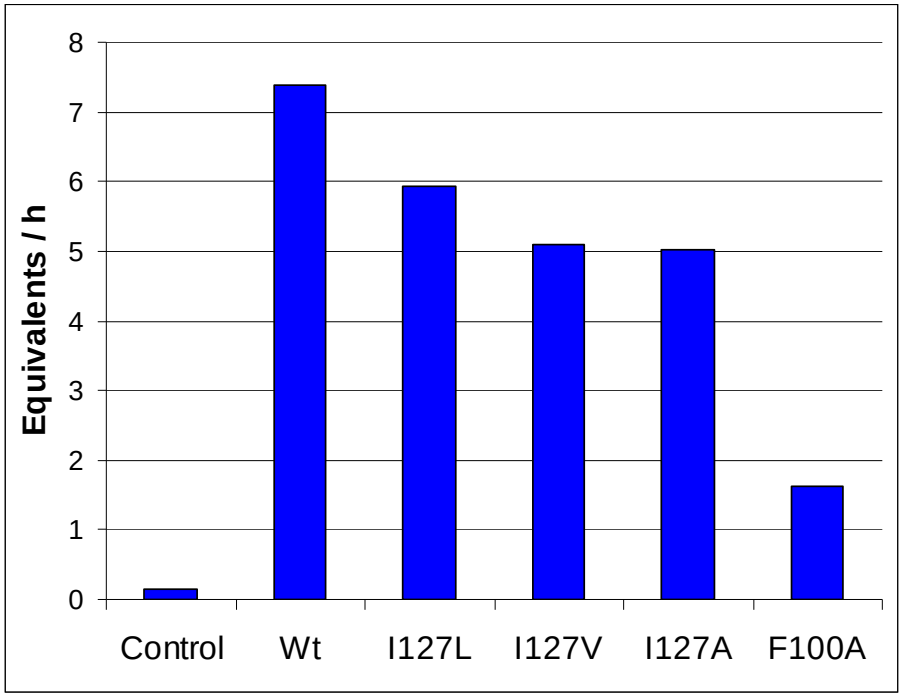

Figure 3.13 – Activity comparison of active site mutations relative to Wt with octadecanal as a substrate.

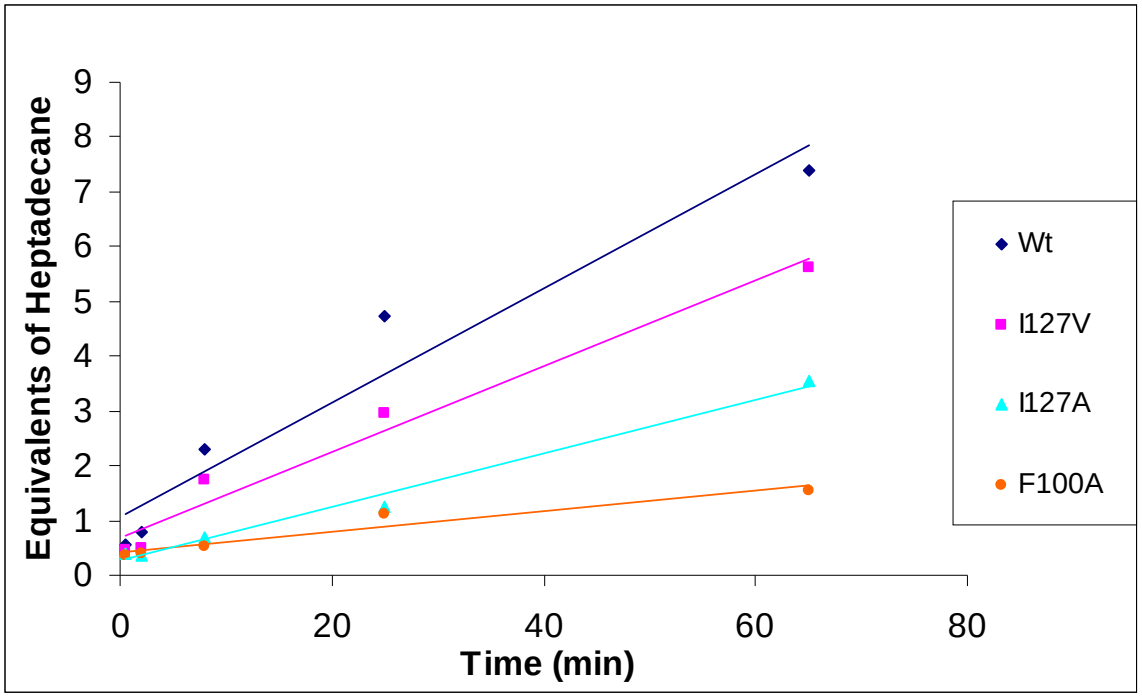

Figure 3.14 – Time course of heptadecane formation from octadecanal for the active site mutants.

The hydrophobic pocket mutant I37F was not active, which was not surprising considering the increase in side chain size, but V41I was observed to be active as indicated in the time course shown in Figure 3.15.

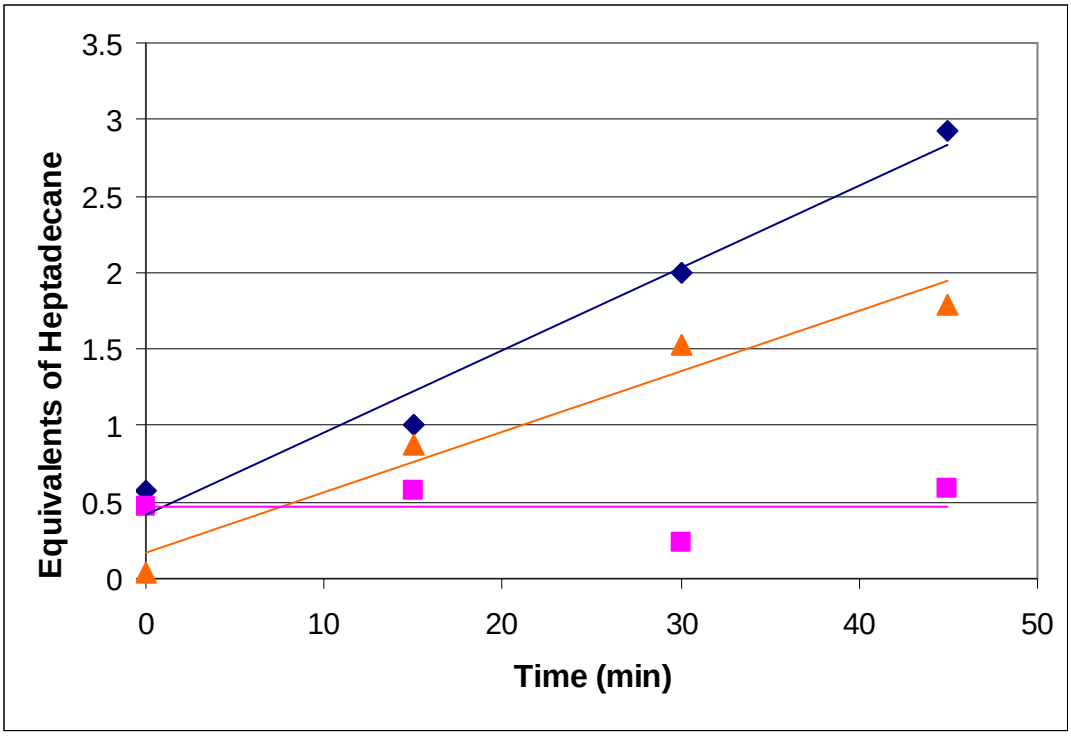

Figure 3.15 – Time course activity of heptadecane formation by hydrophobic pocket mutants with octadecanal. Wt is shown in blue, V41I is shown in orange, and I37F is shown in pink.

The hydrophilic mutants made in the opening of the binding pocket were the least active as shown in Figure 3.16. L194E was essentially inactive, but L194T and I212N were active, at low levels.

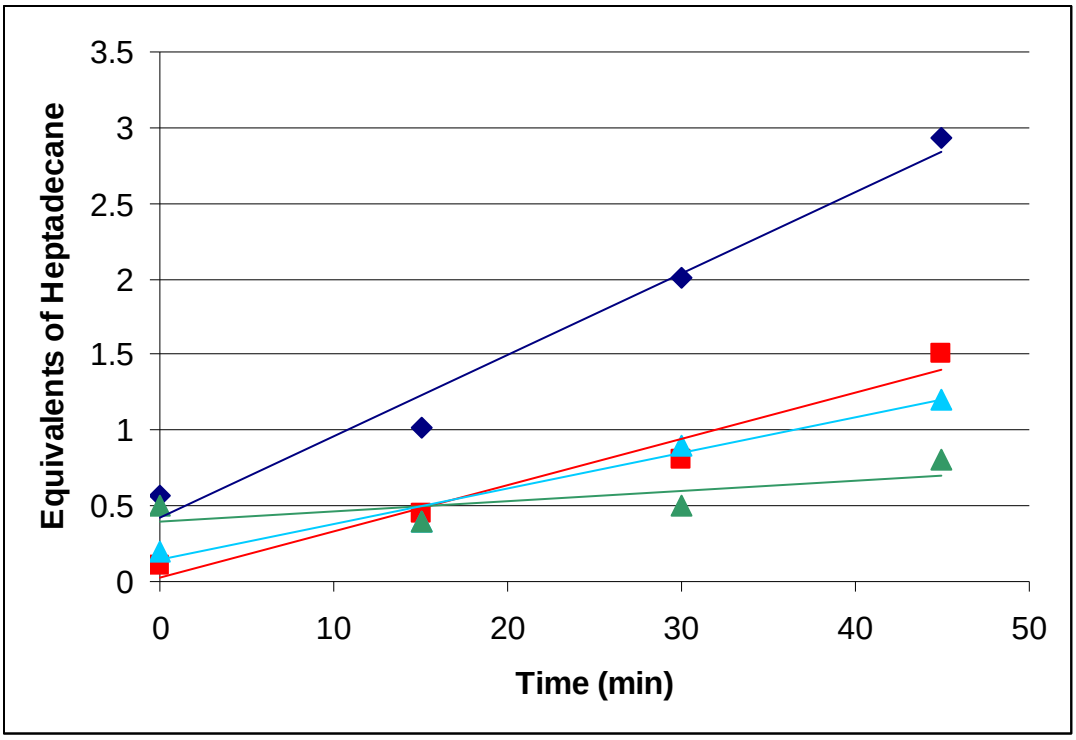

Figure 3.16 – Time course activity of heptadecane formation from octadecanal by hydrophilic mutants in the opening of the binding pocket.

3.3.2.2 Michaelis-Menten Kinetics

The kinetics of heptadecane formation were measured with cADO and the active mutants as shown in Figure 3.17. They were fit to the Michaelis-Menten equation and the apparent kinetic parameters k_{cat}^{app} and K_M^{app} were determined for each. A summary of the kinetic parameters is shown in Table 3.18.

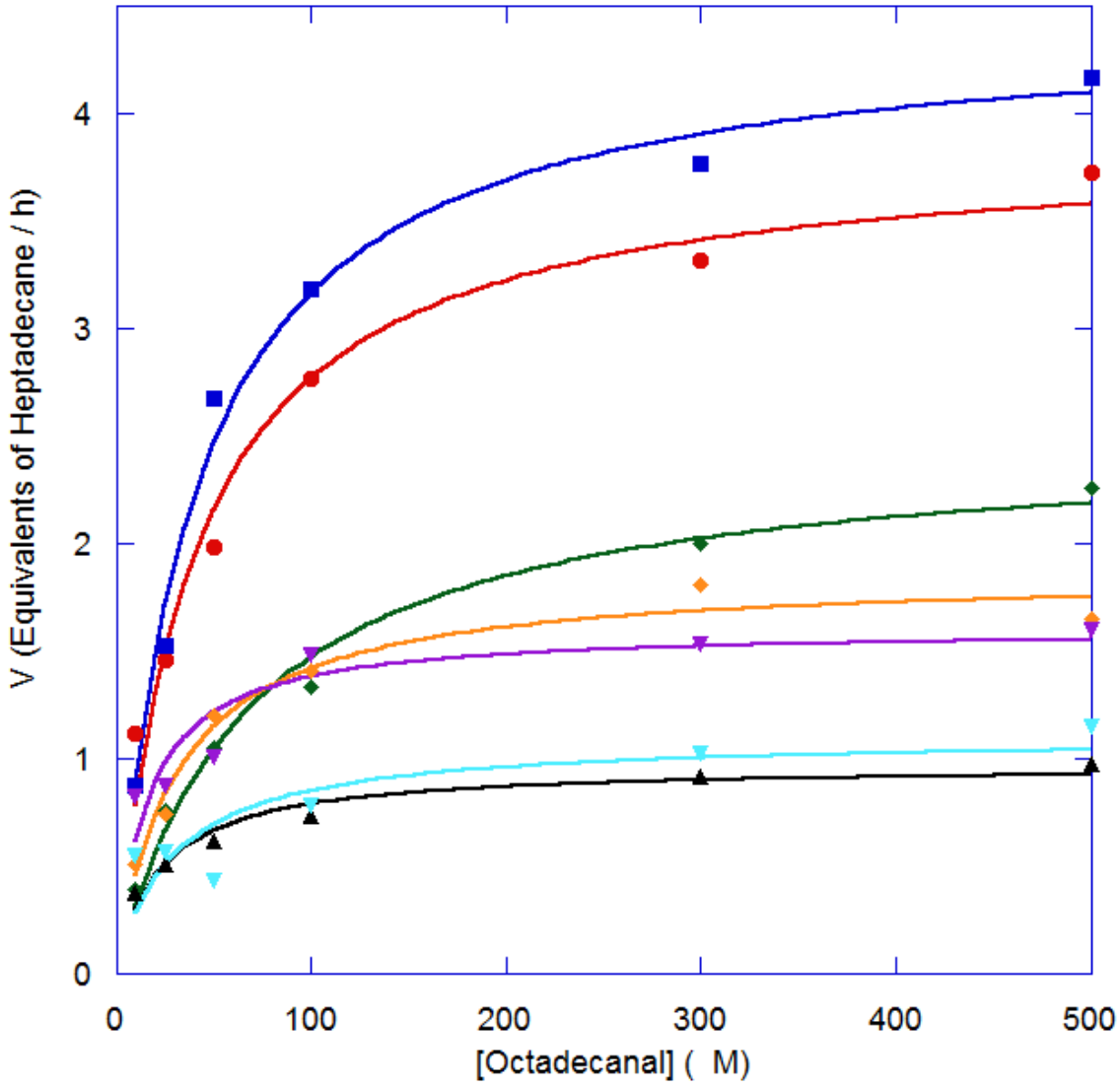

Figure 3.17 – Michaelis-Menten plot of heptadecane formation with Wt (red) and the mutants I127V (blue), I127A (black), V41I (green), L194T (orange), I212N (purple), and L194E (cyan).

Mutation Location	Enzyme	k_{cat}^{app} (min^{-1})	±	K_M^{app} (μM)	±	k_{cat}^{app}/K_M^{app} (mM^{-1} min^{-1})	±
	Wt	0.064	0.0034	39	7.5	1.6	0.32
Active Site	I127V	0.074	0.0026	40	5.0	1.9	0.24
	I127A	0.016	0.0057	22	4.9	0.72	0.30
Hydrophobic Pocket	V41I	0.042	0.0020	69	11	0.61	0.10
Binding Pocket Opening	L194T	0.031	0.0014	31	5.5	1.0	0.18
	I212N	0.027	0.0020	16	5.7	1.7	0.62
	L194E	0.018	0.0029	29	18	0.62	0.40

Table 3.18 – Table of the kinetic parameters of heptadecane formation determined by Michaelis-Menten fits to the plot in Figure 3.17.

3.3.2.3 Implication of Michaelis-Menten Kinetics on Substrate Binding

The k_{cat}^{app} values for the various mutants vary significantly, but with the exception of I127V, none of them are greater than wt. This makes interpretation of the kinetics, and therefore whether substrate binding is a RDS, difficult as it is unclear whether the decrease in activity this represents is a factor of a destabilizing mutation or an effect on the binding of the substrate as we sought to observe. This analysis is further complicated because, as the k_{cat}^{app} values for cADO are so low, small variations between enzyme preparations or assay conditions can result in large effects in the kinetic parameters observed. In fact, any variation of less than 1 equivalent/h is difficult to

interpret. This appears to be the case with the active site mutants as k_{cat}^{app} seems to be inflated for I127V and deflated for I127A relative to the previous activity data displayed in Figure 3.13. This variability is most likely why the observed k_{cat}^{app} for Wt is lower than the previously reported value.[12] Additionally the magnitude of the reported value is dependent on a burst phase that has been difficult to reproduce. However, some interesting observations can be made from this data set.

The kinetic parameter K_M can be useful in describing substrate binding under certain conditions as it is considered to be inversely related to substrate binding strength, although it is important to note that K_M does not necessarily approximate K_d. As such we cannot necessarily make a strong claim about the relatively close K_M^{app} values we determined for the majority of the mutants as they are within error. In the case of V41I, however, there is a significant difference as the K_M^{app} of the mutant is approximately 175% larger than that of the Wt enzyme. This might suggest that octadecanal does not bind as strongly in the V41I mutant. Put another way, these data may suggest that restricting the volume of the hydrophobic pocket in the V41I mutant reduces binding affinity with octadecanal. Based on analysis of the crystal structures this could indicate that the preferred binding conformation of long chain substrates is the one where the aliphatic tail region is buried in the hydrophobic pocket. This is consistent with the position of stearic acid, thought to be a substrate mimic, in the Wt crystal structure.

It should be noted, however, that this result could be due simply to restricting the diameter of the binding channel at the junction where the hydrophobic pocket meets the active site channel and the opening of the binding pocket. Previous studies comparing kinetics of octadecanal deformylation found a reduction in k_{cat} from 0.06 min^{-1} in the Wt

enzyme, the same as observed here, to 0.01 min^{-1} in a V41Y mutant.[21] From analysis of the crystal structure they obtained, it would appear that the bulkier ring of the tyrosine side chain occludes not only the hydrophobic binding pocket but also the space of the main binding channel. In this study, V41I was selected as a more modest mutation to restrict access to the hydrophobic pocket while not interfering with the main binding channel and as a result we observed a k_{cat}^{app} of 0.04 min^{-1}. As this is four fold larger than the k_{cat}^{app} observed for the V41Y mutation, this would suggest that the activity decrease associated with the tyrosine mutant is a result of blocking the main binding channel and, although we cannot rule out the possibility, this also suggests that the isoleucine mutation is not significantly blocking the main binding channel. Therefore, we conclude that the observed increase in K_M^{app} is due primarily to blocking the hydrophobic pocket, likely destabilizing the preferred binding conformation.

Finally, the hydrophilic mutations in the opening of the binding pocket are an interesting case. The polar mutations I212N and L194T are active at low levels, but unsurprisingly the charged mutant L194E is essentially inactive. Interestingly, while all of the hydrophilic mutations in the opening of the binding pocket have much lower k_{cat}^{app} values than Wt, I212N has a k_{cat}^{app}/K_M^{app} comparable to Wt. This appears to be due to I212N being the only mutant with a significantly lower K_M^{app}, within experimental error, than that of the Wt. This might suggest that introducing some polarity into the opening of the binding pocket increased the binding affinity with octadecanal. This effect may be due to elimination of the non-productive binding mode making the active site generally more accessible. Alternatively, and more interestingly, this effect could be due destabilization of the second productive binding mode in which the aldehyde group is

presented towards the active site and the tail is oriented towards to the opening of the binding pocket, which would suggest it is not as productive as originally anticipated. This may also promote the productive binding configuration where the tail is buried in the hydrophobic pocket, and would be consistent with the results observed with the V41I mutant.

3.4 Conclusion

Although this study was unable to definitively resolve the issue of whether substrate binding and product release is a non-chemical RDS, we have been able to learn more about the effects governing octadecanal binding affinity. It appears that hydrophobicity plays a dominant role in this area and that by modulating the hydrophobic volume or introducing hydrophilicity into the binding pocket we can affect and control the substrate affinity, if not improve the rate of reaction. Furthermore, these data suggest that the most productive binding mode is when the tail of the aldehyde substrate is buried in the hydrophobic pocket. Future experiments should focus on mutagenesis introducing polar residues, possibly as double mutants, in more varied positions in both the hydrophobic pocket as well as the binding pocket opening to further explore the effects observed here.

3.5 References

(1) Kallio, P.; Pasztor, A.; Thiel, K.; Akhtar, M. K.; Jones, P. R. (2014) An engineered pathway for the biosynthesis of renewable propane, *Nature commun*, *5*, 4731.

(2) Zhang, F.; Rodriguez, S.; Keasling, J. D. (2011) Metabolic engineering of microbial pathways for advanced biofuels production, *Curr. opin. biotechnol.*, *22*, 775.

(3) Pandelia, M. E.; Li, N.; Norgaard, H.; Warui, D. M.; Rajakovich, L. J.; Chang, W. C.; Booker, S. J.; Krebs, C.; Bollinger, J. M., Jr. (2013) Substrate-triggered addition of dioxygen to the diferrous cofactor of aldehyde-deformylating oxygenase to form a diferric-peroxide intermediate, *J. Am. Chem. Soc.*, *135*, 15801.

(4) Eser, B. E.; Das, D.; Han, J.; Jones, P. R.; Marsh, E. N. G. (2011) Oxygen-Independent Alkane Formation by Non-Heme Iron-Dependent Cyanobacterial Aldehyde Decarbonylase: Investigation of Kinetics and Requirement for an External Electron Donor, *Biochemistry*, *50*, 10743.

(5) Aukema, K. G.; Makris, T. M.; Stoian, S. A.; Richman, J. E.; Munck, E.; Lipscomb, J. D.; Wackett, L. P. (2013) Cyanobacterial aldehyde deformylase oxygenation of aldehydes yields n-1 aldehydes and alcohols in addition to alkanes, *ACS Catal*, *3*, 2228.

(6) Wallar, B. J. L., J. D. (1996) Dioxygen Activation by Enzymes Containing Binuclear Non-Heme Iron Clusters, *Chem. Rev.*, *96*.

(7) Eser, B. E.; Das, D.; Han, J.; Jones, P. R.; Marsh, E. N. (2011) Oxygen-independent alkane formation by non-heme iron-dependent cyanobacterial aldehyde decarbonylase: investigation of kinetics and requirement for an external electron donor, *Biochemistry*, *50*, 10743.

(8) Wallar, B. J. L., J. D. (1996) Dioxygen Activation by Enzymes Containing Binuclear Non-Heme Iron Clusters, *Chem. Rev.*, *96*, 2625.

(9) Jia, C.; Li, M.; Li, J.; Zhang, J.; Zhang, H.; Cao, P.; Pan, X.; Lu, X.; Chang, W. (2015) Structural insights into the catalytic mechanism of aldehyde-deformylating oxygenases, *Protein & cell*, *6*, 55.

(10) Pandelia, M. E.; Li, N.; Norgaard, H.; Warui, D. M.; Rajakovich, L. J.; Chang, W. C.; Booker, S. J.; Krebs, C.; Bollinger, J. M. (2013) Substrate-Triggered Addition of Dioxygen to the Diferrous Cofactor of Aldehyde-Deformylating Oxygenase to Form a Diferric-Peroxide Intermediate, *J. Am. Chem. Soc.*, *135*, 15801.

(11) Buer, B. C.; Paul, B.; Das, D.; Stuckey, J. A.; Marsh, E. N. (2014) Insights into substrate and metal binding from the crystal structure of cyanobacterial aldehyde deformylating oxygenase with substrate bound, *ACS chem biol*, *9*, 2584.

(12) Das, D.; Eser, B. E.; Han, J.; Sciore, A.; Marsh, E. N. G. (2011) Oxygen-independent decarbonylation of aldehydes by cyano-bacterial aldehyde decarbonylase: a new reaction of di-iron enzymes, *Angew. Chem.*, *50*, 7148.

(13) Li, N.; Norgaard, H.; Warui, D. M.; Booker, S. J.; Krebs, C.; Bollinger, J. M. (2011) Conversion of fatty aldehydes to alka(e)nes and foramte by a

cyanobacterial aldehyde decarbonylase: crypric redox by an unusual dimetal oxygenase, *J. Am. Chem. Soc.*, *133*, 7148.
(14) Warui, D. M.; Li, N.; Norgaard, H.; Krebs, C.; Bollinger, J. M.; Booker, S. J. (2011) Detection of Formate, Rather than Carbon Monoxide, As the Stoichiometric Coproduct in Conversion of Fatty Aldehydes to Alkanes by a Cyanobacterial Aldehyde Decarbonylase, *J. Am. Chem. Soc.*, *133*, 3316.
(15) Egorov, A. M.; Matyukhova, S. A.; Anisimov, A. V. (2005) Kinetics and mechanism of the reaction of benzyl bromide with copper in hexamethylphosphoramide, *Int. J. Chem. Kinet.*, *37*, 296.
(16) Cook, M. D. R., B. P. (1982) Liquid Xenon as a Solvent for E.S.R Studies, *J. Chem. Soc., Chem. Commun*, 264.
(17) Xu, M. a. L., J. H. (1995) The Formation fo Gas Phase Benzyl Radicals during the Reaction fo Toluene and Nitros Oxide over Li-MgO and Sr-La2O3 Coupling Catalysts, *J. Chem. Soc., Chem. Commun*, 1203.
(18) Tokumura, K. O., T.; Nosaka, H.; Saigusa, Y.; Itoh, M. (1991) Excited-State and Ground-State Reactivities of Para-Substituted Benzyl Radicals toward Molecular Oxygen, *J. Am. Chem. Soc.*, *113*, 4974.
(19) Das, D.; Ellington, B.; Paul, B.; Marsh, E. N. G. (2014) Mechanistic Insights from Reaction of alpha-Oxiranyl-Aldehydes with Cyanobacterial Aldehyde Deformylating Oxygenase, *ACS Chem. Biol.*, *9*, 570.
(20) Paul, B.; Das, D.; Ellington, B.; Marsh, E. N. (2013) Probing the mechanism of cyanobacterial aldehyde decarbonylase using a cyclopropyl aldehyde, *J. Am. Chem. Soc.*, *135*, 5234.
(21) Khara, B.; Menon, N.; Levy, C.; Mansell, D.; Das, D.; Marsh, E. N.; Leys, D.; Scrutton, N. S. (2013) Production of propane and other short-chain alkanes by structure-based engineering of ligand specificity in aldehyde-deformylating oxygenase, *Chembiochem*, *14*, 1204.
(22) Hayashi, Y.; Yasugi, F.; Arai, M. (2015) Role of Cysteine Residues in the Structure, Stability, and Alkane Producing Activity of Cyanobacterial Aldehyde Deformylating Oxygenase, *PloS one*, *10*, e0122217.

Chapter 4 Protein Electrochemistry

4.1 Introduction

Although cADO is of great interest to the scientific community for its potential as a biofuel-producing enzyme, it is perhaps more interesting for the unique chemistry it performs. All of the ADs perform chemistry that is highly unusual for their class and structure, yet cADO shares an active site nearly identical to that of the well understood non-heme diiron oxygenase MMOH, as shown in Figure 4.1 A and B.[1,2] They have similar requirements for O_2 and external electrons and both perform oxidative chemistry, but the mechanism of oxidation is distinct from MMOH and indeed every other non-heme diiron oxygenase. Based on the structural comparison we would expect cADO to utilize two electrons and O_2 to abstract a hydrogen from a C-H bond, forming a hydroxyl radical that would rebound to oxidize the carbon. Instead cADO employs four electrons and O_2 to perform a nucleophilic addition at the carbonyl carbon that initiates C_1-C_α bond cleavage resulting in two products, including the oxidized carbonyl carbon, and full reduction of the second O atom to water.[3,4] This raises an interesting question as to why cADO is capable of performing this unusual chemistry given that its active site is structurally very similar to MMOH. The question naturally asks “How is the active site of cADO different from MMOH?”

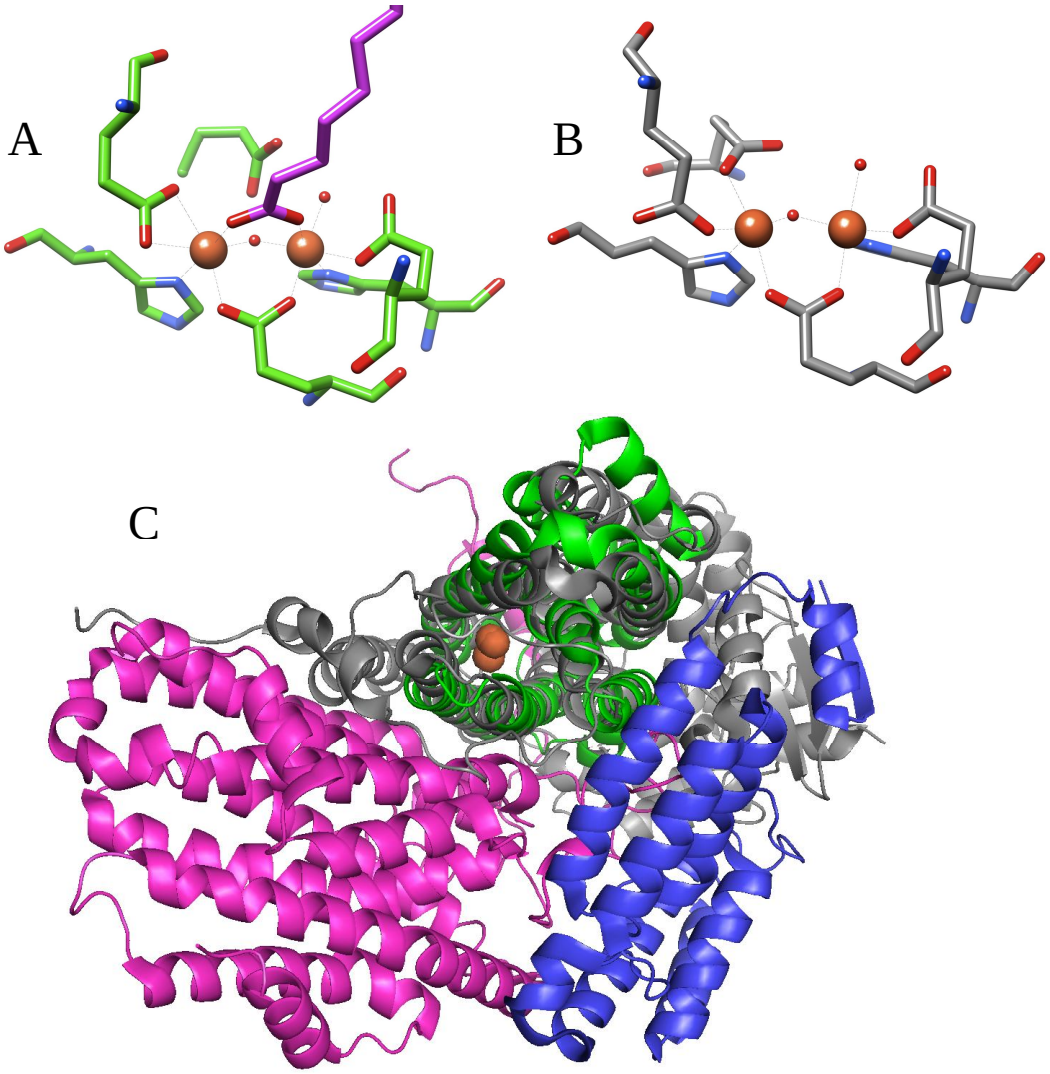

Figure 4.1 – Side by side comparison of the active sites of **A** – cADO and **B** –MMO. **C** – Comparison of the structures of cADO (pdb 2OC5) and MMOH (pdb 1XVC). The structure of cADO, shown in green, is overlaid on the α subunit of MMOH, shown in gray. The additional β and γ subunits of MMOH are shown in pink and blue; the diiron centers of both enzymes closely overlay and are shown in orange. Figures 3A and 3B are based on reference 2.

While the active sites appear nearly identical and the anti-parallel four α-helix bundle fold is conserved, cADO is much smaller and lacks the bulk of the protein architecture present in MMOH, as shown in Figure 4.1 C.[1] This means that it does not contain the binding sites for the cognate reductase or the B component that increases the

activity of MMOH 1000-fold.[5,6] Furthermore, there is evidence to suggest that the complex regulatory control mediated by these associated proteins causes a structural change in the hydroxylase subunit of MMO upon binding of the B component.[7,8] It is possible that the differences observed in the cADO system arise from the lack of this putative activating factor to stimulate a structural change. This would be difficult to test with cADO as no complimentary binding partners have been identified; however, MMOH retains the radical rebound mechanism even without the B component, which suggests this structural change does not affect the fundamental mechanistic pathway.

As the difference in activity does not appear to arise from steric differences in the active site or the larger structural dissimilarities due to size and number of subunits, it would seem plausible that the difference may be a more subtle electronic one. This is supported by Mössbauer spectroscopy indicating the electronic structure of the two iron atoms are nearly equivalent in cADO as a result of identical ligand environments, while in MMO the two iron sites are not homogeneous.[9] Given that beyond the active site itself cADO and MMO do not share a great deal of sequence identity, we can likely attribute this to differences in the amino acids involved in second sphere coordination.

In both cADO and MMO, all of the chemistry occurs between the substrate and the diiron core itself, and there are no additional residues directly involved in the reaction. Therefore, small differences in the ligand environment of the diiron cores, which lead to variations in electrostatic effects and electrochemical reduction potential, might play a significant role in determining the available reaction pathways. The modulation of reduction potential due to manipulation of second sphere coordinating residues has been studied extensively with the cuppredoxin azurin.[10,11] Binding of the B

component also perturbs the second sphere coordination network and the observed conformational change has an additional effect on MMOH from *M. trichosporium*.[7] The reduction potentials of the diiron core of MMOH alone were determined to be E_1^o = +76 mV and E_2^o = +21 mV (± 15 mV vs SHE), yet upon addition of the B component and formation of the MMOH-MMOB complex the observed reduction potentials shifted to E_1^o = -52 mV and E_2^o = -115 mV (± 15 mV).

In this chapter I describe the protein film voltammetry (PFV) studies that I undertook to further explore the electrochemical properties of cADO with the goals of determining the reduction potential, or potentials, of the diiron core and of measuring the kinetics of electron transfer. In these experiments, electrode potential is a variable used to probe the mechanism of cADO. As previously noted in chapter 3, the slow transfer of reducing equivalents at a key point in the mechanism may constitute a non-chemical rate limiting step. Adding the variable of electrode potential may provide insight into this and elucidate other interesting mechanistic features that are otherwise difficult to observe through standard kinetic analyses.

The work described in this chapter was performed in collaboration with the Maldonado Laboratory. Prof. Maldonado provided helpful insight into the analysis of the voltammograms and suggestions for experimental design. Tim Zhang was very helpful in assisting me with performing the electrochemical experiments.

4.2 Materials and Methods

4.2.1 Materials

A 2 mm diameter gold working electrode was obtained from CH Instruments, Inc. Mutant cADO were created using site directed mutagenesis as described previously in Chapter 3 Section 3.2. Recombinant cADO from *P. marinus* MIT9313 was purified as previously described in chapter 2 section 2.3. Spin desalting columns were from Thermo Scientific. HRP was from MP Biomedicals. TCEP was from Gold Biotechnology. H_2O_2, mono and dibasic potassium phosphate, ethanol, potassium chloride and HEPES were from Fisher Chemicals. Octadecanal, heptanal, heptadecane, hexane, phenazine methosulfate, ferrous ammonium sulfate, NADH, pyrogallol and b-mercaptopropionic acid were obtained from Acros Organics.

4.2.2 Protein Film Generation

Gold electrodes 2 mm in diameter were cleaned by successive polishing with 1.0, 0.3, and 0.05 micron alumnia powders then sonicated in water for 15 min. The gold electrodes were then cycled with Ag/AgCl reference and platinum counter electrodes in 1 M sulfuric acid between 0 and 1.2 volts for 1 h at 0.05 V/s. The gold electrodes were then rinsed with water and dried using nitrogen. Alkane-thiol modified gold electrodes were generated by soaking a cleaned gold electrode overnight in a 55 mM solution of 3-mercaptopropionic acid in ethanol and then rinsed with water before addition of enzyme. Wt cADO protein films for cyclic voltammetry were prepared by addition of 3 μL of 100 nM enzyme onto an alkane-thiol modified gold electrode. Films were allowed to dry for

approximately 30 min then rinsed with water before use. Wt cADO films for differential pulse voltammetry were prepared by soaking the modified gold electrode in 300 μM enzyme solution for 30 min and then rinsed with water before use. A21C cADO protein films were prepared by first reducing 1 mM enzyme stocks with 10 mM TCEP for one h. This stock was then diluted to 100 nM and 3 μL of enzyme were added to a cleaned, unfunctionalized gold electrode. Films were allowed to dry approximately 30 min then rinsed with water before use.

4.2.3 Protein Film Voltammetry

Electrochemical experiments were performed using CH Instruments Electrochemical Analyzer models 420a and 760c. Data were collected using a three electrode glass cell with platinum counter and silver/silver chloride reference electrodes at room temperature inside a Faraday cage. 5 mL solutions of 100 mM potassium phosphate 100 mM KCl buffer at pH 7.2 were first purged for 15 min by either nitrogen or argon gas and then maintained under a blanket of that gas for the duration of the experiments. Protein films were generated on a 2mm diameter gold working electrode, as described above. For cyclic voltammetry experiments, the electrode was cycled between 0.1 and -0.8 V at 20 mV/s. No loss in signal was observed over the duration of the experiments. For differential pulse voltammetry experiments, the electrode was scanned from 0.1 V to -0.8V with an incremental potential of 0.02 V, a potential pulse amplitude of 0.05 V, a pulse width of 0.0005 s, a sample width of 0.0001 s, and a pulse period of 0.05 s. Potentials were adjusted to correspond to the standard hydrogen electrode (SHE) scale using $E_{SHE} = E_{SCE} + 241$ mV (at 25^{o}C).

4.2.4 Enzyme Assays

Assays were performed under both aerobic and microaerobic conditions using standard assay conditions as previously described in Chapter 2 section 2.2.3. Activity assays of mutant enzymes were performed only under microaerobic conditions. Reduced mutant activity assays were performed after first incubating the enzyme stock with 10x TCEP for 1h. Quantification of hydrocarbon products was performed as described in Chapter 2 section 2.4.

Initial peroxide formation assays were performed both on aerobic assays that had been reacted for 30 min and microaerobic assays that had been reacted for 1 h at pH 6.8. In these assays 0.02 units of HRP and 1 mM pyrogallol were added to previously reacted cADO assays. The samples were monitored by UV-vis spectroscopy and allowed to react for approximately 3 min until the increase in $A_{420,}$ corresponding to purpurogallin formation, plateaued. H_2O_2 concentrations were calculated based on standard curves.

Peroxidase coupled assays were performed by adding 0.05 units of HRP and 10 mM pyrogallol to aerobic assay solutions before initiating them with NADH. The samples were monitored continuously for 3 min by UV-vis spectroscopy at $A_{420.}$

4.3 Results and Discussion

4.3.1 Cystine Mutant Activity

The first thing to consider in protein film voltammetry (PFV) is the attachment of the enzyme to the electrode in a way that will allow it to remain folded, yet still be close enough to be redox active. To maximize the chance of successful protein film formation two methods of film generation were attempted. The first method used to attach the

enzyme was by direct covalent modification through a free thiol linkage to the gold electrode. However, considering the bare gold surface of the electrode is highly hydrophobic, there was a concern the enzyme might not remain active. The second attachment method was to electrostatically adsorb Wt cADO onto an alkane-thiol SAM that was previously deposited on the gold electrode.

Although cADO lacks the β subunit of MMOH that provides the other half of the reductase component binding cleft, it does share a number of the highly conserved residues implicated in electron transfer to the diiron core.[12] Three of these residues, Lys78, Glu64, and Gly152, were chosen to be mutated to Cys to serve as attachment points to the gold electrode for PFV because of their proximity to the active site and possible role as electron-transfer mediators. Because of the possibility that placing reactive thiols next to the diiron core would cause unfolding that would destabilize the active site, two other residues, A21 and T15, from the flexible tail region of the C-terminus were also mutated to Cys. Three of these mutants were easily purified, stable, and active both under standard conditions and when prepared with the reductant TCEP for surface attachment, as shown in Figure 4.2. Unsurprisingly, the mutants proximal to the active site were unstable and showed reduced activity. However, A21C retained activity at Wt levels. The A21C mutant was used for all further experiments where enzyme was covalently linked to the gold electrode.

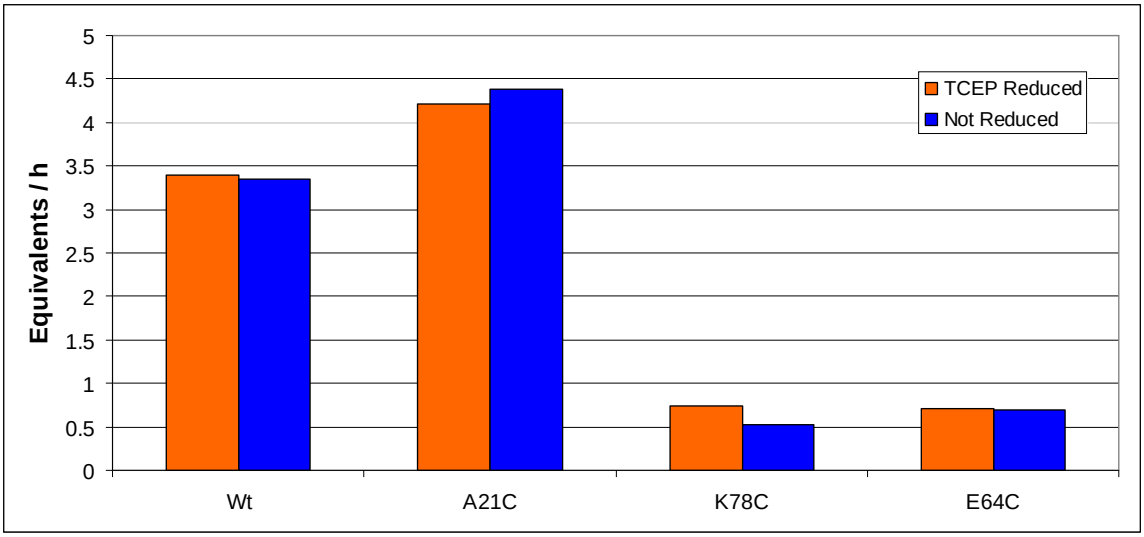

Figure 4.2 – Background corrected activity comparison of Cys mutants to Wt with octadecanal under standard conditions, shown in blue, or when previously reduced for 1 h with TCEP, shown in orange.

4.3.2 Non-Catalytic Voltammetry

PFV can be a powerful tool in the investigation of enzyme mechanisms and kinetics, in that the magnitude of the current provides a direct way to measure the rate of electron transfer, and therefore the rate of reaction, under catalytic conditions.[13,14] Typical experiments involve a three electrode cell as described in Figure 4.3 with working, counter, and reference electrodes connected to a potentiostat machine. The potentiostat applies an excitation waveform, varying the working electrode potential over time, and records the response waveform as a function of the current drawn by the electrode vs its reduction potential. In PFV, the measured current is directly proportional to the rate of electron transfer and, in catalytic voltammetry, the rate of catalysis. The limiting current (i_{lim}), where the change in current (Δi) is zero, represents the electrode potential at which electron transfer is no longer rate limiting and can be used in favorable cases to determine the rates of electron transfer.

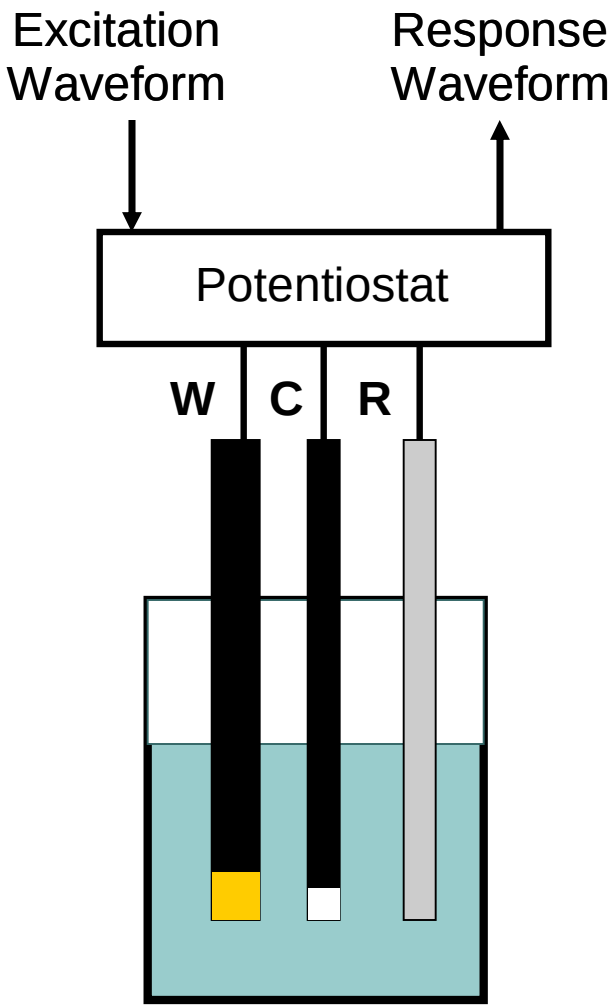

Figure 4.3 – Standard three electrode reaction set-up for PFV with a gold working electrode (**W**), platinum counter electrode (**C**), and Ag/AgCl reference electrode (**R**).

Additionally, it is capable of providing information while using very small quantities of enzyme – in favorable cases sub picomolar concentrations. However, there are limitations in that the protein must be able to be tethered to an electrode and must remain redox active. Also, to quantitatively evaluate catalytic data in a meaningful way, a non-catalytic signal must be observed, which can be challenging as the signal is usually quite small, making observation difficult. Fitting this piece of data can provide two parameters that are necessary to interpret catalytic data and perform kinetic analyses.

First is the reduction potential or potentials of one or more redox active centers in an enzyme. This information is frequently obscured under catalytic conditions. The second piece is the electroactive coverage. This provides the number of electrons transferred from the electrode to the protein film in a single reduction cycle, quantitating how much enzyme is attached to the surface and remains active.

The non-catalytic signal proved to be too small to reliably determine using cyclic voltammetry, however, we were able to determine the midpoint reduction potential using the complimentary technique differential pulse voltammetry (DPV), as shown in Figure 4.5. Unlike cyclic voltammetry, which employs a linear function to vary the electrode potential over time, or square wave voltammetry, which accomplishes the same variation in electrode potential in a series of small steps; the DPV excitation waveform uses a series of small, isolated pulses to incrementally vary the electrode potential, as shown in Figure 4.4 A, B, and C respectively. In DPV current measurements are taken immediately before and after each pulse. Measuring the current this way allows amplification of the signal to noise ratio by reducing the effect of the current charging the double layer during the pulse and only extracting the faradaic current.[15]

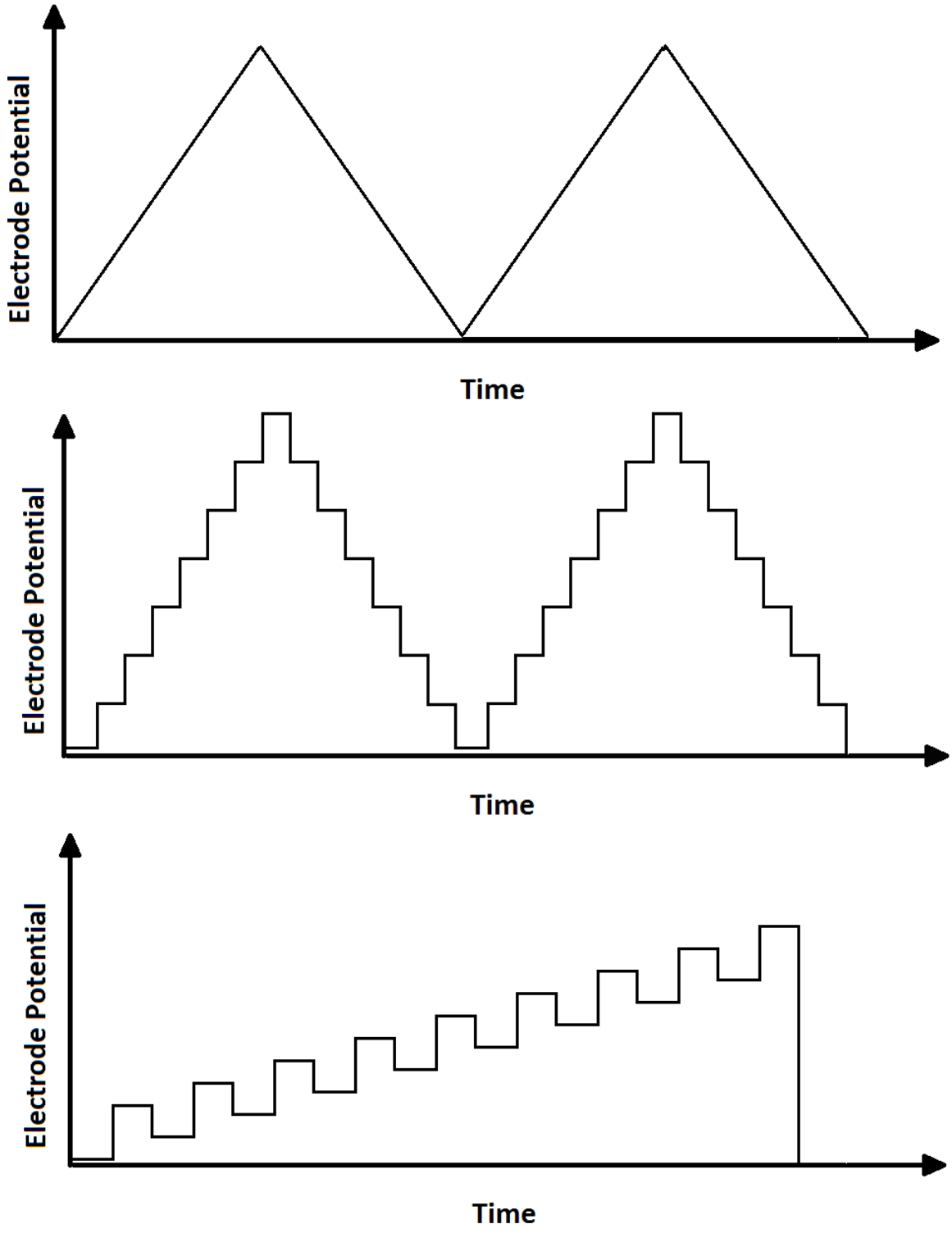

Figure 4.4 – Excitation waveforms for **A** – cyclic voltammetry, **B –** square wave voltammetry, and **C** – differential pulse voltammetry (DPV).

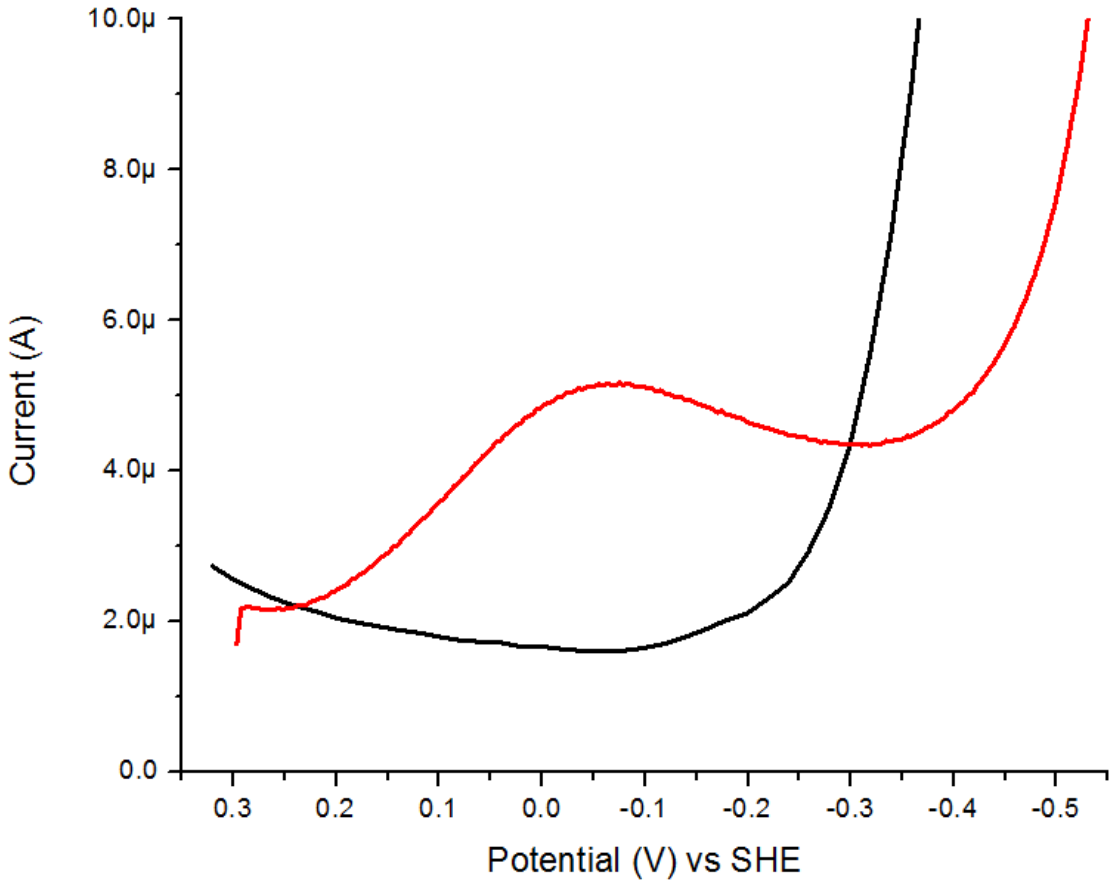

Figure 4.5 – Differential Pulse Voltammogram of the alkane-thiol functionalized electrode, shown in black, and the Wt cADO protein film, shown in red.

DPV experiments were performed using the alkane-thiol functionalized gold electrode with or without high concentration solutions (~300 μM) of Wt cADO adsorbed to the surface. Only one broad peak was observed indicating a midpoint reduction potential for cADO of $E^{o'}$ = -73 mV (± 10 mV vs SHE). While this is approximately the same as observed for the MMOH-MMOB complex, MMOH is capable of shifting approximately 132 mV to a higher reduction potential. [7] This is significant because it allows MMOH to become a more favorable electron acceptor. Under standard assay conditions PMS is used as an electron mediator, however, it would appear that at +80

mV, PMS has a higher reduction potential than cADO.[16] This would cause it be a less efficient electron donor to cADO and may be resulting in a slow electron rate transfer.

Unfortunately, because this experiment also required much higher enzyme concentrations than the cyclic voltammetry experiments described below, the electroactive coverage was not able to be determined at this time for interpretation of the catalytic signals. However, qualitative analyses of the features present in two distinct catalytic signals have proven to be mechanistically informative.

4.3.3 Catalytic Voltammetry with Heptanal

Cyclic voltammetry experiments were performed using the A21C mutant covalently linked to a clean gold electrode in a three electrode cell under argon gas. Small (less than 100 μL) quantities of aerated buffer containing heptanal were exchanged for equivalent volumes of buffer in the reaction cell while maintaining the argon atmosphere. Although we were unable to determine the electroactive coverage, because the concentrations of the films aliquoted on the electrode were only 100 nM, we are confident in the attachment of the enzyme to the surface of the electrode and that some portion is redox active. A significant catalytic wave was observed in the presence of heptanal that increased with substrate concentration, as shown in Figure 4.6. Furthermore this wave is distinct from the second catalytic wave with only oxygen present.

While we cannot precisely determine the rate or number of turnovers without knowing the electroactive coverage, the magnitude of the i_{lim} is orders of magnitude large than what we would expect for a non-catalytic signal. This suggests that there are multiple turnovers per 45 second cycle, which indicates a rate much higher than the

current maximum turnover numbers measured in solution of ~1 min^{-1}. Even without the electroactive coverage, calculating the current drawn by the enzyme at the i_{lim} with 200 μM heptanal we can estimate product turnover. Assuming all of the enzyme used in the film generation is bound and active, this puts a lower limit on the k_{obs} of 0.63 s^{-1}. This suggests that the rate of heptanal turnover in solution is at the very least an order of magnitude slower than what the enzyme is capable of under optimal electron transfer conditions. This observation lends support to the idea that there may be a binding interaction between cADO and its chemical or protein electron mediator, rather than simply a transient association, that would be a significantly slow step.

However, this estimation is complicated by the observation that the enzyme is able to react catalytically with O_2 in the absence of aldehyde as described below in section 4.3.4. We cannot rigorously determine from this data what contribution to the current is due to aldehyde turnover and what may be from the O_2 turnover to peroxide. It may be that in the presence of aldehyde substrate all of the reducing equivalents are used to produce alkane, but this seems unlikely. If we assume that the O_2 being shunted to the peroxide formation pathway remains the same regardless of aldehyde and background correct the calculation then the lower limit of k_{obs} for alkane formation drops to 0.43 s^{-1}, which is still significantly faster than observed in solution. The truth most likely lies somewhere in the middle as the Bollinger group has reported there are two distinct forms of the enzyme-substrate reactant complex that lead to formation of the peroxy-hemiacetal intermediate.[17] Their observation suggests that the order of binding of aldehyde and O_2, while introducing kinetic complexity, does not prohibit and that some quantity of the enzyme reacting with O_2 may contribute the formation of alkane.

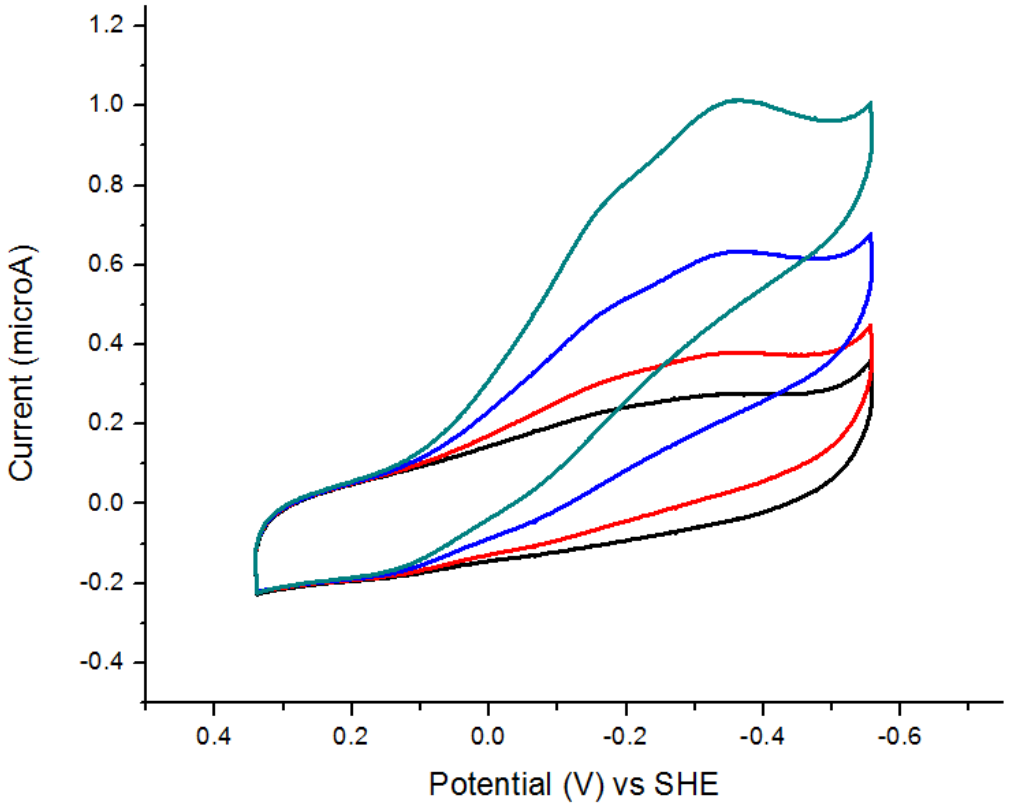

Figure 4.6 – Catalytic cyclic voltammogram of A21C on gold with heptanal. The black trace shows the background signal of the protein film without heptanal. The red, blue, and teal traces show the increase in current upon addition of 50, 100, and 200 µM heptanal respectively. A boost is evident at E= -210 mV and a switch at E= -370 V.

Interestingly, there are two additional features present in the wave that are informative. First, the increase in current at E = -210 mV immediately following the first i_{lim} (i_{lim1}) is known as a "boost." This feature, which allows the resolution of two distinct i_{lim}, is infrequently observed, but is indicative of a second redox couple distinguishable in the signal.[14,18] i_{lim1} at E = -160 mV likely corresponds to the initial reduction event, in this case the reduction of the diiron core from the resting diferric to the active diferrous state, because it occurs at the same potential where O_2 is reduced when no aldehyde is present.

The second i_{lim} (i_{lim2}) at E= -340 mV would, therefore, be suggestive of the key, second electron injection in step III of the mechanism.

Although it seems plausible that we observe this second reduction event, given that the second electron transfer is so crucial to aldehyde turnover, there is an alternative explanation for this effect. We cannot rule out this possibility that the i_{lim1} is only visible because of a competing reaction with O_2 and that i_{lim2} is the only limiting current for aldehyde turnover. If this boost does represent the observation of a distinct second electron transfer, this suggests the potentials at which the initial and second electron injection steps are no longer rate limiting are different. With further study these could provide rate constants for the two distinct electron transfer steps.

The second feature, is a "switch-off" that occurs at E= -370 mV where the current is attenuated after the observed maximum at i_{lim2}, but before it increases to an overpotential at E= -510 mV. This feature indicates that the second electron transfer occurred at a faster rate in the specific reduction potential window where the current was at i_{lim2}, or before it became fully reduced.[14,19,20] In other words, the second electron transfer occurs at an intermediate oxidation state, or in a mixed valent species. Returning to chapter 2, this appears to answer the question of whether the second electron injection is a single two electrons injection or multiple subsequent one electron injection steps, as illustrated in Figure 2.6 A and B. This switch provides evidence supporting the proposed mechanism in 2.6 B and the commonly proposed mechanism of two separate one electron transfers.

4.3.4 Catalytic Voltammetry with O_2

Elimination of oxygen is important in the preparation of samples for PFV because in significant concentrations it will be reduced by the electrode and produce an interfering and erratic signal, however, cADO requires O_2 for activity. The reaction cell was prepared under three different atmospheric conditions, nitrogen gas, argon gas, or in an anaerobic glovebox, in order to optimize the O_2 concentration to allow for catalysis without background interference. In the anaerobic glovebox neither any catalytic signals, nor any O_2 contamination were observed. Under nitrogen or argon gas, catalytic signals were observed with heptanal in the presence of the protein film while no contaminating signal was observed with a bare electrode. This suggested O_2 was in sufficiently low concentrations to prevent contaminating signals, while still in high enough concentration to maintain enzymatic activity. Reliably controlling the oxygen concentration proved difficult as on some occasions where the cell was purged extensively with argon, the heptanal catalytic wave was lost, which we attribute to limiting O_2.

Most surprisingly, however, under nitrogen or argon gas with low, but not limiting, O_2 an enzyme dependent catalytic wave was observed in the absence of aldehyde, as shown in Figure 4.7. The i_{lim} (i_{lim3}) for this wave occurs at the same potential as the initial reduction of cADO observed in the heptanal catalytic wave, i_{lim1}. It was hypothesized this signal was due to the catalytic reduction of O_2 by electrode reduced cADO. This is surprising as previous studies have suggested aldehyde must be bound first in order to trigger oxygen binding.[17] In the absence of aldehyde we might expect the diferrous enzyme to react slowly with oxygen and decay to the diferric resting state by releasing H_2O.[21] Although it seems plausible that H_2O_2 could be an alternative byproduct

of this decay, we would expect this process to be slow and not on the same order of magnitude as the catalytic wave with heptanal, suggesting multiple turnovers per cycle. Indeed, calculating the turnover rate at i_{lim3}, where E = -150 mV, gives the lower limit of H_2O_2 turnover as 0.20 s^{-1}. Logically, this leads to one of two conclusions. Either the rate of decay of the iron-peroxy species is being perturbed from physiological conditions by the stress applied by the electrode, or the rate of decay of the iron-peroxy species occurs on a much faster timescale than the scan rate.

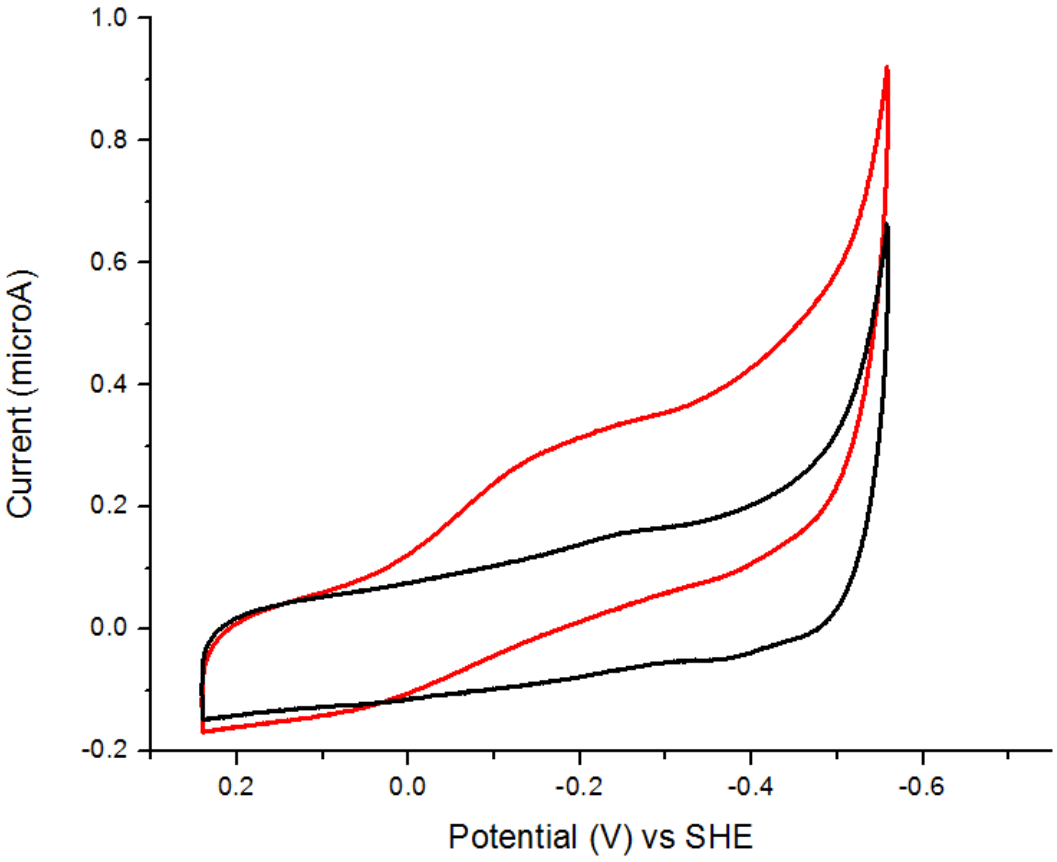

Figure 4.7 – Catalytic cyclic voltammetry of Wt cADO with O_2 on alkane-thiol funtionalized gold. The black trace shows the background of the alkane-thiol modified gold without enzyme. The red trace shows the catalytic wave upon addition of cADO.

4.3.5 Hydrogen Peroxide Formation

To confirm that cADO can react with O_2 and electrons to produce H_2O_2 physiologically and that the suspected peroxide formation is not solely a result of the electrode, peroxidase coupled assays were performed. The PMS/NADH reducing system and cADO were reacted with and without each other in the presence of O_2 for 30 min and subsequently analyzed for peroxide formation in a pyrogallol-horseradish peroxidase (HRP) coupled assay. These results were also compared to samples reacted microaerobically for 1 h to approximate typical assay conditions. These assays were not performed on a shorter timescale because the change in absorption of the NADH and PMS interfered with that of the pyrogallol to purpurogallin transition in the peroxidase half of the coupled assay. Enzyme samples had been previously iron loaded and desalted to remove excess iron. We do not expect there to be significant quantities of free iron in solution. The enzyme binds metals very tightly and requires an extensive purification process involving several metal chelators to remove the bound metals. Iron bound nonspecifically to the surface of the enzyme would be expected to react with free aldehyde, which has not been observed in associated activity assays.

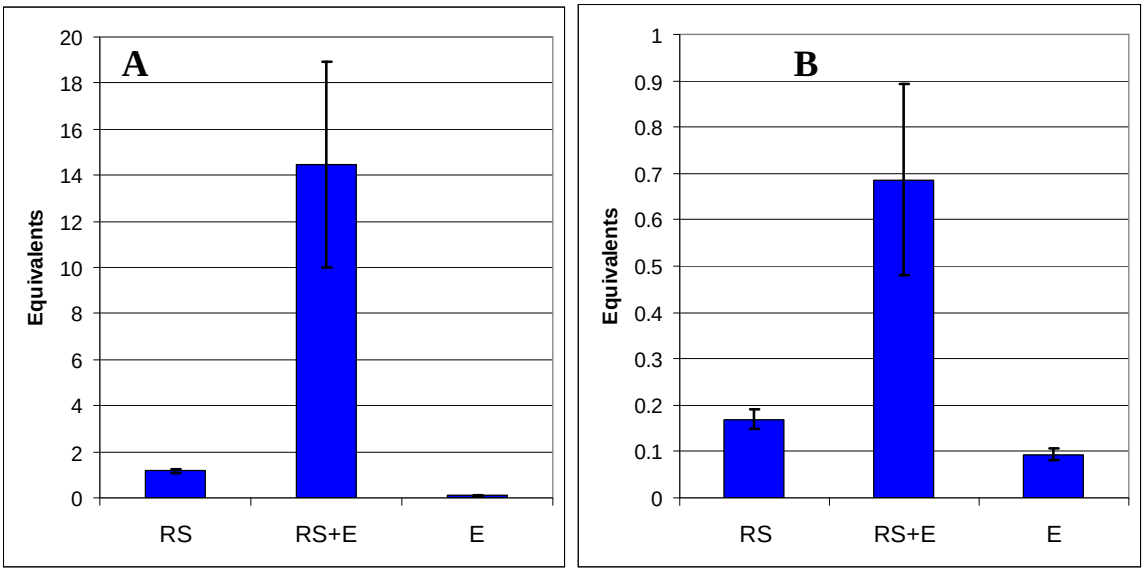

Figure 4.8 – Peroxide formation by a PMS/NADH reducing system (RS) alone, cADO (E) alone, or reducing system and cADO combined (RS+E). **A –** Aerobic and **B –** microaerobic solutions were monitored for 30 and 60 min respectively before analysis of peroxide concentration via coupled peroxidase assay.

The results in Figure 4.8 indicate that cADO was able to turn over O_2 to H_2O_2 14 times (± 4.5) in 30 min the presence of reducing system under aerobic conditions. This is compared to less than a single turnover of peroxide by the reducing system alone. However, this apparent rate of 0.47 ± 0.15 min^{-1} significantly underestimates the k_{cat} of this reaction. Under aerobic assay conditions the reducing system has been observed to oxidize completely in approximately 5 min. [22,23] This is readily apparent as the assay solution turns bright yellow, indicating only the oxidized form of PMS remains and that all of the NADH has been consumed. Therefore, we estimate that the rate of H_2O_2 formation is closer to ~2.8 ± 0.9 min^{-1}. It should also be noted that the H_2O_2 produced in this assay only accounts for 10-20% of the total reducing equivalents available. It is likely, therefore, that NADH oxidation is still uncoupled from this reaction, as has been previously observed for alkane production.[22] Microaerobically, far less H_2O_2 was formed

suggesting that fewer reducing equivalents are consumed in this reaction, but the observed trend is the same. That fewer reducing equivalents are shunted this way is consistent with the observation that under microaerobic conditions the reducing system is still viable for the duration of the assay. The fact that there is no color change suggests that NADH remains in excess.

Previously it had been assumed in the literature that the rapid futile cycling of NADH, PMS, and O_2 to produce H_2O_2 independent of enzyme was responsible for the short lifetime of the aerobic assay.[1] Furthermore, H_2O_2 production was determined to be responsible for inhibiting cADO.[23] This finding suggests that it is in fact cADO that is futilely cycling reducing equivalents in a futile peroxide shunt type mechanism to produce the H_2O_2 enzymatically.

4.3.6 Mechanistic Implication of Catalytic O_2 Reduction

Many non-heme and P450 type iron oxygenases have been shown to use H_2O_2 as a replacement for oxygen and external reducing equivalents in what is deemed a peroxide shunt mechanism.[21] In this way, the enzyme can recoup oxygen and electrons lost to oxidative decay. cADO is not capable of utilizing H_2O_2 in this manner and is instead inhibited by it. This means cADO not only has an alternative mechanism that diverges from the activity of alkane production, but also is distinct from other iron oxygenases. This has significant implications for alkane production and provides further support as to why the reaction is so slow without having a chemical RDS. Building on the generally accepted mechanism in Figure 1.6 and based on the new evidence available, I propose the following more comprehensive mechanism for cADO in Figure 4.9.

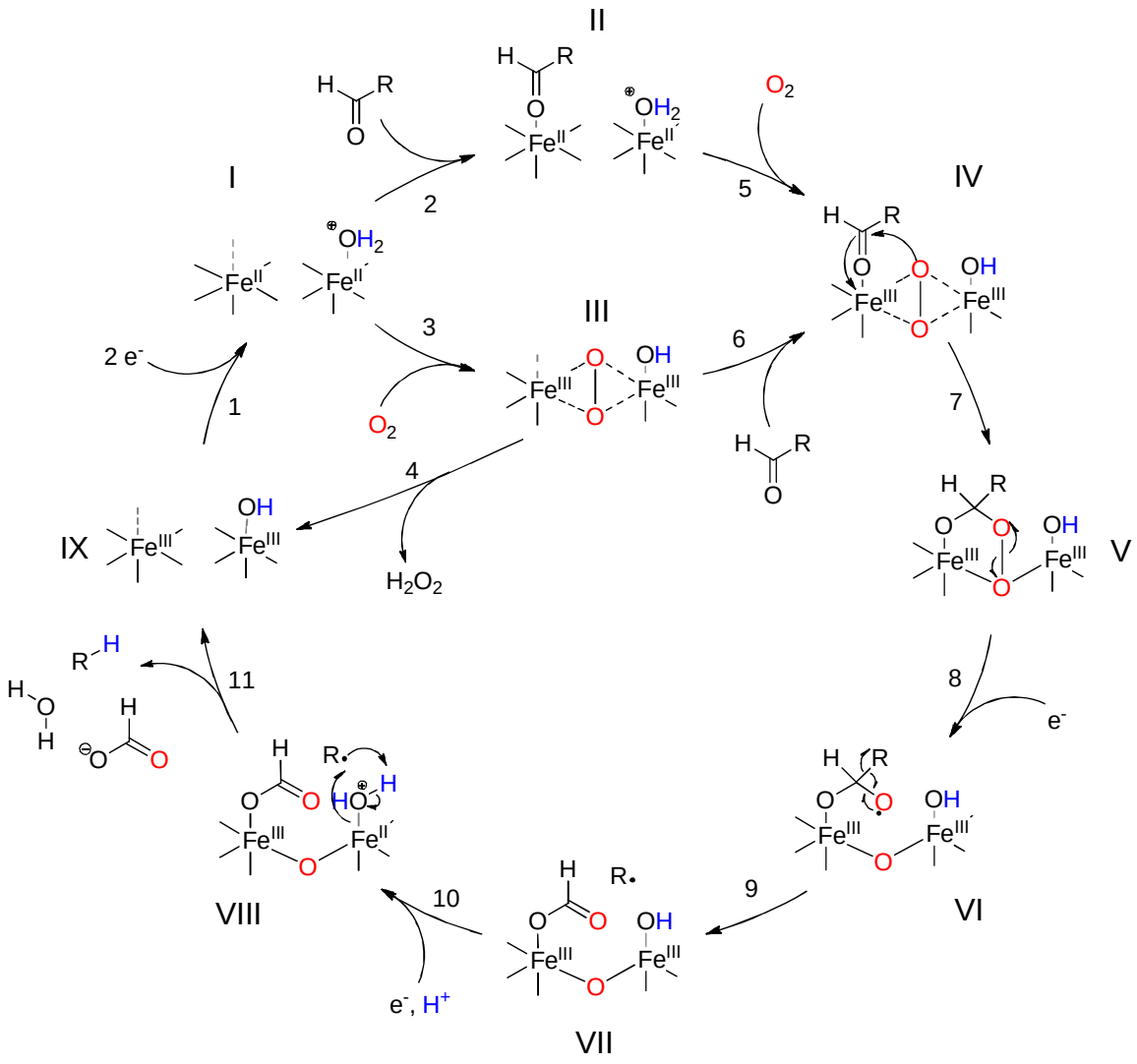

Figure 4.9 – Proposal for a new, more comprehensive mechanistic interpretation of the reactivity of cADO.

The primary addition to the previously published mechanism is the addition of the futile cycling of O_2 to peroxide, comprising steps 3 and 4, that is supported by the observation of the catalytic O_2 wave in conjunction with the coupled peroxidase assays. Although previous studies by Bollinger et al have claimed that prior binding of the aldehyde is “essential” to trigger oxygen binding, this study shows that is clearly not the

case. Their experiment following the formation and decay of the peroxy-hemiacetal intermediate by UV-vis spectroscopy did not fit to a simple model of 2 irreversible steps. [17] In fact, the data were fit to a model with two formation phases with differing rate constants arising from two distinct reactant states and each having a decay phase with the same rate constant. This kinetic complexity supports a mechanism in which either substrate can bind in either order, creating a branched pathway with two reactant states that reunites at intermediate IV. This also provides the evidence for inclusion of step 6. Although there is no direct evidence for this, it is also possible that intermediate IV is capable of decaying through this futile cycle and producing H_2O_2. Intermediates IV and V are thought to be in a rapid equilibrium and reaction of the "stable" peroxy-hemiacetal (V) with reduced ^{OMe}PMS only produced ~0.5 equivalents of alkane product. This could suggest either the electron transfer was decoupled or that the intermediate V might have been trapped as intermediate IV and decaying through this mechanism.

The "switch-off," where current is attenuated after reaching i_{lim2}, observed in the catalytic heptanal wave provides evidence that the later electron injections in steps 8 and 10 are in fact two discrete electron transfers. This mechanism also incorporates the findings from the SIE study in chapter 2 with a multiple site electron-proton transfer (MS-EPT) in step 10 including an iron bound aquo ligand. In the end, the sluggish nature of the alkane producing pathway may be the result of a combination of slow aldehyde binding relative to O_2 and more favorable partitioning towards the futile peroxide shunt pathway.

4.4 Conclusions

This work presented in this chapter provides a strong preliminary study for the electrochemical investigation of cADO. With a few further experiments, particularly determination of the electroactive coverage possibly through square wave voltammetry, this area of study could provide a wealth of information. Although we were unable to provide the in-depth kinetic analysis at this time with electron transfer rate constants, we did make several interesting mechanistic observations. The midpoint reduction potential was determined to be comparable to that of the *M. trichosporium* MMOH-MMOB complex and supporting evidence was found for the key electron injection step being two single electron transfers. Most interestingly, however, were the implication of electron transfer from the reducing system as a rate limiting step in solution experiments and the discovery of a futile cycle pathway possibly responsible for low alkane production through a partitioning effect. This may not have answered the question of why cADO and MMO perform different chemistry, but it does provide possible solutions to the question of why the enzyme is so slow.

4.5 References

(1) Marsh, E. N. G.; Waugh, M. W. (2013) Aldehyde Decarbonylases: Enigmatic Enzymes of Hydrocarbon Biosynthesis, *ACS Catal.*, *3*, 2515.

(2) Das, D.; Eser, B. E.; Han, J.; Sciore, A.; Marsh, E. N. (2011) Oxygen-independent decarbonylation of aldehydes by cyanobacterial aldehyde decarbonylase: a new reaction of diiron enzymes, *Angew Chem Int Ed Engl*, *50*, 7148.

(3) Li, N.; Norgaard, H.; Warui, D. M.; Booker, S. J.; Krebs, C.; Bollinger, J. M., Jr. (2011) Conversion of fatty aldehydes to alka(e)nes and formate by a cyanobacterial aldehyde decarbonylase: cryptic redox by an unusual dimetal oxygenase, *J. Am. Chem. Soc.*, *133*, 6158.

(4) Warui, D. M.; Li, N.; Norgaard, H.; Krebs, C.; Bollinger, J. M., Jr.; Booker, S. J. (2011) Detection of formate, rather than carbon monoxide, as the stoichiometric coproduct in conversion of fatty aldehydes to alkanes by a cyanobacterial aldehyde decarbonylase, *J. Am. Chem. Soc.*, *133*, 3316.

(5) Wallar, B. J. L., J. D. (1996) Dioxygen Activation by Enzymes Containing Binuclear Non-Heme Iron Clusters, *Chem. Rev.*, *96*.

(6) Baik, M. N., M.; Friesner, R. A.; Lippard, S. J. (2003) Mechanistic Studies on the Hydroxylation of Methane by Methane Monoxygenase, *Chem. Rev.*, *103*, 2385.

(7) Paulsen, K. E. L., Y.; Fox, B. G.; Lipscomb, J. D.; Munck, E.; and Stankovich, M. T. (1994) Oxidation-Reduction Potentials of the Methane Monooxygenase Hydroxylase Component from *Mehtylosinus trichosporium* OB3b, *Biochemistry*, *33*, 713.

(8) Lee, S. J.; McCormick, M. S.; Lippard, S. J.; Cho, U. S. (2013) Control of substrate access to the active site in methane monooxygenase, *Nature*, *494*, 380.

(9) Aukema, K. G.; Makris, T. M.; Stoian, S. A.; Richman, J. E.; Munck, E.; Lipscomb, J. D.; Wackett, L. P. (2013) Cyanobacterial aldehyde deformylase oxygenation of aldehydes yields n-1 aldehydes and alcohols in addition to alkanes, *ACS Catal*, *3*, 2228.

(10) Marshall, N. M.; Garner, D. K.; Wilson, T. D.; Gao, Y. G.; Robinson, H.; Nilges, M. J.; Lu, Y. (2009) Rationally tuning the reduction potential of a single cupredoxin beyond the natural range, *Nature*, *462*, 113.

(11) Clark, K. M. Y., Y.; Marshall, N. M.; Sieracki, N. A.; Nilges, M. J.; Blackburn, N. J.; van der Donk, W. A.; Lu, Y. (2010) Transforming a Blue copper into a Red Copper Protein: Engineering Cysteine and Homocysteine into the Axial Postition of Azurin Using Site-Directed Mutagenesis and Expressed Protein Ligation, *J. Am. Chem. Soc.*, *132*, 100093.

(12) Merkx, M. K., D. A.; Sazinsky, M. H.; Blazyk, J. L.; Muller, J.; Lippard, S. J. (2001) Dioxygen Activation and Methane Hydroxylation by Soluble Methane Monooxygenase: A Tale of Two Irons and Three Proteins, *Angew Chem Int Ed*, *40*.

(13) Bertrand, C. L. a. P. (2008) Direct Electrochemistry of Redox Enzymes as a Tool for Mechanistic Studies, *Chem. Rev.*, *108*, 2379.

(14) Armstrong, F. A. (2005) Recent developments in dynamic electrochemical studies of adsorbed enzymes and their active sites, *curr opin chem biol*, *9*, 110.

(15) Ianniello, R. M. L., T. J.; Yacynych, A. M. (1982) Differential Pulse Voltammetric Study of Direct Electron Transfer in Glucose Oxidase Chemically Modified Graphite Electrodes, *Anal. Chem.*, *54*, 1098.
(16) Dutton, P. L. (1978) Redox Potentiometry: Determination of Midpoint Potentials of Oxidation-Reduction Components of Biological Electron-Transfer Systems, *Methods in enzymology*, *54*.
(17) Pandelia, M. E.; Li, N.; Norgaard, H.; Warui, D. M.; Rajakovich, L. J.; Chang, W. C.; Booker, S. J.; Krebs, C.; Bollinger, J. M. (2013) Substrate-Triggered Addition of Dioxygen to the Diferrous Cofactor of Aldehyde-Deformylating Oxygenase to Form a Diferric-Peroxide Intermediate, *J. Am. Chem. Soc.*, *135*, 15801.
(18) Heering HA, W. J., Armstrong FA; (1997) Direct detection and measurement of electron relays in a multicentered enzyme: voltammetry of electrode-surface films of E. coli fumarate reductase, an iron-sulfur flavoprotein, *J. Am. Chem. Soc.*, *119*, 11628.
(19) Angove HC, C. J., Richardson DJ, Butt JN; (2002) Protein film voltammetry reveals distinctive fingerprints of nitrite and hydroxylamine reduction by a cytochrome c nitrite reductase, *J Biol Chem*, *277*, 23374.
(20) Gwyer JD, A. H., Richardson DJ, Butt JN; (2004) Redox-triggered events in cytochrome c nitrite reductase, *Bioelectrochemistry*, *63*, 43.
(21) kovaleva, E. G. N., M. B.; Chakrabarty, S.; and Lipscomb, J.D. (2007) Finidng INtermediates in the O2 Activtion Pathways of Non-Heme Iron Oxygenases, *Acc. Chem. Res.*, *40*, 475.
(22) Eser, B. E.; Das, D.; Han, J.; Jones, P. R.; Marsh, E. N. (2011) Oxygen-independent alkane formation by non-heme iron-dependent cyanobacterial aldehyde decarbonylase: investigation of kinetics and requirement for an external electron donor, *Biochemistry*, *50*, 10743.
(23) Andre, C.; Kim, S. W.; Yu, X. H.; Shanklin, J. (2013) Fusing catalase to an alkane-producing enzyme maintains enzymatic activity by converting the inhibitory byproduct H2O2 to the cosubstrate O2, *Proc.Natl. Acad. Sci. USA*, *110*, 3191.

Chapter 5 Conclusions

5.1 Overview

The initial investigations of cADO were full of promise and the expectation that it would form the cornerstone of a net carbon neutral biosynthetic pathway to drop-in biofuel production. The enzyme identified by Schirmer et al was small, stable, and soluble with a crystal structure already available and an obvious structural similarity to a well studied class of enzymes, the non-heme diiron oxygenases.[1] This made it an excellent alternative to studying the membrane-bound, and notoriously difficult to purify, plant and insect ADs. The initial investigations by our lab and others rapidly established that cADO utilized molecular oxygen, an external reducing system, and a diiron core to deformylate aldehydes with a wide range of chain lengths.[2-6] The Booker, Krebs, and Bollinger collaboration proved the existence of the proposed peroxy-hemiacetal intermediate species using a combination of spectroscopic techniques.[7] Our lab not only confirmed the radical nature of the mechanism, but determined both its lifetime and the rate of electron-proton transfer (EPT) through the use of cyclopropyl and oxiranyl radical clock substrate analogs.[8,9] However, as our comprehension of the unusual mechanistic features of cADO has grown throughout these experiments, it has become increasingly clear that the kinetics of alkane formation are simply too slow to provide a viable pathway to sustainable biofuel production.

Although the observed rate of *in vitro* alkane formation has been improved through better experimental design since the initial characterization of the enzyme, from 3 turnovers / 20 h to 1 min^{-1}, this activity is orders of magnitude slower than can be reasonably compensated for by system engineering.[2,3,5] Determining the source of this sluggishness is the major challenge remaining in the study of this enzyme. My investigations into the mechanism of cADO have been performed with this in mind. The work presented here has expanded our current knowledge about this enzyme, but just as importantly it has exposed new avenues for study that may be fruitful in improving the rate of the reaction.

5.1.1 Multiple Site Electron-Proton Transfer

In the initial labeling studies performed on cADO, the proton transferred to the alkyl radical to form the alkane product was determined to originate from the solvent.[2] Through study of the solvent isotope effects (SIE) on cADO, we have determined that the source of that proton is an iron-bound water ligand. Although no SIE was observed on the rate, using a novel method, we generated a proton inventory from the mass ratio of labeled and unlabeled products.[10] This technique directly informed on the isotopic fractionation at the site of proton transfer, allowing the $^{D_2O}SIE_{obs}$ value to be calculated as 2.19 ± 0.02. This effect on V/K corresponds to a highly inverse fractionation factor (Φ_{obs}) of 0.457 that is characteristic of a metal-hydroxide proton donor with two hydrogen bonds. Because this effect is purely on V/K and informs on the enrichment of protium, we attribute this to an equilibrium isotope effect (EIE) resulting from the pre-equilibration of protium and deuterium at the iron-bound water ligand.

Aside from determining the identity of the proton donor, this study provides a negative control that confirms proton transfer is not rate limiting. The radical clock substrates used to determine the lifetime of the radical suggested electron transfer was very fast, on the order of 10^4 to 10^5 s^{-1}, and that it likely originated directly from the metal center.[8,9] That no SIE on the rate was observed is consistent with this and together they suggest a multiple site electron-proton transfer (MS-EPT). This conclusion also created indicated that a non-chemical step may be rate determining.

5.1.2 Substrate Specificity

Following the conclusion of the SIE study, mutagenesis and substrate analogs were used to probe the non-chemical steps of substrate binding and/or product release. This area of study provided the fewest firm conclusions and we were unable to rule out substrate binding or product release as rate limiting. The phenylacetaldehyde derived substrate analogs, intended for stabilizing and trapping the product radical, were uninformative in this regard. They did, however, provide some insight into strength of the hydrophobic effect as a driving force for substrate binding, even to the point of overcoming clearly unfavorable steric effects. The mutagenesis experiments proved to be interesting for understanding substrate specificity when compared with the recent crystal structures of cADO indicating multiple substrate binding conformations may be interfering with activity.[11] The mutants were generally destabilizing, but two variants, I212N and V41I, showed significant changes in K_M^{app} with octadecanal. As a hydrophilic mutant intended to be slightly destabilizing for non-productive substrate binding in the opening of the binding pocket, I212N surprisingly had a lower K_M^{app} than the Wt

enzyme. The V41I mutant designed to occlude the hydrophobic pocket showed the largest variance with a K_M^{app} significantly larger than Wt. Taken together these data suggest that the binding conformation of long chain substrates with the polar head group exposed to the active site and the long aliphatic tail buried in the hydrophobic pocket is the most preferred. That no rate enhancement was observed, is unsurprising, however these results are interesting and further study may be able to improve substrate affinity while retaining stability and activity.

5.1.3 Electrochemistry

The protein electrochemistry studies on cADO proved to be very mechanistically informative, despite not knowing the electroactive coverage. The catalytic cyclic voltammograms observed when cADO reacted with heptanal and O_2 allowed for the lower limits of turnover rate to be calculated as 0.43 s^{-1} and 0.20 s^{-1} respectively. This result alone indicates a significantly higher activity with PFV than in solution assays, and these values almost certainly underestimate the true k_{cat} for these reactions.[2,3,12] Although, this may simply be due to optimizing electron transfer through the variable of reduction potential, these results do suggest that the electrochemistry plays a significant role in modulating the activity of cADO. The observation of the second catalytic wave was unexpected, but lead to the discovery of an alternative mechanism for cADO and a branch point in the mechanism of alkane production. It seems likely that the partitioning of reducing equivalents and O_2 between alkane formation and futile cycling to produce H_2O_2 is one source of kinetic complexity that has resulted in the observation of slow reaction rates.

The role of the reducing system has long been a point of contention in the study of cADO.[2,13] With no native reducing system identified, we have never been able to know whether our kinetic analyses come close to approximating the system as it is *in vivo* or if cADO is slow by natural design. Fortunately, expanding our investigations to include protein electrochemistry seems to have resolved this issue. That the lower limits on turnover rate were determined to be at least an order of magnitude larger than those observed in solution assays suggests that the reducing system is involved in a non-chemical rate limiting step, at least under current *in vitro* conditions. Although, this may simply be a result using a poor electron mediator as differential pulse voltammetry experiments determined the midpoint reduction potential of cADO to be -73 ± 10 mV (vs SHE), much lower than the reduction potential for PMS (+80 mV). This suggests a second source of complexity in the solution assays because PMS will be a less efficient electron donor to cADO.[14]

The goal of the electrochemical investigation of cADO was to determine how it differed from MMO. It would appear the answer to this question, electrochemically speaking, was that it did not. The midpoint potential for cADO was approximately the same as that for MMO.[15] However, the catalytic protein film voltammetry did result in two observations that may have answered the original question of why cADO is slow.

5.2 Future Directions

First and foremost, further experiments are necessary to complete the protein electrochemistry dataset. A number of interesting features were observed and, with determination of the electroactive coverage by standardizing film generation conditions or using square wave voltammetry, the catalytic signals could be analyzed more

thoroughly. This would allow for the accurate determination of a number of kinetic parameters for the formation of alkane and peroxide as opposed to only the lower limit of turnover rate that we have now.

A number of control experiments will need to be performed using a Clark electrode to determine the concentration and background subtract the contribution of oxygen in these systems. Catalytic experiments with heptanal and oxygen will need to be performed using a Clark electrode to have more rigorous control of the oxygen concentration in the reaction cell. This will allow for accurate kinetic parameters to be assigned to the side reaction of cADO and O_2. Additionally coupled catalytic heptanal and peroxide formation experiments will need to be performed to determine the ratio governing partitioning and whether the rate of peroxide formation is dependent on the presence of aldehyde. To ensure any rate enhancement observed is not simply due to the electrode, *in vitro* assays using different electron mediators with reduction potentials in the range of -340 mV, where electron transfer is no longer rate limiting, should also be explored.

5.2.1 Fusion Protein

In the event that further investigation into the electrochemistry of cADO does not lead to the understanding and rate enhancement necessary for making the system relevant for biofuels production, the next step in the project would be to design cADO-MMO fusion proteins to try and utilize the rate enhancing activity of the complimentary MMOR and MMOB proteins.[16] While the obvious approach would be to combine cADO with the β and γ subunits of MMOH, this would be unlikely to be successful as the protein-protein

interaction surfaces of the MMOH subunits are largely hydrophobic, while the surface of cADO is strongly charged. The amount of mutation necessary to get cADO to interact with the other subunits would undoubtedly destroy the stability of the enzyme.

An alternative method to generating an active and stable fusion protein would be to attempt to transplant the deformylation activity of cADO into the protein matrix of MMO. This type of activity transplant will likely prove challenging and require much trial and error, but has been successful before when both proteins have a similar fold.[17] This could potentially be accomplished through mutations leading to careful manipulation of the second sphere coordination residues in the hydroxylase subunit of MMOH. If the ligand state of the diiron core in MMO is perturbed to mimic that of cADO the deformylation chemistry may be imparted to an enzyme that already has well understood interactions with the reductase and B components.

5.3 References

(1) Schirmer, A.; Rude, M. A.; Li, X.; Popova, E.; del Cardayre, S. B. (2010) Microbial biosynthesis of alkanes, *Science*, *329*, 559.

(2) Das, D.; Eser, B. E.; Han, J.; Sciore, A.; Marsh, E. N. (2011) Oxygen-independent decarbonylation of aldehydes by cyanobacterial aldehyde decarbonylase: a new reaction of diiron enzymes, *Angew Chem Int Ed Engl*, *50*, 7148.

(3) Eser, B. E.; Das, D.; Han, J.; Jones, P. R.; Marsh, E. N. (2011) Oxygen-independent alkane formation by non-heme iron-dependent cyanobacterial aldehyde decarbonylase: investigation of kinetics and requirement for an external electron donor, *Biochemistry*, *50*, 10743.

(4) Li, N.; Chang, W. C.; Warui, D. M.; Booker, S. J.; Krebs, C.; Bollinger, J. M., Jr. (2012) Evidence for only oxygenative cleavage of aldehydes to alk(a/e)nes and formate by cyanobacterial aldehyde decarbonylases, *Biochemistry*, *51*, 7908.

(5) Li, N.; Norgaard, H.; Warui, D. M.; Booker, S. J.; Krebs, C.; Bollinger, J. M., Jr. (2011) Conversion of fatty aldehydes to alka(e)nes and formate by a cyanobacterial aldehyde decarbonylase: cryptic redox by an unusual dimetal oxygenase, *J. Am. Chem. Soc.*, *133*, 6158.

(6) Warui, D. M.; Li, N.; Norgaard, H.; Krebs, C.; Bollinger, J. M., Jr.; Booker, S. J. (2011) Detection of formate, rather than carbon monoxide, as the stoichiometric coproduct in conversion of fatty aldehydes to alkanes by a cyanobacterial aldehyde decarbonylase, *J. Am. Chem. Soc.*, *133*, 3316.

(7) Pandelia, M. E.; Li, N.; Norgaard, H.; Warui, D. M.; Rajakovich, L. J.; Chang, W. C.; Booker, S. J.; Krebs, C.; Bollinger, J. M. (2013) Substrate-Triggered Addition of Dioxygen to the Diferrous Cofactor of Aldehyde-Deformylating Oxygenase to Form a Diferric-Peroxide Intermediate, *J. Am. Chem. Soc.*, *135*, 15801.

(8) Das, D.; Ellington, B.; Paul, B.; Marsh, E. N. G. (2014) Mechanistic Insights from Reaction of alpha-Oxiranyl-Aldehydes with Cyanobacterial Aldehyde Deformylating Oxygenase, *ACS Chem. Biol.*, *9*, 570.

(9) Paul, B.; Das, D.; Ellington, B.; Marsh, E. N. (2013) Probing the mechanism of cyanobacterial aldehyde decarbonylase using a cyclopropyl aldehyde, *J. Am. Chem. Soc.*, *135*, 5234.

(10) Waugh, M. W.; Marsh, E. N. (2014) Solvent isotope effects on alkane formation by cyanobacterial aldehyde deformylating oxygenase and their mechanistic implications, *Biochemistry*, *53*, 5537.

(11) Buer, B. C.; Paul, B.; Das, D.; Stuckey, J. A.; Marsh, E. N. (2014) Insights into substrate and metal binding from the crystal structure of cyanobacterial aldehyde deformylating oxygenase with substrate bound, *ACS chemical biology*, *9*, 2584.

(12) Andre, C.; Kim, S. W.; Yu, X. H.; Shanklin, J. (2013) Fusing catalase to an alkane-producing enzyme maintains enzymatic activity by converting the inhibitory byproduct H2O2 to the cosubstrate O2, *Proc. Natl. Acad. Sci. USA*, *110*, 3191.

(13) Zhang, J.; Lu, X.; Li, J. J. (2013) Conversion of fatty aldehydes into alk (a/e)nes by in vitro reconstituted cyanobacterial aldehyde-deformylating oxygenase with the cognate electron transfer system, *Biotechnol Biofuels*, *6*, 86.

(14) Dutton, P. L. (1978) Redox Potentiometry: Determination of Midpoint Potentials of Oxidation-Reduction Components of Biological Electron-Transfer Systems, *Methods in enzymology*, *54*.
(15) Paulsen, K. E. L., Y.; Fox, B. G.; Lipscomb, J. D.; Munck, E.; and Stankovich, M. T. (1994) Oxidation-Reduction Potentials of the Methane Monooxygenase Hydroxylase Component from *Mehtylosinus trichosporium* OB3b, *Biochemistry*, *33*, 713.
(16) Wallar, B. J. L., J. D. (1996) Dioxygen Activation by Enzymes Containing Binuclear Non-Heme Iron Clusters, *Chem. Rev.*, *96*, 2625.
(17) Lu, Y. B., S. M.; Pfister, T. D. (2001) Engineering Novel Metalloproteins: Design of Metal-Binding Sites in to Native Protein Scaffolds, *Chem. Rev.*, *101*, 3047.

Appendix A : Synthesis of Substrate Analogs

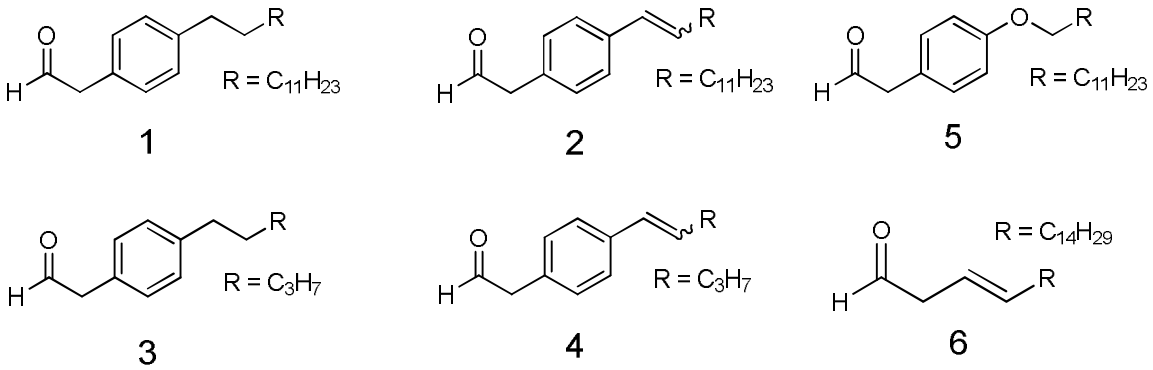

Figure S.1 – Substrate analogs synthesized to assay cADO. **1** — 2-(4-tridecylphenyl)acetaldehyde **2** — unsaturated 2-(4-(tridec-1-en-1-yl)phenyl) acetaldehyde **3** — 2-(4-pentylphenyl) acetaldehyde **4** — 2-(4-(penten-1-en-1-yl) phenyl)acetaldehyde **5** — 2-(4-(dodecyloxy)phenyl)acetaldehyde and **6** — (E)-octadec-3-enal.

A.1 Synthesis of 2-(4-acylphenyl)acetaldehyde derivatives

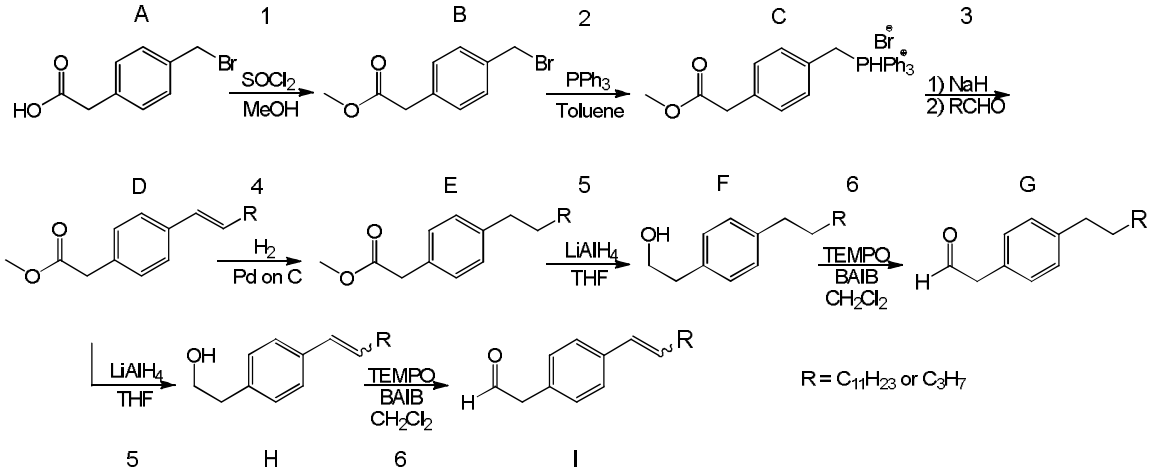

Figure S.2 – General synthesis of 2-(4-acylphenyl)acetaldehyde derivatives.

The syntheses of substrate analogs **1**, **2**, **3**, and **4** was accomplished using the general protocol as shown in Figure 3.6. In step 1, 5g of 2-(4-(bromomethyl)phenyl) acetic acid (**A**) was dissolved in excess dry MeOH to which 250 μL of $SOCl_2$ were added. The mixture was left to stir overnight at which point it was quenched with base, the organic layer was extracted with ethyl acetate, and the product was dried by rotary evaporation. The product, methyl 2-(4-(bromomethyl)phenyl)acetate (**B**), was obtained in 93.4% yield.

Methyl 2-(4-((triphenyl-phosphonium-bromide)methyl)phenyl)acetate (**C**) was synthesized in step 2 according to a literature procedure by refluxing 1 equivalent of **B** and 0.8 equivalent of triphenyl phosphine in 10 equivalents of dry toluene at 130^{o}C for 24 hours under nitrogen.[1] The product was an insoluble salt collected by filtration and washed with hexanes. The salt, **C**, was dried using a rotary evaporator to obtain a 64% yield.

The Wittig reaction in step 3 was performed according to a literature procedure.[2,3] Dodecanal was the aldehyde used in the syntheses of **1** and **2.** Butyraldehyde was the aldehyde used in the syntheses of **3** and **4.** Under nitrogen, 1 g of the **C** was dissolved in dry THF to which 1.25 equivalents of NaH were added dropwise at room temperature. The reaction mixture was stirred for 90 min and turned yellow. 1.25 equivalents of aldehyde in dry, nitrogen purged THF, were added dropwise and the reaction was left overnight. The reaction was quenched with HCl and diluted with water and ethyl acetate. The mixture was washed with saturated $NaHCO_3$ and the organic layer was extracted. The organic layer was washed with brine, dried over sodium sulfate, filtered, and evaporated using a rotary evaporator. The dried, crude product was packed onto silica

and purified using flash chromatography in 95% hexanes to 5% ethyl acetate. The product was identified by TLC and the solvent was removed using a rotary evaporator. The stereospecificity of the double bond was not controlled for in this reaction and the products contained a mixture of the cys and trans forms. In the syntheses of **1** and **2** intermediate **D** was obtained in a yield of a 52%. In the syntheses of **3** and **4** intermediate **D** was obtained in a yield of a 38% and was carried directly on to step 5**.**

Hydrogenation of **D** in step 4 was performed in the syntheses of **1** and **3.** 1 g of Pd on C was dried on a watch glass at 300^{o}C for 1 h, covered with foil, and left to cool in a desicator. 150 mg of **D** were dissolved in 5 mL of ethyl acetate and purged with nitrogen gas. A small spatula of Pd on C was added to the solution and the flask was quickly backfilled with nitrogen and stoppered. A balloon containing hydrogen gas under slight pressure was connected to the purged flask and all other gas lines were removed. After 36 h of constant stirring under hydrogen, the reaction mixture was filtered through a sintered glass frit and rinsed with hot ethyl acetate. The filtrate was collected and evaporated using a rotary evaporator to obtain **E**. The product was verified by NMR and obtained in 100% yield.

In step 5, the reduction intermediate **E** (in the syntheses of **1** and **3**) or intermediate **D** (in the syntheses of **2** and **4**) was accomplished according to a literature procedure.[4] 150 mg of **D** or **E** were dissolved in 1 mL of THF under nitrogen. An excess of $LiAlH_4$ (3 equivalents) was added dropwise to the solution at 0^{o}C. The reaction was stirred at room temperature overnight, then quenched with concentrated HCl and diluted with water. The mixture was extracted with diethyl ether and the organic layer was back

extracted with brine, dried over sodium sulfate, filtered, and evaporated using a rotary evaporator. The products **F** or **H** were identified by NMR and obtained in 100% yield.

The final step, 6, was accomplished using a TEMPO oxidation according to a literature procedure.[5,6] 80 mg of **F** or **H** were dissolved with 0.1 equivalents of (2,2,6,6-tetramethylpiperidin-1-yl)oxyl (TEMPO) in CH_2Cl_2 at room temperature. To initiate the reaction 1.5 equivalents of [bis(acetoxy)iodo]benzene were added. The reaction was monitored by TLC until no starting material remained. The reaction mixture was purified directly by flash chromatography using 98:2 hexanes to ethyl acetate. The products **G** or **I** were determined by TLC and the solvent removed by rotary evaporation. to obtain a yield of 75%. In the syntheses of **1** and **3** the product **G** was obtained in yields of 61% and 57% respectively. In the syntheses of **2** and **4** the product **I** was obtained in yields of 68% and 51% respectively. The identity of the products was confirmed by TLC and NMR.

Characterization of 2-(4-tridecylphenyl)acetaldehyde (1)

^{1}H NMR (400 MHz, $CDCl_3$) δ 9.72 (t, *J* = 2.4 1H), 7.17-7.01 (dd, 4H), 3.63 (d, *J* = 2 Hz, 2H), 2.57 (t, *J* = 7.6 Hz, 2H), 1.60-1.54 (m, 2H), 1.40-1.20 (m, 20H), 0.86 (t, *J* = 7.2 Hz, 3H); ^{13}C NMR (100 MHz, $CHCl_3$) δ 199.73, 142.20, 129.46, 129.03, 128.84, 50.21,35.56, 31.90, 31.45, 29.65, 29.57, 29.50, 29.34, 29.30, 22.67, 14.11.

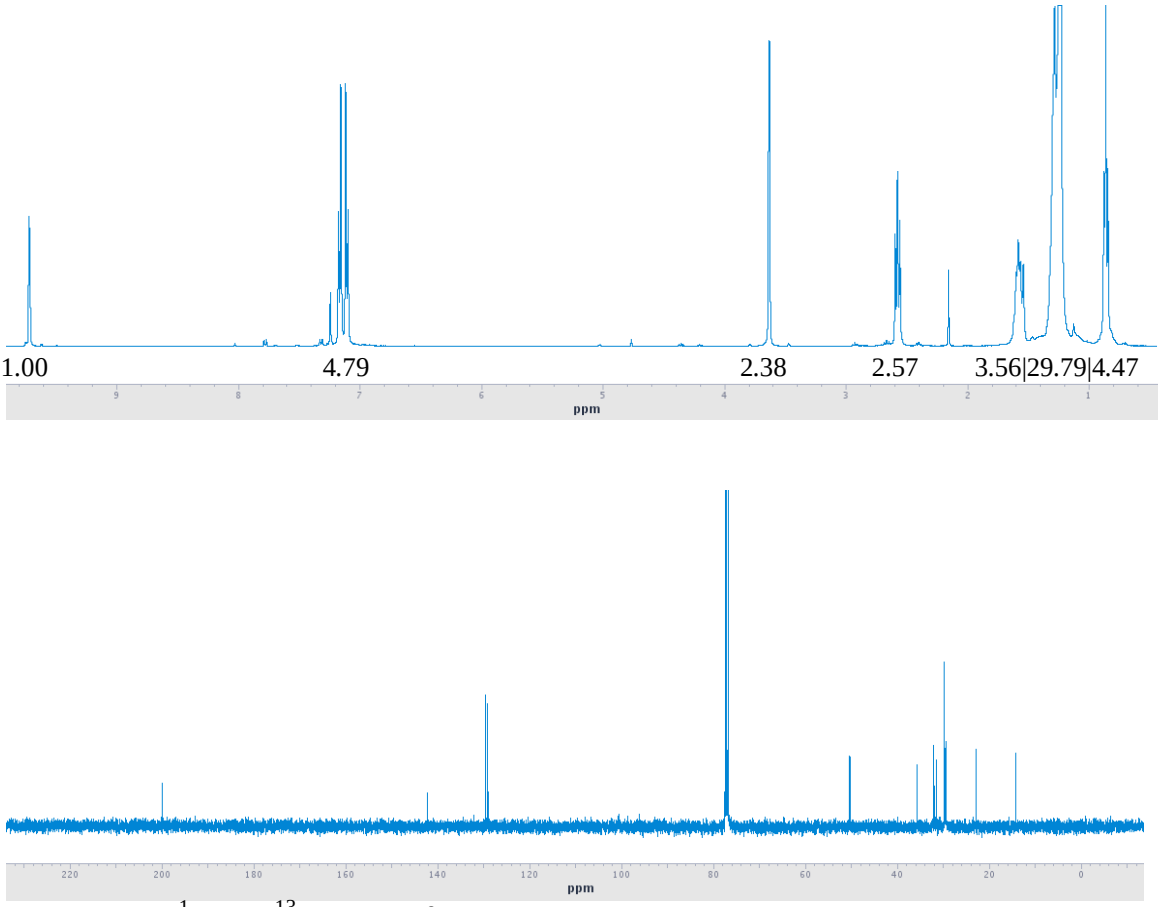

Figure S.3 – ^{1}H and ^{13}C NMR of 2-(4-tridecylphenyl)acetaldehyde (**1**)**.**

Characterization of 2-(4-(tridec-1-en-1-yl)phenyl) acetaldehyde (2)

^{1}H NMR δ 9.70 (t, *J* =2.4 1H), 7.33-7.11 (dd, *J* = 8 Hz, 4H), 6.41-6.17 (dm, 2H), 3.64 (d, *J* = 2 Hz, 2H), 2.21-2.16 (q, *J* = 7.2 Hz, 2H), 1.46-1.40 (q, *J* = 6.8 Hz, 2H), 1.28-1.24 (m, 16H), 0.86 (t, *J* = 7 Hz, 3H)

^{13}C NMR δ 199.42, 137.23, 129.72, 129.35, 129.01, 126.46, 50.27, 33.03, 31.90, 29.65, 29.62, 29.60, 29.50, 29.33, 29.21, 22.67, 14.10

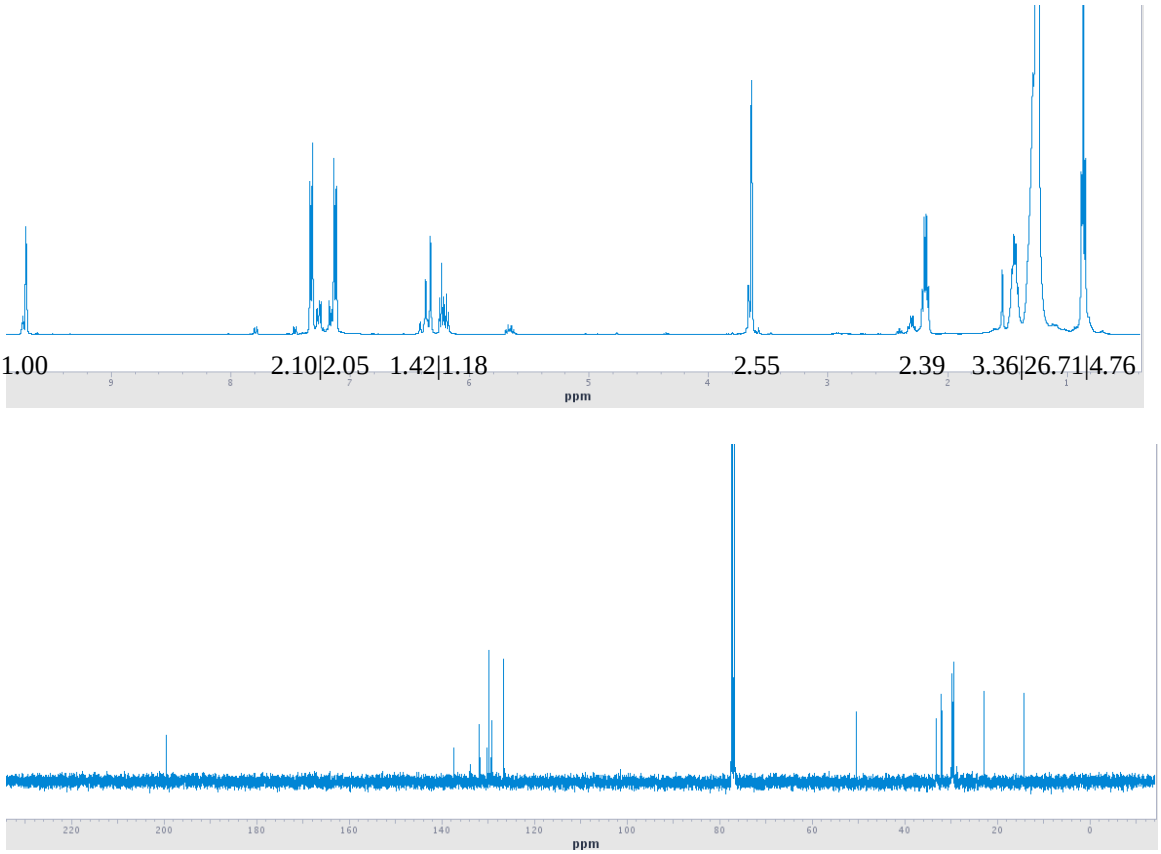

Figure S.4 – ^{1}H and ^{13}C NMR of 2-(4-(tridec-1-en-1-yl)phenyl) acetaldehyde (**2**).

Characterization of 2-(4-pentylphenyl) acetaldehyde (3)

^{1}H NMR δ 9.72 (t, *J* = 2.4 1H), 7.18-7.10 (dd, *J* = 8 Hz, 4H), 3.63 (d, *J* = 1.6 Hz, 2H), 2.60-2.56 (t, *J* = 7.8 Hz, 2H), 1.65-55 (m, 2H), 1.4-1.2 (m, 6H), 0.88 (s, *J* = 6.6 Hz, 3H)

^{13}C NMR δ 199.71, 142.17, 129.47, 129.04, 128.87, 52.21, 35.53, 31.48, 31.13, 22.52, 14.01

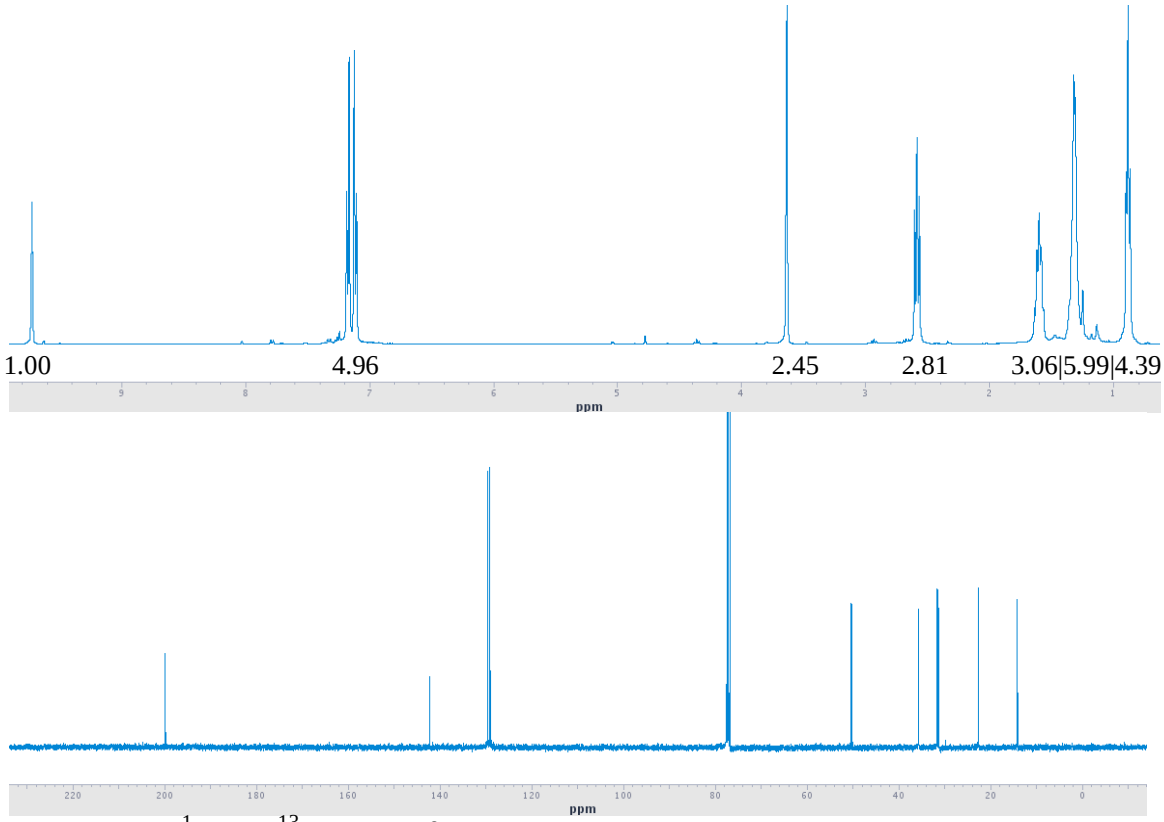

Figure S.5 – ^{1}H and ^{13}C NMR of 2-(4-pentylphenyl) acetaldehyde (**3**).

Characterization of 2-(4-(penten-1-en-1-yl) phenyl)acetaldehyde (4)

^{1}H NMR δ 9.71 (t, *J* = 2.4 1H), 7.34-7.11 (dd, *J* = 8 Hz, 4H), 6.40-6.18 (dm, 2H), 3.66-3.64 (d, *J* = 8 Hz, 2H), 2.20-2.15 (q, *J* = 7.2 Hz, 2H), 1.53-1.44 (m, 2H), 0.937 (t, *J* = 7.2 Hz, 3H)

^{13}C NMR δ 199.42, 137.20, 129.73, 129.36, 129.35, 129.24, 126.48, 50.26, 35.09, 22.49, 13.71

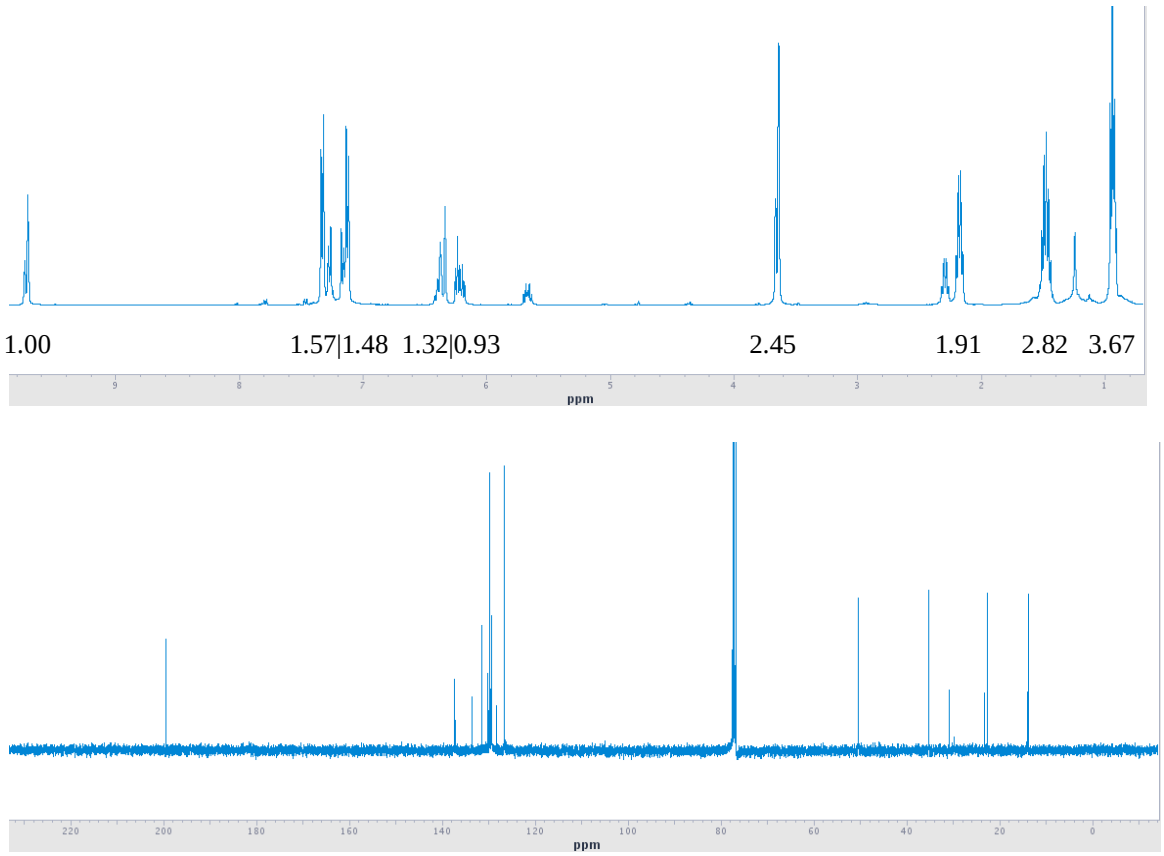

Figure S.6 – ^{1}H and ^{13}C NMR of 2-(4-(penten-1-en-1-yl) phenyl)acetaldehyde (**4**).

A.2 Synthesis and Characterization of 2-(4-(dodecyloxy)phenyl)acetaldehyde (5) and the product standard 1-methyl-4-dodecyloxy-benzene (11)

The synthesis of f **5** was accomplished in four steps according to literature procedures. The starting material 2-(4-hydroxyphenyl)acetic acid was methyl esterified with thionyl chloride as previously described in step 1 of the general synthesis of the 2-(4-acylphenyl)acetaldehyde derivatives to obtain methyl 2-(4-methyoxyphenyl) acetate in 68% yield. To a solution of dry acetone and saturating potassium carbonate, 1.5 g of methyl 2-(4-methyoxyphenyl) acetate and 1.1 equivalents of 1-bromododecane were added. The mixture was refluxed overnight, separated by filtration, and the filtrate was evaporated using a rotary evaporator. The crude product was separated by flash

chromatography using 9:1 hexanes to ethyl acetate. The intermediate methyl 2-(4-(dodecyloxy)phenyl) acetate was identified by TLC, evaporated to dryness, and confirmed by NMR to obtain 78.1% yield. This intermediate was then subjected to $LiAlH_4$ reduction and TEMPO oxidation as described in steps 5 and 6 of the general synthesis of the 2-(4-acylphenyl)acetaldehyde derivatives to produce the product **5** in 72.5% yield. The identity of the product was confirmed by NMR.

^{1}H NMR δ 9.70 (t, *J* = 2.4 1H), 7.11-6.87 (dd, *J* = 8.4, 4H), 3.94-3.91 (t, *J* = 6.6, 2H), 3.60 (d, *J* = 2.4, 2H), 1.78-1.74 (m, 2H), 1.44 (m, 2H), 1.33-1.26 (m, H), 0.89-0.85 (t, *J* = 6.8, 3H)

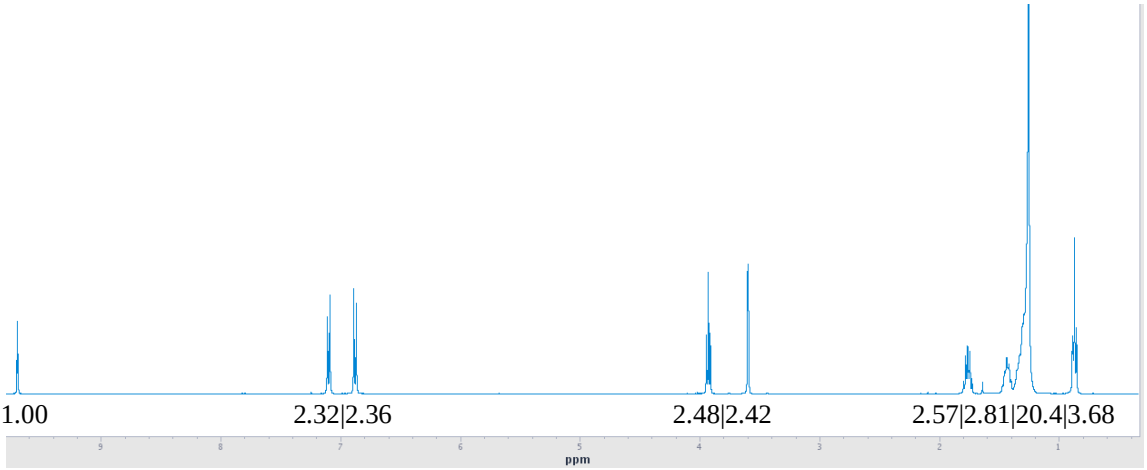

Figure S.7 – ^{1}H and ^{13}C NMR of 2-(4-(dodecyloxy)phenyl)acetaldehyde (**5**).

The synthesis of the product standard for **5**, 1-methyl-4-dodecyloxy-benzene, was accomplished using using *p*-cresol as the starting material in the reaction conditions described for the synthesis of **5.** The product was identified by NMR.

^{1}H NMR δ 7.07-6.77 (dd, *J* = 8.4, 4H), 3.91 (t, *J* = 6.8, 2H), 3.39 (t, *J* = 6.8, 2H), 2.28 (s, 3H), 1.90-1.81 (m, 2H), 1.44-1.39 (m, 2H), 1.27 (m, 14H), 0.89 (t, *J* = 6.8, 3H)

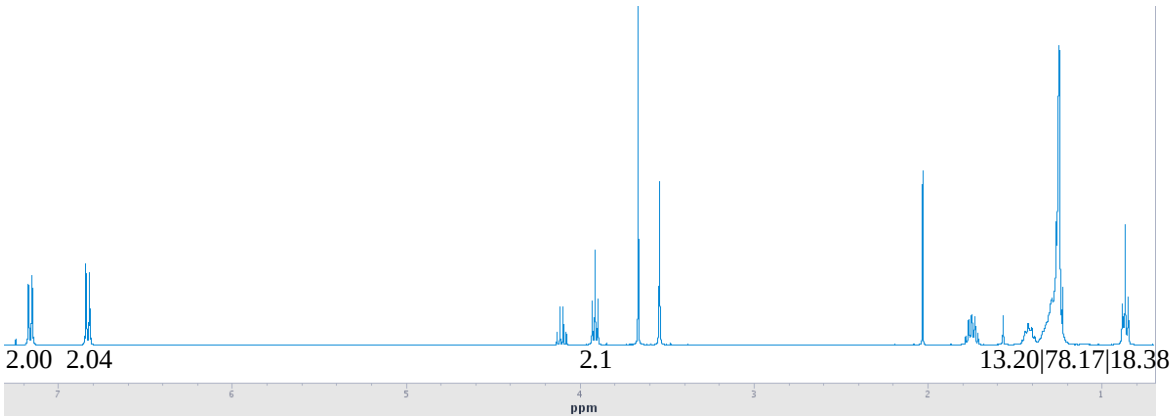

Figure S.8 – ^{1}H NMR of 1-methyl-4-dodecyloxy-benzene (**11**).

A.3 Synthesis and Characterization of (E)-octadec-3-enal (6)

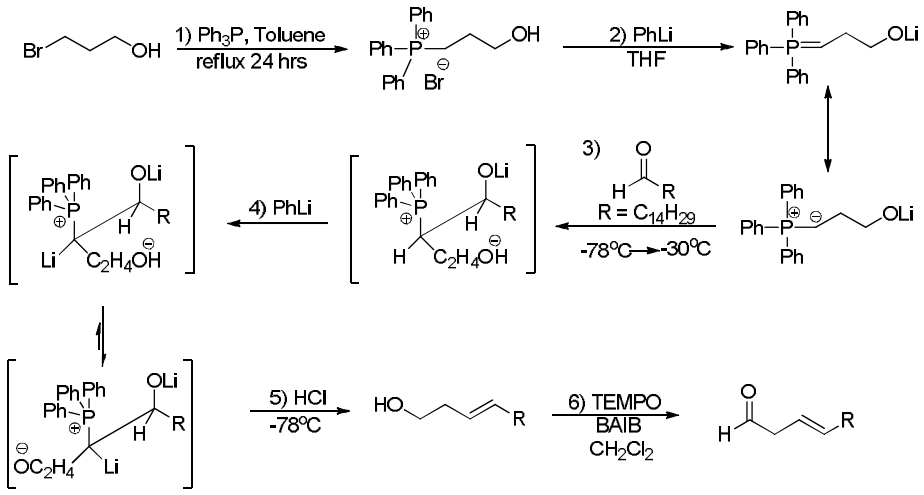

Figure S.9 -- Synthesis of **6** — (E)-octadec-3-enal via the Schlosser modification of the Wittig reaction.

The synthesis of **6** was accomplished in three steps from the starting material 3-bromoproan-1-ol as shown in Figure 3.5. 3-hydroxypropyl-triphenylphosphonium bromide was synthesized according to a literature procedure by refluxing 2 equivalents of 3-bromo-1-propanol and 1 equivalent of triphenyl phosphine in 10 equivalents of dry toluene for 24 hours under nitrogen.[1] The product was an insoluble salt collected by

filtration and washed with hexanes. The salt was dried using a rotary evaporator to obtain an 85.4% yield.

The Schlosser modification of the Wittig reaction[2,7] was employed using pentadecanal and the 3-hydroxypropyl-triphenylphosphonium bromide to form trans-octadec-3-enol. 1.75 equivalents of phenyl lithium were added dropwise at room temperature to a solution of 1 equivalent of 3-hydroxypropyl-triphenylphosphonium bromide dissolved in THF and under nitrogen. The resulting clear red solution was cooled to -78^{o}C in an acetone dry ice bath. 0.75 equivalents of pentadecanal were added to the solution at -30^{o}C and stirred for 20 min, resulting in a cream colored solution. 0.75 equivalents of n-butyl Lithium were added dropwise and the resulting dark red solution was kept at -30^{o}C for 30 min, then at -78^{o}C for 15 min. 2.1 equivalents of HCl in diethyl ether was added causing immediate decolorization. A 10:1 mixture of tert-butanol (22.5 eq.) to potassium tert-butyl oxide (2.25 eq) was added and the reaction mixture was stirred for one hour at room temperature. The reaction mixture was diluted with H_2O and extracted with diethyl ether. The organic layer was washed with diethyl ether, dried with sodium sulfate, and evaporated using a rotary evaporator. The product was extracted from tripenyl phosphine oxide by filtration with hexanes, which were removed by rotary evaporation, to obtain a 50% yield of (E)-octadec-3-en-1-ol.

(E)-octadec-3-en-1-ol was oxidized to (E)-octadec-3-en-1-ol (6) using a TEMPO oxidation according to the literature.[5,6] 1 equivalent of (E)-octadec-3-en-1-ol was brought up to 1 M in CH_2Cl_2 at room temperature and mixed with 0.1 equivalents of (2,2,6,6-tetramethylpiperidin-1-yl)oxyl (TEMPO). 1.1 equivalents of [bis(acetoxy)iodo]benzene was added and the reaction was allowed to stir until no alcohol was observed by TLC.

The reaction mixture was purified directly by flash chromatography using 9:1 hexanes to ethyl acetate. The product (E)-octadec-3-en-1-al (6) was determined by TLC and the solvent removed by rotary evaporation to obtain a yield of 75%. The compound was identified by TLC and NMR.

^{1}H NMR δ 9.58 (t, *J* = 4, 1H), 5.57-5.38 (dm, 2H), 3.03 (m, 2H), 2.01-1.95 (m, 2H), 1.31-1.18 (m, 24H), 0.81 (t, *J* = 12, 3H)

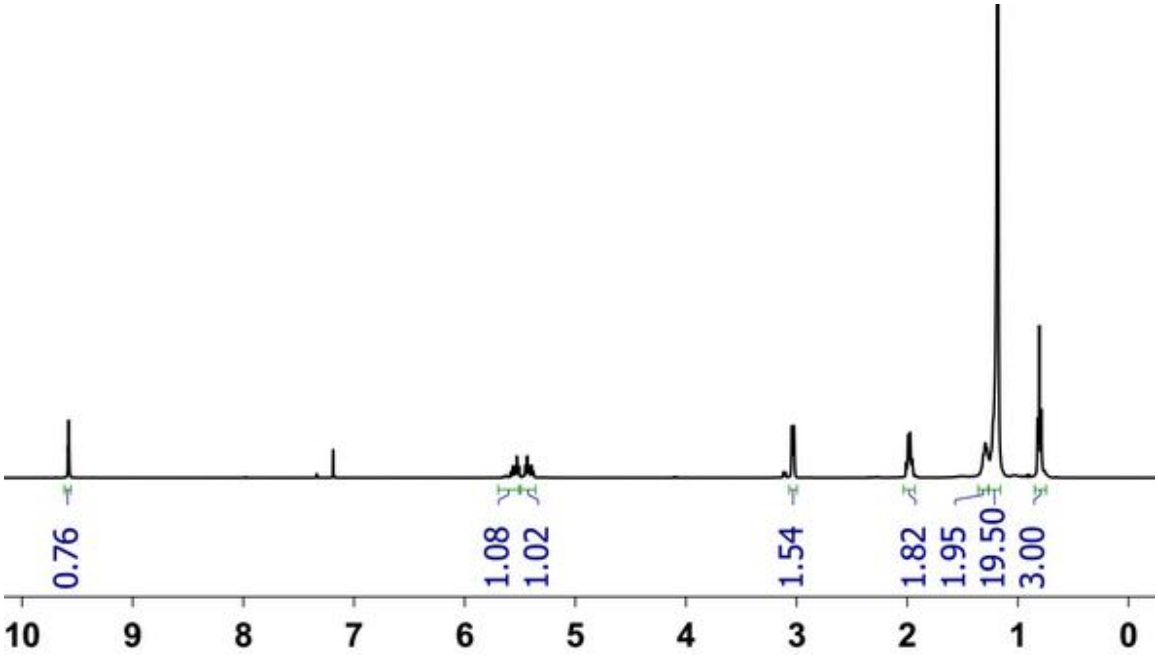

Figure S.10 – ^{1}H NMR of (E)-octadec-3-enal (**6**).

A.4 Synthesis of 1-methyl-4-tridecyl-benzene (7) and 1-methyl-4-(tridec-1-en-1-yl)benzene (8)

The syntheses of **7** and **8** were accomplished using reaction conditions previously described in the general synthesis of the 2-(4-acylphenyl)acetaldehyde derivatives. First, the starting material 1-(bromomethyl)-4-methylbenzene was reacted with triphenyl phosphonium using the conditions outlined in step 2. The resulting the

bromophosphonium salt was obtained in 94.5% yield and used in the Wittig reaction with dodecanal described in step 3 to produce **8** in 62% yield. The hydrogenation reaction conditions described in step 4 was then performed on **8** to produce the **7** in 95% yield, which was verified by NMR.

Characterization of 7

^{1}H NMR δ 7.07 (s, 4H), 2.56 (t, *J* = 7.6, 2H), 2.31 (s, 3H), 1.65-1.53 (m, 2H), 1.38-1.22 (m, 20H), 0.88 (t, *J* = 6.4, 3H)

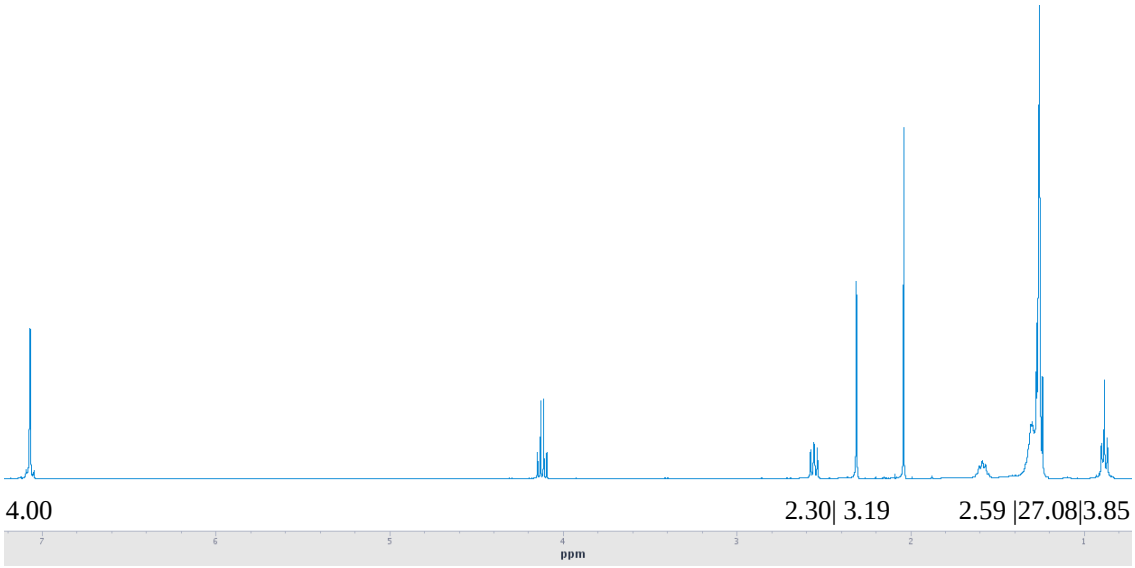

Figure S.11 – ^{1}H NMR of 1-methyl-4-tridecyl-benzene (**7**)

Characterization of 8

^{1}H NMR δ 7.24-7.07 (dd, *J* = 8.4, 4H), 6.4-6.1 (dm, 2H), 2.35-2.230 (d, *J* = 8.8, 2H), 2.20-2.10 (q, *J* = 6.4, 2H), 1.50-1.39 (m, 2H), 1.39-1.19 (m, 16H), 0.90-0.82 (t, *J* = 6.8, 3H)

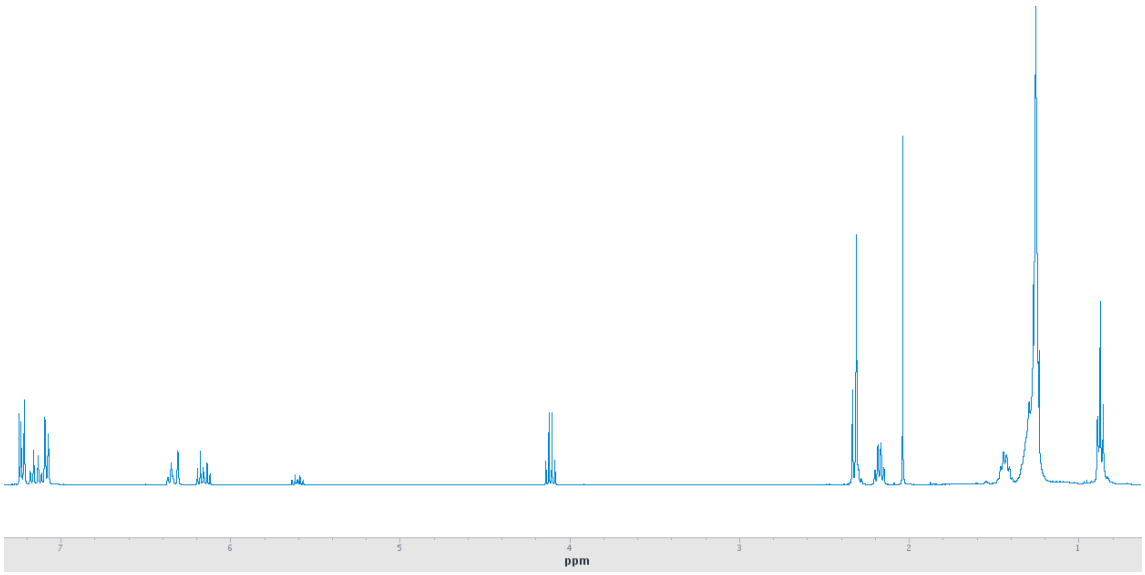

Figure S.12 – ^{1}H NMR of 1-methyl-4-(tridec-1-en-1-yl)benzene (**8**).

A.5 References

(1) Bulman Page, P. C. V., H.; Batchelor, K. J.; Hindley, S. J.; Edgar, M.; Beswick, P. (2003) Synthesis of an Isomer of the Oxaspirobicyclic Tetronic Acid Unit of the CCK-B Receptor Antagonist Tetronothiodin, *Synlett*, *7*, 1022.

(2) Schlosser, M. T., H. B.; Schaub, B. (1985) The Betaine-Ylid Route to Trnas-Alkenols, *Tetrahedron Letters*, *26*, 311.

(3) Wadsworth, D. H. S. I., O. E.; seus, E.J.; Ford Jr, J.A. (1964) The Stereochemistry of hte Phosphonate Modification of the Wittig Reaction, *Wadsworth, Schupp, Seus, and Ford*, *30*, 680.

(4) Gaylord., N. G. In *Comprehensive Organic Synthesis*; Wiley-Interscience: New York, 1956; Vol. 35, p 107.

(6) Antonella De Mico, R. M., Luca Parlanti, Andrea Vescovi, and; Piancatelli, G. (1997) A Versatile and Highly Selective Hypervalent Iodine (III)/ 2,2,6,6-Tetramethyl-1-piperidinyloxyl-Mediated Oxidation of Alcohols to Carbonyl Compounds, *J. Org. Chem*, *62*, 6974.

(7) Schlosser, M. a. C., K. F. (1966) Trans-Selectove Olefin Syntheses, *Angew Chem Int Ed*, *5*, 126.